Université Mohamed Khider – Biskra

Faculté des Sciences et de la technologie

Département : Génie Mécanique

Réf : ………………

جامعة محمد خيضر بسكرة

كليـة العلـوم و التكنولوجيــا

قسم: الهندسة الميكانيكية

المرجع: …………

Thèse présentée en vue de l'obtention
Du diplôme de
Doctorat en : Métallurgie

Spécialité: Métaux industriels

Etude du comportement mécanique et tribologique d'une couche de nitrures de chrome déposée par un traitement duplex sur un acier faiblement allié

Présentée par:

MOKHTARA Soheib

Soutenue publiquement le: 05/10/2021

Devant le jury composé de :

BOUMERZOUG Zakaria	**Professeur**	**Président**	**Université de Biskra**
ZIDANI Mosbah	**Professeur**	**Rapporteur**	**Université Batna 2**
MECHACHTI Saïd	**Professeur**	**Rapporteur adjoint**	**Université d'Annaba**
BELIARDOUH Nasser Eddine	**Professeur**	**Examinateur**	**Université d'Annaba**
BENTAMAM ElHachmi	**Professeur**	**Examinateur**	**Université de Biskra**
MERZOUGUI Abdelkrim	**Professeur**	**Examinateur**	**Université de Biskra**

Thesis submitted for obtaining the degree of

Doctorate in: Metallurgy

Specialty: Industrial metals

Study of the mechanical and tribological behaviour of a chromium nitrides layer deposited by a duplex treatment on a low alloy steel

---

Presented by:

MOKHTARA Soheib

Thesis defended publicly on: 05/10/2021

The jury members:

BOUMERZOUG Zakaria	**Professor**	**Chairman**	**University of Biskra**
ZIDANI Mosbah	**Professor**	**Supervisor**	**University Batna 2**
MECHACHTI Saïd	**Professor**	**Co-supervisor**	**University of Annaba**
BELIARDOUH Nasser Eddine	**Professor**	**Examiner**	**University of Annaba**
BENTAMAM ElHachmi	**Professor**	**Examiner**	**University of Biskra**
MERZOUGUI Abdelkrim	**Professor**	**Examiner**	**University of Biskra**

ACKNOWLEDGEMENTS

ABSTRAT

The present work aims at producing a chromium nitrides layer by plasma nitriding of a hard chromium electroplated layer in a pure nitrogen atmosphere (duplex surface treatment) and to study the effect of the nitrogen pressure of plasma nitriding on the structural, morphological, mechanical and tribological properties of the obtained chromium nitrides layer. Several characterisations and testing techniques were used to achieve the objectives of this work, including X-ray diffraction, scanning electron microscopy (SEM), optical microscopy (OM), energy dispersive spectroscopy (EDS), microhardness test, nanoindentation test and ball-on-disk test. The results showed that a Cr_2N layer was successfully produced by plasma nitriding of a hard chromium electroplated layer in a pure nitrogen atmosphere. Furthermore, it was found that the nitrogen pressure of plasma nitriding significantly affected the surface properties of the plasma nitrided hard chromium electroplated layer. Indeed, plasma nitriding of the hard chromium electroplated layer at low nitrogen pressure did not significantly improve the morphological, mechanical and tribological properties of the surface of the hard chromium electroplated layer. On the other hand, increasing the nitrogen pressure led to a noticeable improvement in the mechanical and tribological properties of the hard chromium electroplated layer surface.

Keywords: Low alloy 35NCD6 steel; Duplex surface treatment; Hard chromium electroplating; Plasma nitriding; Nitrogen gas pressure; Chromium nitrides; Nanoindentation; Wear resistance; Micro-cracks.

ملخص

يهدف هذا العمل إلى إنتاج طبقة من نيتريدات الكروم عن طريق النترجة بالبلازما لطبقة كروم صلبة مرسبة كهربائيا في وسط مكون من النيتروجين النقي (المعالجة السطحية المزدوجة) ودراسة تأثير ضغط النيتروجين في النترجة بالبلازما على التركيب البنوي والشكلي والخصائص الميكانيكية والترايبولوجية لطبقة نيتريدات الكروم المحصل عليها. تم استخدام العديد من أدوات التوصيف وتقنيات الاختبار لتحقيق أهداف هذا العمل ، وتشمل : حيود الأشعة السينية والمسح المجهري الإلكتروني (SEM) والفحص المجهري الضوئي (MO) والتحليل الطيفي المشتت للطاقة (EDS) ، واختبار الصلادة، واختبار التسنن النانوي و اختبار الكرة على القرص. أظهرت النتائج أن طبقة Cr_2N تم إنتاجها بنجاح بواسطة النترجة بالبلازما لطبقة الكروم الصلبة المرسبة كهربائياً في وسط مكون من النيتروجين النقي. بالإضافة إلى ذلك ، وجد أن ضغط النيتروجين في النترجة بالبلازما يؤثر بشكل كبير على خصائص سطح طبقة الكروم الصلب المرسبة كهربائيًا والمنترجة بالبلازما. في الواقع ، لم تعمل النترجة بالبلازما لطبقة الكروم الصلب المرسبة كهربائيا عند ضغط النيتروجين المنخفض على تحسين الخصائص المورفولوجية والميكانيكية والترايبولوجية لسطح طبقة الكروم الصلب المرسبة كهربائيا بشكل كبير. وبالمقابل ، أدت زيادة ضغط النيتروجين إلى تحسن ملحوظ في الخصائص الميكانيكية والترايبولوجية لسطح طبقة الكروم الصلب المرسبة كهربائيا.

كلمات مفتاحية: الفولاذ 35NCD6، المعالجة السطحية المزدوجة، الترسيب الكهربائي للكروم الصلب، النترجة بالبلازما، ضغط النتروجين الغازي، نيتريدات الكروم، التسنن النانوي، مقاومة الحت، الشقوق الدقيقة.

RESUME

Le présent travail vise à produire une couche de nitrures de chrome par nitruration au plasma d'une couche électrodéposée de chrome dur dans une atmosphère d'azote pur (traitement de surface duplex) et à étudier l'effet de la pression d'azote de la nitruration au plasma sur les propriétés structurelles, morphologiques, mécaniques et tribologiques de la couche de nitrures de chrome obtenue. Plusieurs caractérisations et techniques d'essai ont été utilisées pour atteindre les objectifs de ce travail, notamment la diffraction des rayons X, la microscopie électronique à balayage (MEB), la microscopie optique (MO), la spectroscopie à dispersion d'énergie (EDS), le test de microdureté, le test de nanoindentation et le test de la bille sur disque. Les résultats ont montré qu'une couche de Cr_2N a été produite avec succès par nitruration au plasma d'une couche électrodéposée de chrome dur dans une atmosphère d'azote pur. De plus, il a été constaté que la pression d'azote de la nitruration au plasma affectait de manière significative les propriétés de surface de la couche électrodéposée de chrome dur nitrurée au plasma. En effet, la nitruration au plasma de la couche électrodéposée de chrome dur à faible pression d'azote n'a pas amélioré de manière significative les propriétés morphologiques, mécaniques et tribologiques de la surface de la couche électrodéposée de chrome dur. En revanche, l'augmentation de la pression d'azote a conduit à une amélioration notable des propriétés mécaniques et tribologiques de la surface de la couche électrodéposée de chrome dur.

Mots clés : Acier faiblement allié 35NCD6 ; Traitement de surface duplex ; Electrodéposition de chrome dur ; Nitruration au plasma ; Pression d'azote gazeux ; Nitrures de chrome ; Nanoindentation ; Résistance à l'usure ; Microfissures.

TABLE OF CONTENTS

LIST OF FIGURES

LIST OF TABLES

GENERAL INTRODUCTION

GENERAL INTRODUCTION

Mechanical metal parts are subject to various types of solicitation: tribological, mechanical, electrochemical,...etc. The objective of researchers has always been to improve the response of metal parts to these solicitations. The approach used to achieve this objective differs from one research group to another, with some targeting the material of construction, others the surrounding environment, others the contact surface between the material and the environment, and others the whole system.

In systems where the dominant solicitations are of a tribological and mechanical nature, such as in the interaction of interconnected gears, the appropriate solution is usually to improve the mechanical and tribological properties of the metal part surface by means of surface treatment, surface coating or a combination of them. The latter combination is called "duplex surface engineering", which can be defined as the application of two surface engineering techniques to produce a new layer with combined properties or to supplement the drawbacks of one of them by the other [1]. Successful combinations include the use of thermochemical surface treatment with the application of a coating.

One of the duplex surface treatments that has attracted attention in recent decades is the combination of hard chrome electroplating and plasma nitriding. Hard chromium electroplating is a widely used technique in the industry as it offers many advantages in terms of hardness, wear resistance and corrosion resistance [2]. However, it has some limiting properties, such as surface micro-cracks, high internal residual stresses and reduced hardness at high temperatures, which can affect its performance under severe working conditions. In order to improve its properties and reduce its drawbacks, the surface of electroplated hard chromium can be modified by surface treatment techniques such as ion implantation, gas nitriding and plasma nitriding. The resulting layer usually consists of chromium nitrides with outstanding wear and corrosion resistance characteristics.

The duplex surface treatment consisting of hard chrome electroplating and plasma nitriding is advantageous as it represents an economical alternative to other expensive surface engineering techniques with comparable resulting properties. In addition, it can be easily implemented in the

industry by adding the complementary technique to the existing chrome electroplating or plasma nitriding industries.

The objectives of this thesis are to produce a chromium nitrides layer by plasma nitriding of hard chromium electroplated layer in a pure nitrogen gas atmosphere and to study the effect of the nitrogen pressure of plasma nitriding on the structural, morphological, mechanical and tribological properties of the resulting chromium nitrides layer. The results of this thesis can contribute to filling the gap in the research work on the use of pure nitrogen as a nitriding atmosphere in plasma nitriding of a hard chromium electroplated layer, as well as the gap in the research work on the effect of nitrogen pressure of plasma nitriding on the surface properties of the plasma nitrided hard chromium electroplated layer. Moreover, they can help to determine the possibility of applying the resulting chromium nitrides layer to metal parts that require good mechanical and tribological performance.

The thesis consists of three chapters. The first chapter is composed of four main parts: the first part presents steel types and their microstructural and mechanical properties, the second covers metal coating processes, the third presents common thermochemical treatments of steels and the fourth summarises the literature review on nitriding of chromium coatings.

The second chapter is devoted to the presentation of the substrate material and the description of the different experimental methods used to characterise the properties of the resulting layer.

The third chapter presents the experimental results concerning the structural, morphological, mechanical and tribological properties of the resulting layer and a study of the effect of nitrogen pressure in plasma nitriding on the surface properties. The experimental results are discussed and compared with some research work in the literature where necessary.

Finally, general conclusions and suggestions for future works are presented in the last part of the thesis.

BACKGROUND

AND

LITERATURE REVIEW

I. BACKGROUND AND LITERATURE REVIEW

I.1. Introduction

This chapter is divided into four main parts. The first part presents the types of steel and the characteristics of each type in terms of microstructure and mechanical properties. After that, the second part explores the techniques used in the deposition of metallic coatings and the general principle of each technique. In essence, the electroplating technique principle and properties are presented in details. The third part presents the main thermochemical surface treatment techniques. From the thermochemical techniques, nitriding principle and types are detailed with a special focus on plasma nitriding principle and properties. Finally, the fourth part is a state of the art about the nitriding of chromium coatings. In this part, we present the Cr-N system and its properties, the mechanism that governs the formation of chromium nitrides, and the properties of the surface of the chromium electroplated layer after gas and plasma nitriding as reported in the literature.

I.2. Types of Steel

Steels are ferrous alloys that are composed mainly of iron. Generally, they can be classified according to the nature and amount of alloying elements into three groups, namely: plain carbon steels, low-alloy steels, and high alloy steels.

I.2.1. Plain carbon steels

Plain carbon steels are solid solutions of iron and a percentage of carbon with a limited concentration of residual impurities like manganese [3]. Generally, the microstructure of a plain carbon steel is formed of ferrite and pearlite phases [4]. The proportion of each phase depends on the carbon amount. The change in phase proportions affects the properties of plain carbon steels, which in turn affects the application filed. This kind of steels is used for a broad range of applications such as in automobile parts, wiring products, sheets and strips [5].

I.2.2. Low-alloy steels

The application domains of steels can be extended by the addition of alloying elements such as chromium, molybdenum and nickel. when the total amount of added elements is under 10 %,

the steel is called low-alloy steel [3]. The alloying elements can improve the mechanical properties of steel in terms of hardness and toughness, especially after heat-treatment, also they can enhance its resistance to degradation under certain surrounding conditions [6]. In general, a low alloy steel contains an amount of molybdenum in the range of 0.5 - 1 % in order to improve the creep strength. In addition, it contains an amount of chromium between 0.5 and 9 % to enhance the resistance against corrosion, rupture and graphitisation. Moreover, a small amount of carbide-forming elements such as vanadium, nobium and titanium is added in order to improve the hardness by precipitation strengthning or for grain refinement [7].

In the heat treatment process of low alloy steels, the austinitising step takes longer time than in carbon steels because of the low dicossiation rate of alloying elements in the austenite phase [8]. After austenitising, other steps can take place according to the heat treatment type. Different heat treatments such as normalising, annealing, quenching and tempering can be performed considering to the effect of treatment on microstructure and the targeted properties. Heat-treated low alloy steels can be used in many applications, like in railway wheels and tracks, gears, crankshafts, and machine parts [3].Generally, low-alloy steels have better mechanical properties than plain carbon steels [6].

I.2.3. High-alloy steels

A high alloy steel contains a total amount of alloying elements that exceeds 10% [6]. Generally, high alloy steels are classified into three categories, Cobalt and molybdenum secondary hardening steels, maraging steels and precipitation hardening stainless steels [8]. Each category of high alloy steels is treated in a way to have the maximum of desirable mechanical properties based on the properties of elements that it contains. In effect, secondary hardening steels must be quenched and tempered to benefit from the high amount of carbide-forming elements (Mo, V, Cr and W) that they contain. The formed and dispersed carbides produce a secondary hardening steel with high strength and toughness properties that make them suitable for high strength structural applications [8]. The second category of high alloy steels corresponds to maraging steels. This type of steel is composed of a very low amount of carbon (maximum of 0.03%), high amount of nickel (17-19%) in addition to a lower amount of cobalt (8–12%), molybdenum (3–5%), titanium (0.2–1.8%) and aluminium (0.1–0.15%) [9]. The maraging steel has a martensitic base microstructure with dispersed precipitates obtained after austinitising, slow rate cooling and aging heat treatment,

which gives it a unique combination of high tensile strength with high resistance to fracture toughness [9]. Because of their unique properties, maraging steels are used usually in aircraft industry. Finally, the third category of high alloy steels consists of stainless steels. They are ferrous alloys that are characterised by a high amount of chromium (at least 11 wt%), which makes them highly resistive to corrosion environments [3].

Stainless steels are classified into three types according to the main phase in their microstructure, namely: ferritic, austenitic and martensitic. The mechanical properties of stainless steels are enhanced by the addition of other alloying elements such as molybdenum, tungsten and vanadium [8]. Based on their properties, stainless steels can be used in a variety of industrial applications, including automotive, aerospace and utensils.

I.3. Metallic Coatings

The surface of a metal is often subjected to different kind of damage that can deteriorate its properties. This damage can be induced by corrosion and wear due to the interaction between the metal and its surrounding environment. Therefore, the surface of a metal is generally coated or treated using surface engineering techniques, which can extend the life cycle of parts made from that metal. Surface engineering techniques can be classified according to their microstructural or compositional effect on the metal surface. Figure I.1 shows a diagram of the classification of surface engineering techniques. In this section, we focus on the techniques used in making compositional modification, especially the coatings that are based on metals.
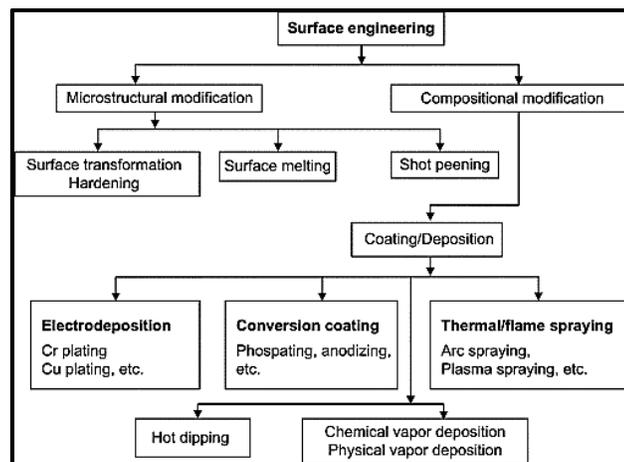
Figure I.1: General classification of surface engineering techniques used in metallurgical industries [10]

I.3.1. Hot dipping

Hot dipping is a technique of metallic coating that consists of immersing the part to be coated in molten coating metal. The hot dipping process starts by degreasing and fluxing the part to be coated, and after immersion during a controlled time, the part is removed from the dipping bath. Within a period of time, the molten coating metal dries and forms a coating layer on the coated part. The properties of the resulting coating depend on surface preparation, molten coating metal composition, dipping bath temperature, dipping duration and substrate material [11]. In practice, the metals that can be deposited by hot dipping are zinc, aluminium, lead and tin [12]. A schematic illustration of the hot dipping process is presented in Figure I.2.
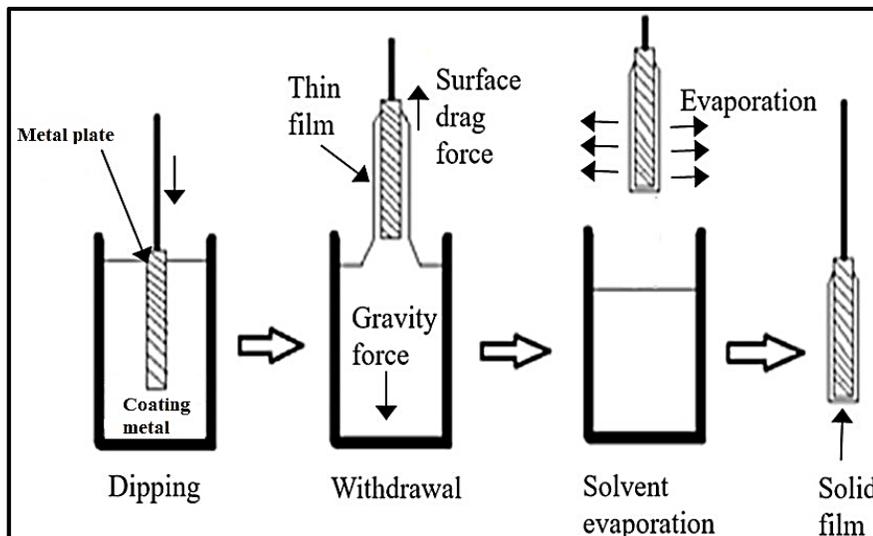
Figure I.2: Schematic illustration of the hot dipping process [13]

I.3.2. Thermal spraying

The principle of thermal spray coating consists of spraying molten or in plastic state metal, which can be form of wire, rod or powder, onto the surface to be coated using a stream of compressed gas. The sprayed metal arrives to the surface in the form of droplets with a high velocity, hence the metal droplets are flattened. The accumulation of flattened metal droplets covers the surface and forms the coating. A schematic illustration of the process is presented in Figure I.3. In order to obtain a good adherence, the surface of the substrate material must be clean and rough. Thermal spray coatings are classified according to the method used in melting or

softening the coating material. Generally, these methods comprise flame, resistance, arc, induction and plasma [11].
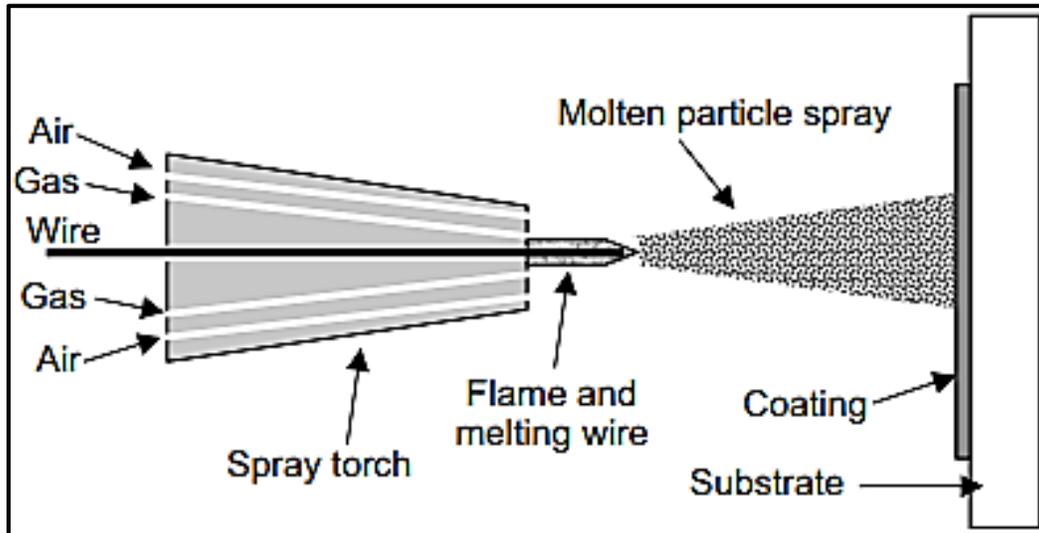
Figure I.3: Schematic illustration of the thermal spraying process [14]

I.3.3. Conversion coating

Conversion coatings are applied to metals in order to prepare their surface to subsequent painting or to protect the surface from corrosion. The conversion process starts when a metal part is immersed in an aqueous solution to induce the oxidation of the surface. In absence of external voltage, the process is driven by the chemical reactions in the immersing bath, thus it is called a chemical conversion. Whereas, when the electricity is passed through the immersed metal part that represents the anode, the process is controlled by the applied external voltage and the chemical reaction in the anode, and in this case, it is called an electrochemical conversion or anodising. Figure I.4 presents a schematic illustration of the anodising process. Because of their wide usage, phosphating and chromating are well-known in the industry sector.
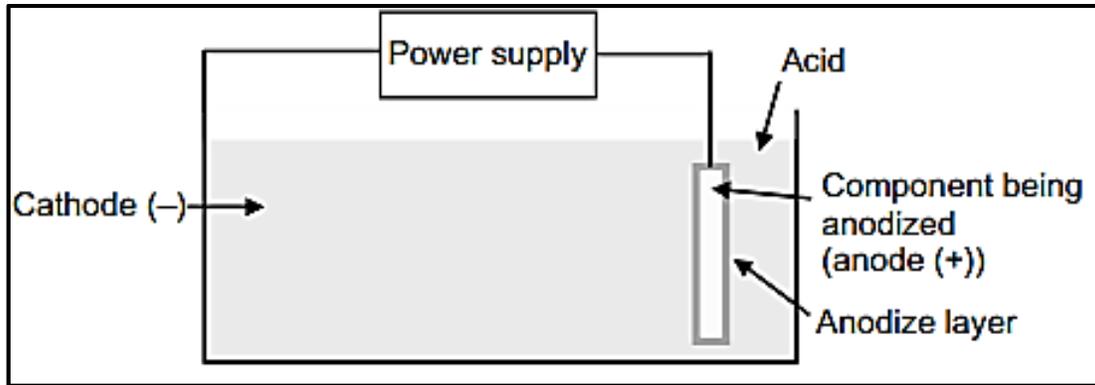
Figure I.4: Schematic illustration of the anodising process [14]

I.3.4. Chemical vapour deposition

Chemical vapour deposition is a coating technique that was introduced in industry in the late of the sixties. Its principle consists of producing a coating from the interaction between reactant gases and heated substrate material in an atmospheric pressure. Though, the resulting coating is usually formed of carbides, nitrides, borides or oxides. An illustration of the chemical vapour deposition process is presented in Figure I.5.
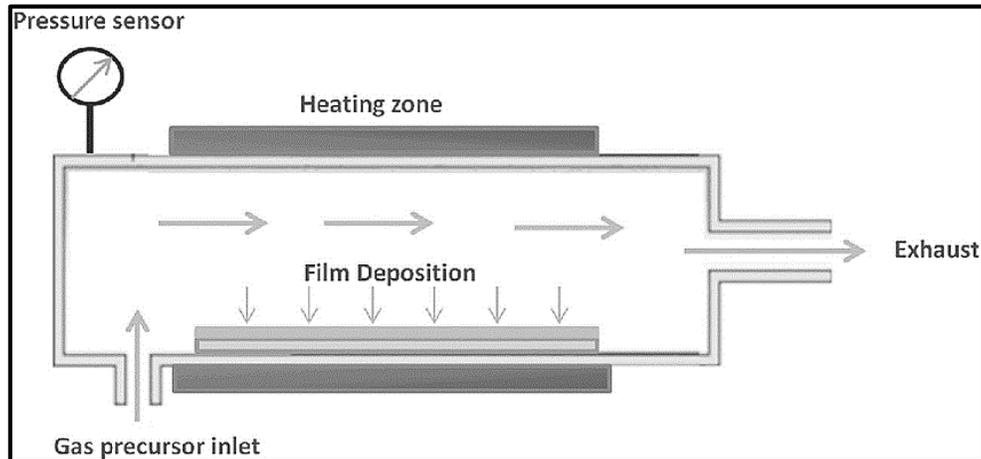
Figure I.5: Schematic illustration of the chemical vapour deposition process [15]

I.3.5. Physical vapour deposition

The process of physical vapour deposition basically describes the deposition of metal atoms or molecules on a substrate material in a vacuum chamber. In cases where nitrogen, methane or oxygen are introduced in the vacuum chamber, a coating composed of nitrides, carbides or oxides is formed. The technique used in obtaining the coating metal atoms determines the physical vapour

deposition type. In effect, when the metal atoms are evaporated from a heated target, the technique is called evaporation. Whereas, when the metal atoms are obtained from the impact between accelerated argon ions and the target, the technique is called sputtering. Finally, when the metal atoms are obtained by evaporation or plasma and they are accelerated toward a biased substrate, the technique is called ion plating. Metals that can be physically vapour deposited include aluminium, copper, titanium, gold, platinum, chrome and nickel [14]. Figure I.6 shows a schematic illustration of the physical vapour deposition process.
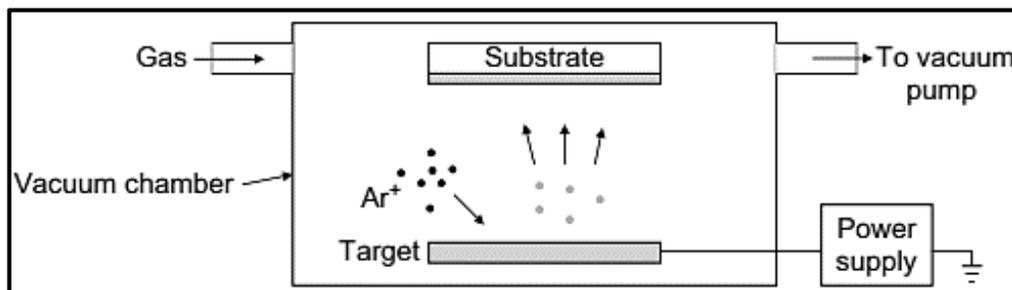
Figure I.6: Schematic illustration of physical vapour deposition process [14]

I.3.6. Metal Electroplating

Metal electroplating is a process in which metal cations migrate from an electrolyte to a target surface, where they are reduced to metal atoms by electrons [16]. The source of the electrons used in the reduction process determines the type of the metal deposition process. when the electrons are from an external source, the process is called an electrolytic deposition [17]. Whereas, in the case of no external source of electrons, the process is called electroless or chemical deposition [17].

I.3.6.1. Electrolytic plating

The technique of metal deposition from an electrolytic solution is based on electrochemistry principles. In the absence of an external voltage source, a metal exposed to an electrolyte oxidises. The general equation that governs the oxidation process is presented in the equation I-1. The produced metal cations are transported to the electrolyte, and the surface of the metal is negatively charged. When the equilibrium is attained, the reaction is stopped.

$$M = M^{n+} + n\acute{e} \hspace{3cm} \text{(I-1)}$$
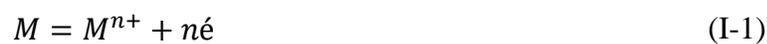
When the metal is connected to a source of electrons, it becomes more negatively charged, and the positively charged ions (cations) of the metal to be deposited are attracted to it. This phenomenon represents the basis of the metal electroplating process. A schematic illustration of the process is presented in Figure I.7.
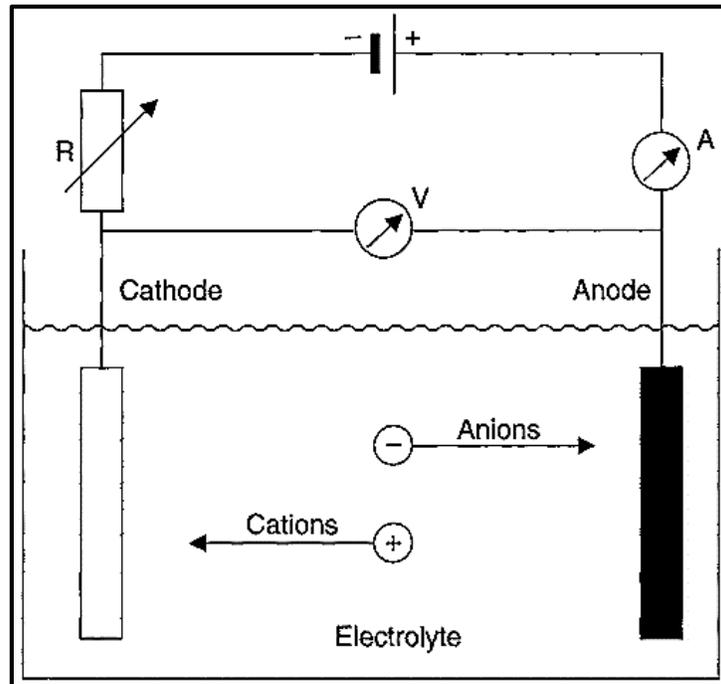
Figure I.7: Schematic illustration of metal electroplating process [17]

Direct, alternative, and pulsed currents can be used as a source of electrons in the deposition process. The current type affects the properties of the deposited layer. Deposition of metals from aqueous solution using direct current represents the conventionally used method. The transport of cations from the solution to the cathode under the passage of direct current is governed by three main phenomena, namely: migration, convection, and diffusion [17]. The potential gradient initiated after circuit closure causes the migration of cations to the cathode and anions to the anode. The movement of ions (cations and anions) is in the order of micrometres per second [17]. The slow movement of ions, because of obstacles composed of molecules of other species in the solution, and viscosity indicate that the contribution of migration in cations transport can be negligible. Another phenomenon that contributes to cations transport is convection, which can be defined as the movement of all the aqueous solution under an external force, or by the difference in density induced by temperature. The movement of ions by convection is negligible near the electrodes, where another phenomenon called diffusion takes place. The region near to cathode

surface is called the diffusion or the Nernestian layer [17]. The transport of cations in this layer is induced by the difference in concentration between the solution and the cathode surface. When metal cations reach the cathode surface, they are discharged and transformed into a metal layer. Figure I.8 shows a schematic illustration of the processes involved during an electrolytic plating.
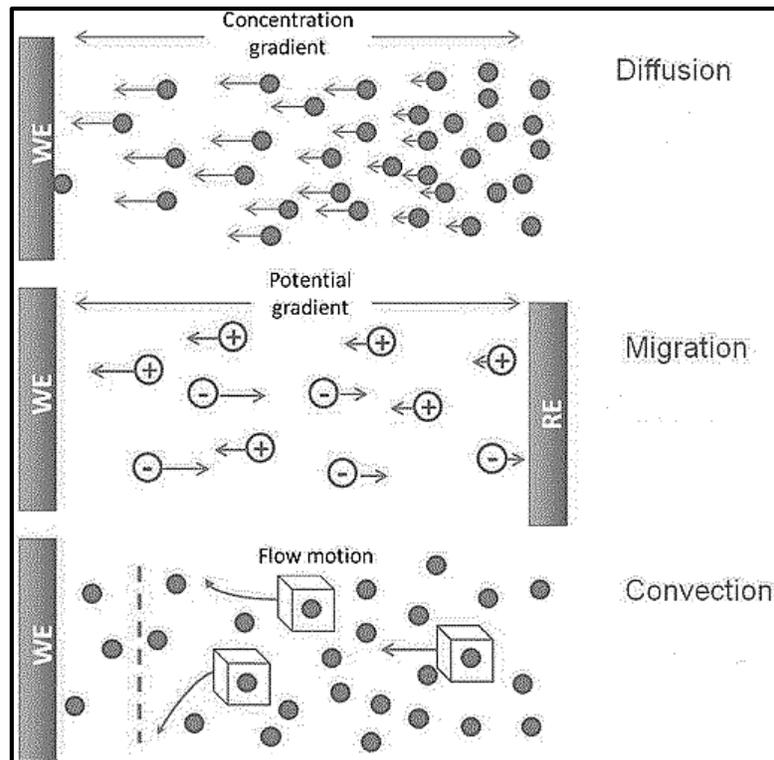
Figure I.8: Schematic illustration of the processes involved during electrolytic plating [18]

After a period of time, the ions of the coating metal in the electrolyte are consumed. The replacement of metal ions in the solution can be done by injecting a metal salt formed by the metal to be deposited or by using a sacrificial anode made by the metal to be deposited. The metals that can be electrodeposited from an aqueous solution are shown inside the bold line in Figure I.9.

Ia	IIa	IIIa	IVa	Va	VIa	VIIa	VIII			Ib	IIb	IIIb	IVb	Vb	VIb	VIIb	O
1 H																1 H	2 He
3 Li	4 Be											5 B	6 C	7 N	8 O	9 F	10 Ne
11 Na	12 Mg											13 Al	14 Si	15 P	16 S	17 Cl	18 Ar
19 K	20 Ca	21 Sc	22 Ti	23 V	24 Cr	25 Mn	26 Fe	27 Co	28 Ni	29 Cu	30 Zn	31 Ga	32 Ge	33 As	34 Se	35 Br	36 Kr
37 Rb	38 Sr	39 Y	40 Zr	41 Nb	42 Mo	43 Tc	44 Ru	45 Rh	46 Pd	47 Ag	48 Cd	49 In	50 Sn	51 Sb	52 Te	53 I	54 Xe
55 Cs	56 Ba	57 La	72 Hf	73 Ta	74 W	75 Re	76 Os	77 Ir	78 Pt	79 Au	80 Hg	81 Tl	82 Pb	83 Bi	84 Po	85 At	86 Rn
87 Fr	88 Ra	89 Ac	104 Ku														

Figure I.9: Metals that can be electrodeposited from an aqueous solution [17]

I.3.6.1.1. Chromium electroplating

Chromium is characterised by shininess good appearance, high resistance to corrosion, and resistance to galling [19]. These properties make it suitable for many decorative and engineering applications. In applications where resistance to wear and corrosion are most needed, the chromium is deposited in thicker thickness than in decorative purposes, and in this case, it is called "hard chromium". The Bath used in the electroplating process of both decorative and hard chromium is generally composed of chromic and sulphuric acids with concentrations in a typical electrolyte of 250-400 g/l and 2.5-4 g/l, respectively, and the typical ratio between the two acids must be CrO_3: SO_4^{2-} 100:1[19]. In the electroplating process, the chromium existed in the form of chromic acid in the electrolyte is transformed into its solid form at the cathode surface [20]. After a period of time, the concentration of chromium in the bath is reduced, so a replenishment process by the addition of chromic acid takes place.

There are many parameters that control the electroplating process other than species concentration, namely: solution acidity, current density, voltage and temperature [20]. The characteristics of electroplated chromium depend on process parameters. For a fixed value of one parameter, there is an optimum range of the others. Generally in decorative deposits, chromium is deposited on an undercoating layer of nickel [20]. The thickness in decorative chromium deposits is generally between 0.25 and 2 micrometres [19]. However, hard chromium deposits are electroplated directly on substrate surface with a thickness up to 0.5 mm, depending on the application [19], [20]. The thickness of chromium affects the stress state in the coated layer. The

increase in thickness leads to an increase in tensile stress which in turn leads to cracks [19]. The density of cracks in the chromium layer determines its resistivity to corrosion because the corrosion is developed generally from the surface cracks. A density range of 30-80 cracks/mm can result an acceptable corrosion resistance [19]. Thick chromium deposits are generally corrosion and wear resistive [21]. They can be used in applications such as in crankshafts, pump shafts, plastic moulds, dies, cams...etc.

I.3.6.2. Electroless plating

The main characteristic of this plating technique is the absence of any external source of electricity. The process of electroless plating takes place in a bath composed mainly of the salt of the metal to be deposited and the reducing species. In effect, the bath composition and the catalytic effect of the substrate surface represent the main factors in the electroless plating process. In the presence of metal salts, reducing species and a catalytic surface, the thickness of the coating resulting from this plating process can evolve continuously. Thus, the electroless plating can also be called autocatalytic plating [22].

I.4. Thermochemical Surface Treatments

Thermochemical surface treatments are the surface engineering techniques that modify the chemical composition of the surface through the addition of chemical elements such as carbon, nitrogen and boron, under the effect of temperature. Their main objective is to improve the hardness, the wear-resistance and the corrosion properties of part surfaces. Thermochemical surface treatment techniques are determined according to the element added to the surface. The most important techniques are: carburising, carbonitriding, nitriding and nitrocarburising [23].

I.4.1. Carburising

Carburising is a thermochemical surface treatment technique. Generally, it is used in case hardening of low carbon steels. The principle of carburising consists of incorporating carbon atoms in the surface of steels. Based on carbon atoms source, the carburising technique can be divided into five methods or types, gas carburising, vacuum carburising, plasma (ion) carburising, salt bath carburising and pack carburising. The process of carburising starts by heating the steel part above the A_3 temperature in the carbon steel phase diagram (Figure I.10) in order to obtain the austenite

phase in the material. After the carburising process, the parts are quenched and heat-treated to keep the properties of the hardened case and to restore the properties of the bulk material, respectively. The carburising technique can produce a case hardened layer with a carbon content between 0.8 and 1 wt% [24].
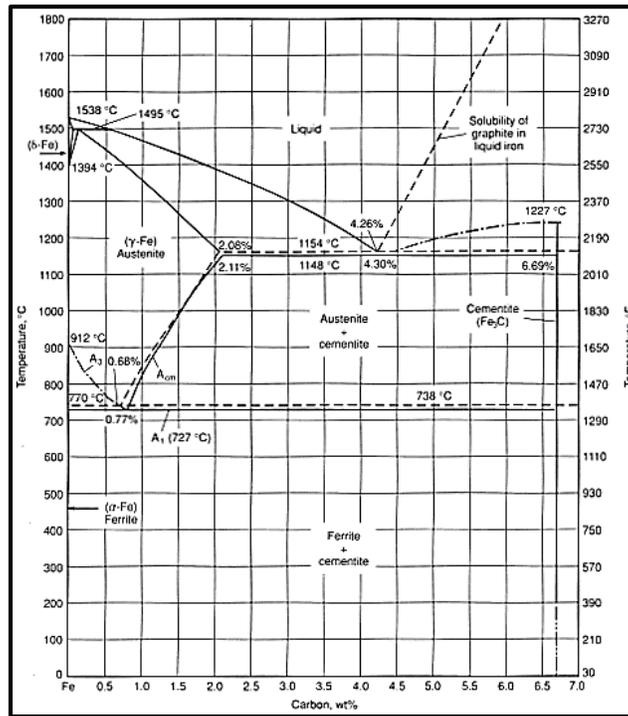
Figure I.10: Iron-carbon phase equilibrium diagram up to 6.67 wt% C [24]

I.4.2. Carbonitriding

Carbonitriding is a thermochemical surface treatment technique that differs from carburising by the addition of ammonia gas to the carbonitriding atmosphere as a source of nitrogen atoms. It is applied on steel parts in order to enhance their mechanical and tribological surface properties by the formation of carbides and nitrides. The process of carbonitriding starts when nitrogen and carbon atoms diffuse into the steel part surface, in the austenite phase, under the effect of temperature. In order to obtain a hardened case composed of martensite and nitrides, carbonitrided parts are subjected to a quenching step after the carbonitriding process. The hardened case obtained by carbonitriding is not thick in comparison to that obtained by carburising, because of the difficulty of carbon diffusion caused by the inhibition effect of nitrogen. Therefore, the case thickness obtained by carbonitriding is usually between 75 and 750 um [24].

I.4.3. Nitriding

I.4.3.1. Principle of the nitriding process

Nitriding is a thermochemical surface treatment process. It was developed at the beginning of the 20th century. The process consists of introducing nascent nitrogen into a metal surface from a nitrogen-rich medium. Depending on medium type, gaseous, liquid, or solid, different nitriding techniques have been developed. However, in the industry sector, the gas, salt bath and ion (plasma) nitriding are the widely used techniques because of their adaptability to mass production. One of the main advantages of nitriding in comparison to the conventional thermochemical surface treatment "carburising" is its ability to maintain nitrided part dimensions, except for a slight change caused by nitrogen diffusion in the metal matrix. Nitriding is applied in different industrial applications such as in the manufacture of aircraft, automotive components, and turbine generation systems.

I.4.3.2. Techniques of nitriding

I.4.3.2.1. Salt bath nitriding

In salt bath nitriding process, a molten salt based on cyanides and cyanates is used as a nitriding medium. The typical commercial bath used for salt bath nitriding is generally composed of sodium and potassium salts, with an operating temperature of about 565°C [24]. The nitriding process in the bath takes place when cyanides are decomposed to form cyanates. This chemical process leads to the liberation of nitrogen atoms, which are subsequently diffuse into the steel surface. This kind of baths can be used in the nitriding of wide range of steels, like tool and low alloy steels. The case depth obtained in salt bath nitriding is generally low, as a consequence, this technique is not suitable for applications that require deep cases [24].

I.4.3.2.2. Gas nitriding

The process of gas nitriding consists of subjecting a metal part, usually made of steel, to a nitrogenous gas at a predefined temperature. Generally, the gas used for this purpose is ammonia, and the temperature used for all steels is ranging between 495 and 565°C. The nitriding process occurs when ammonia is dissociated on the steel surface under temperature into nascent nitrogen and hydrogen (equation I-2). After that, an amount of nascent nitrogen diffuses into the steel

surface and another amount reacts with other nitrogen atoms to form nitrogen gas (equation I-3). Whereas, the nascent hydrogen is subsequently transformed into hydrogen gas (equation I-4) [24]. Figure I.11 shows a schematic illustration of the reactions involved in the gas nitriding process of steels.

$$NH_3 \rightarrow 3H + N \qquad\qquad\qquad\qquad\qquad (I\text{-}2)$$

$$2N \rightarrow N_2 \qquad\qquad\qquad\qquad\qquad (I\text{-}3)$$

$$2H \rightarrow H_2 \qquad\qquad\qquad\qquad\qquad (I\text{-}4)$$
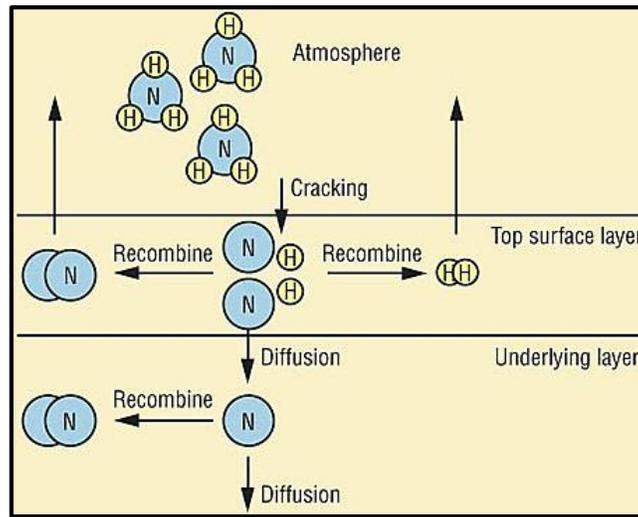
Figure I.11: The reactions in surface and subsurface during gas nitriding process [25]

Gas nitriding of steels results in two different phases, a compound or white phase and a diffusion phase. The compound phase is formed of epsilon (ε) and gamma prime ($\grave{\gamma}$) phases, while the diffusion phase is composed of stable nitrides resulting from the interaction between the diffused nitrogen and nitride-forming elements in the steel like chromium, aluminium, molybdenum...etc. Gas nitriding technique has a variety of industrial applications because of its role in improving mechanical, tribological, and corrosion properties of steels.

I.4.3.2.3. Plasma nitriding

Plasma is defined as the fourth state of matter. It is obtained by ionising gas using heat, radiation, or electrical discharge. It consists of an electron collection, free radicals derived from the ionised gas, ions of both charges (positive and negative), and photons. The glow discharge phenomenon represents the basis of plasma nitriding. This phenomenon takes place when gas is

placed between two electrodes connected to direct current (DC) power supply. In Figure I.12, the curve current-voltage presents the characteristics of glow discharge, where the "abnormal glow discharge" zone is the part used in the plasma nitriding process.
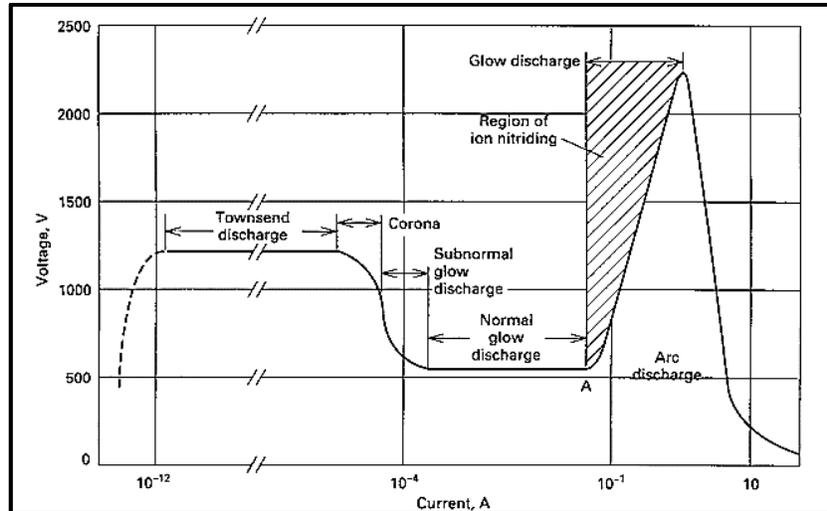
Figure I.12: Characteristics of glow discharge in argon [24]

        Generally, a gas mixture of nitrogen and hydrogen is used in plasma nitriding of steels. In a vacuum and under an electric field,   nitrogen and hydrogen molecules are cracked into ions to form the plasma, and the positive nitrogen ions are attracted to the cathode (the workpiece). Consequently, the accelerated nitrogen ions bombard the workpiece surface under the high voltage used in plasma nitriding. Ion bombardment cleans the surface, heats the workpiece and provides active nitrogen [24]. Figure I.13 shows a schematic illustration of the processes that take place during the ion-surface interaction.   Adsorbed nitrogen atoms are then diffused into the metal surface under the effect of temperature. In addition to temperature, gas composition and pressure, DC voltage and current, and time are the parameters that control the plasma nitriding process. The typical range of each plasma nitriding parameter is presented in Table I.1.
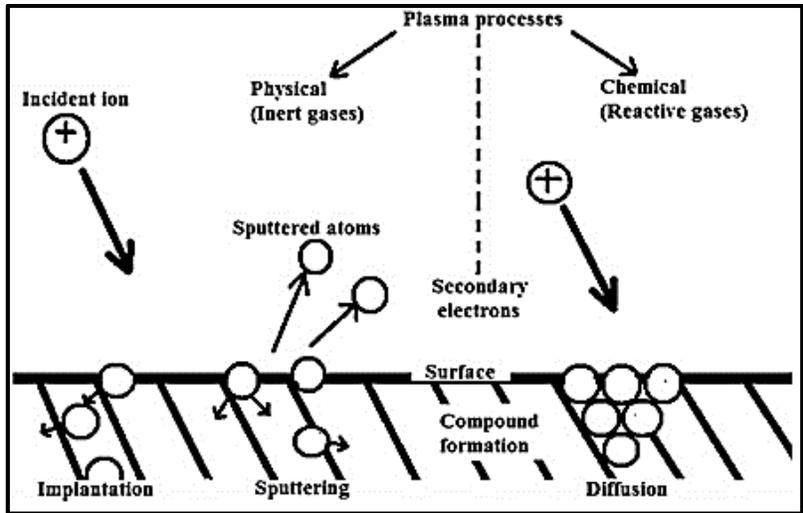
Figure I.13: Schematic illustration of the ion-surface interaction processes [26]

Although the plasma nitriding technique has many advantages such as pollution reduction, high diffusion speed and low energy consumption, it has some problems like the difficulty to obtain reproducible properties of nitrided parts, surface distortions caused by arcing and the overheating of small parts [26], [27].

Table I.1: Typical parameter ranges of plasma nitriding technique [28]

Temperature (°C)	Gas mixture	Gas pressure (Torr)	Voltage (V)	Current density (mA/cm²)	Time
450-650	Hydrogen + Nitrogen	1-10	400-800	0.5-5	Minutes to more than 10 hours

I.5. Nitriding of Chromium Coatings

I.5.1. Chromium-nitrogen system

Chromium is a chemical element that is one of the transition metals. Chromium coatings are characterised by their resistance to corrosion as well as their good appearance, thus they are used for decorative purposes in many applications. In addition to above-mentioned properties, thick chromium coatings are hard and wear-resistant. Insertion of nitrogen atoms in the chromium

crystalline structure creates chromium nitrides. According to the Cr-N equilibrium phase diagram presented in Figure I.14, two chromium nitride phases are created depending on nitrogen content and temperature, namely: CrN and Cr_2N. The equilibrium equations of Cr/Cr_2N and Cr_2N/CrN systems are as the following [29]:

$$2Cr\ (s) + \frac{1}{2} N_2(g) \rightleftharpoons Cr_2N(s) \qquad\qquad\qquad (I\text{-}5)$$

$$Cr_2N(s) + \frac{1}{2} N_2(g) \rightleftharpoons CrN(s) \qquad\qquad\qquad (I\text{-}6)$$
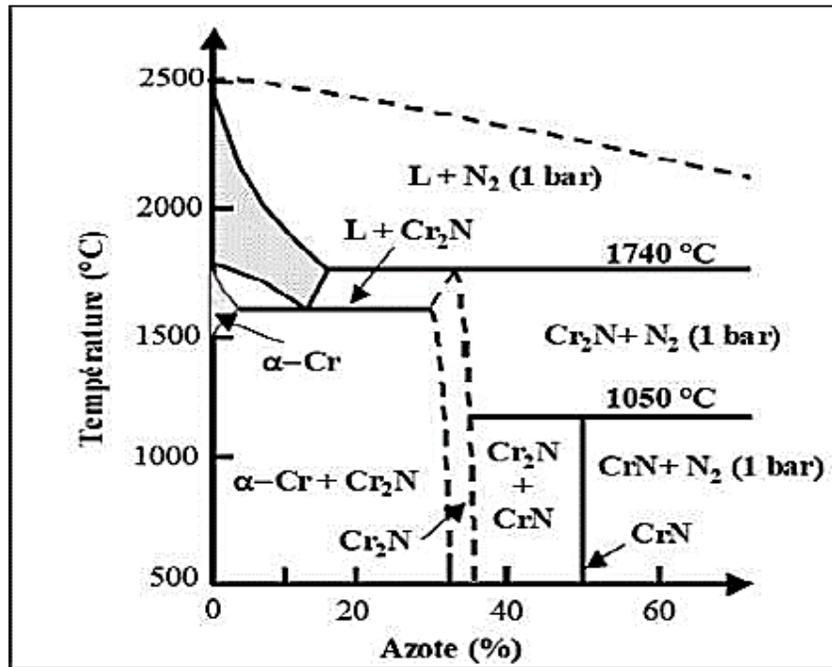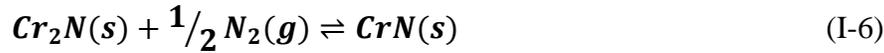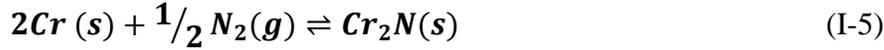
Figure I.14: Phase diagram of Cr-N system in function of nitrogen percentage [30]

CrN has a face-centred cubic structure, and it is formed between 49.5 and 50 at. % of nitrogen. Whereas, Cr_2N has a hexagonal crystalline structure, and it is in turn formed between 30 and 33.3 at. % of nitrogen. This observation indicates that the stability domain of CrN is very narrow in comparison to Cr_2N. Also, it is noted that a biphasic domain formed of CrN and Cr_2N is formed between the stability domains of both nitrides. A number of physical and mechanical properties of chromium and both chromium nitrides is presented in the Table I.2.

Table I.2: Physical and mechanical properties of chromium nitrides [31], [32]

Property	Cr	β-Cr$_2$N	CrN
Crystal structure	bcc	Hexagonal	fcc
Density (g.cm^{-3})	7.14	6.54	6.18
Linear expansion coefficient (10^{-6} °C^{-1})	6.6	9.41 (20-1100 °C)	2.3 (20-800 °C) 7.5 (850 – 1040 °C)
Decomposition temperature (°C)		1500 – 1650	1083-1500
Microhardness (HV$_{0.05}$)	800 - 1000	1600	1100

The comparison of the hardness of chromium with both chromium nitrides indicates that although Cr is denser, its hardness is the lowest. It is noted also that the highest hardness value corresponds to Cr$_2$N phase. This high hardness is due to the covalent bonds in hexagonal chromium nitride (Cr$_2$N) [33]. In addition to the intrinsic property of compounds that form the coating, stress state and microstructure contribute also to its hardness [34]. The mechanical and tribological properties of a chromium nitride coating depend on the depositing technique. Researchers have studied the chromium nitride layer deposited by different surface coating technologies. The techniques used in the deposition of chromium nitride films are often based on physical vapour deposition (PVD) and chemical vapour deposition (CVD) technologies. However, PVD based techniques such as magnetron sputtering [35], [36] and cathodic arc evaporation [37], [38], are among the most used techniques. These surface engineering techniques can produce chromium nitride films in a one-step process. Researchers have also investigated the possibility to produce chromium nitride films in more than one step process using duplex surface engineering technology, as in the case of the combination of a chromium coating and nitriding.

I.5.2. Mechanisms of chromium nitrides formation

Nitriding is a thermochemical process because it depends mainly on temperature, time, and gas concentration. The nitriding of chromium and the formation of chromium nitrides are controlled by thermodynamic conditions. The nitriding of chromium process starts when nascent nitrogen that comes from the interaction between chromium and nitriding gas at the chromium surface diffuses through the interstitial vacancies of the chromium lattice. In regions where the

concentration of nitrogen reaches 30 at. %, Cr_2N phase begins to form according to the equation (I-5). Then, as the nitriding process continues, Cr_2N transforms to CrN in regions that contain 50 at% of nitrogen [39]. This sequence of chromium nitride formation has been reported by many researchers [40]–[43]. The sequence of chromium nitrides formation is related to diffusion behaviour of nitrogen into chromium metal and its nitrides. The formation of CrN and Cr_2N phases on the chromium surface during nitriding limits the diffusion of nitrogen into the chromium, resulting in reduced film thickness growth. The effect of chromium nitrides on diffusion kinetics is due to their higher density compared to chromium [44]. Table I.3 presents the nitrogen diffusion constants (D_0) and the activation energies (Q) of nitrogen diffusion into chromium and its nitrides (CrN and Cr_2N) reported by a number of researchers in the literature.

Table I.3: Comparison of diffusion constants and activation energy of nitrogen into chromium

Phase	Process	Diffusion constant, D_0 (m^2/s)	Activation energy (kJ/mol-K)	Reference
Cr	Gas nitriding (NH_3-Ar)	7.7×10^{-4}	239.6	[43]
	Gas nitriding (N_2)	23.9×10^{-4}	269.1	[40]
	Plasma nitriding (N_2+H_2)	0.00041×10^{-4}	131.4	[45]
Cr_2N	Gas nitriding (N_2)	3.51×10^{-4}	258.3	[40]
CrN	Gas nitriding (N_2)	0.018×10^{-4}	281.8	[40]

It is noted from Table I.3 that the activation energy of nitrogen diffusion into chromium during plasma nitriding is the lowest. This low activation energy is a result of the high kinetic of the plasma nitriding process as compared to gas nitriding [45].

The properties of the chromium nitride film depend on the techniques used for chromium deposition as well as those used for nitriding.

I.5.3. Gas nitriding of chromium coatings

Many researchers have studied the process of gas nitriding of chromium as well as the chromium nitride film obtained from this process. Taguchi and Kurihara have reported that the formation of chromium nitrides starts at 600°C [41]. Their finding was based on the mass gain of chromium powder during gas nitriding in pure nitrogen, which was recorded at different nitriding temperatures, as shown in Figure I.15.
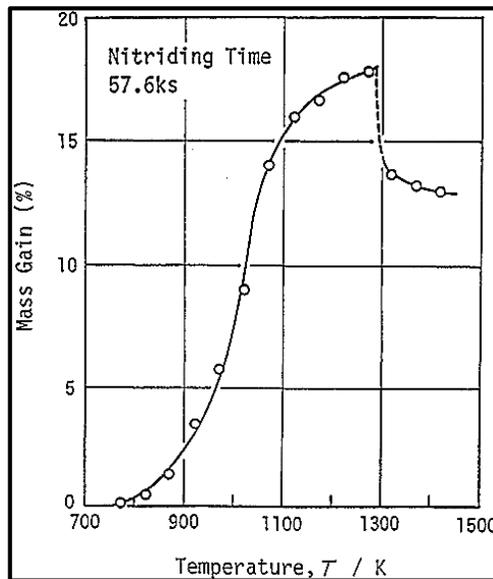
Figure I.15: Effect of nitriding temperature on gain mass [41]

In the case where NH_3 gas is used as a nitriding atmosphere, the cracking temperature of NH_3 gas on the chromium surface determines the starting point of the nitriding process. This temperature is about 700°C, and it depends on the catalytic effect of the nitrided material in addition to the level of surface finish [46]. Generally, The surface of gas nitrided chromium is rough, and it has a grey dark colour as reported by many researchers [39], [43]. In addition to these surface characteristics, the surface contains a number of micro-cracks in the case of gas nitriding of electroplated chromium [46], [47]. Figure I.16 shows SEM micrograph of chromium electroplated steel after gas nitriding at 900°C.
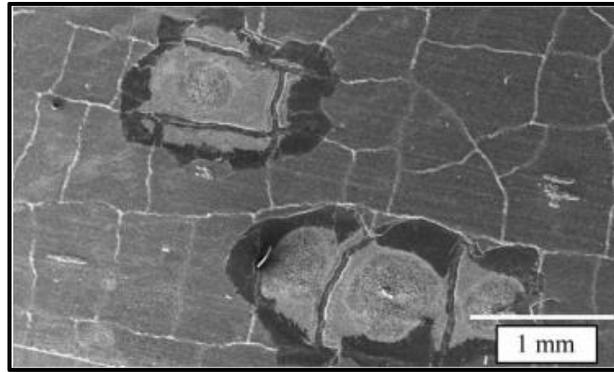
Figure I.16: Micrograph of chromium electroplated steel after gas nitriding at 900°C [46]

The cross-section view of samples subjected to chromium coating and gas nitriding shows a layered microstructure. This microstructure is composed mainly of a mixture of CrN and Cr_2N, Cr_2N, and Cr(N) layers from the upper surface to the pure chromium layer, respectively[39], [46]. In the case of chromium electroplated and gas nitrided steel, another layer of chromium carbides grows from the interface between the steel surface and the chromium coating [43], as shown in Figure I.17. The growth of the above-mentioned layers depends basically on nitriding time and temperature, as the increase in one of them makes the layers more distinguished [39], [46]. Taguchi and Kurihara have reported that the nitriding of chromium starts at 600°C and until 700°C, the surface is composed of Cr and Cr_2N [41]. After that, between 700-1000°C, the surface transformes into a mixture of CrN and Cr_2N. Then, above 1100°C, the CrN decomposes to Cr_2N. The thickness of the nitrided film depends on nitriding temperature and time. for instance, at a nitriding temperature of 800°C, the thickness goes from 4.5 um after 1 hour of nitriding to 43.1 um after 142 hour [39].
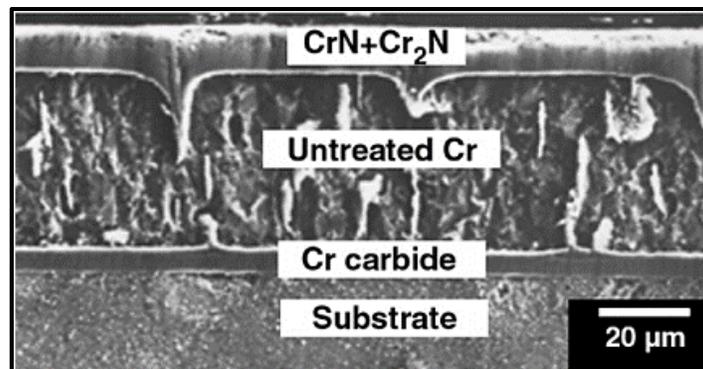
Figure I.17: Cross-section SEM micrograph of chromium electroplated and gas nitrided steel at 850°C for 6h [43]

The layered microstructure reflects the cross-section hardness profile reported by many researchers [39], [43], [46]. The peak hardness is often recorded near the surface due to the existence of chromium nitrides. Then, the hardness decreases gradually to its lowest value at the annealed chromium layer. However, when the substrate sample is made of steel, the hardness increases at the interface between steel and chromium coating due to the existence of hard chromium carbides. The hardness of gas nitrided chromium coating can reach a value of about 19 GPa [43], depending on gas nitriding parameters and the chromium nitrides existed in the nitrided surface. The hardness of the chromium nitride film can also be affected by the state of stress in the film. The main sources of stress can be the residual stress that generally accompanies the deposition of chromium, the compressive stress induced at high nitriding temperatures during the formation of chromium nitrides due to the large unit cell parameters of chromium nitrides in comparison to that of chromium metal [39], [48], and the stress caused by the difference in coefficient of thermal expansion between the chromium coating and steel. The residual stress decreases with the increase of nitriding time and temperature [48]. Gas nitriding of a chromium coating deteriorates the wear resistance of the chromium coating, especially at high nitriding temperature [48]. Basu et al. have reported that the cause of this deterioration is the high surface roughness, in addition to the brittleness of the film caused by the increase in Cr_2N phase amount[48].

I.5.4. Plasma nitriding of chromium coatings

In order to avoid the drawbacks accompanying the gas nitriding of chromium coatings, and to benefit from the fast kinetics of plasma nitriding, many researchers have used plasma nitriding to make chromium nitride layer on chromium coatings. In effect, diffusion of nitrogen atoms into chromium during plasma nitriding is slightly different compared to gas nitriding as proposed by Dasgupta et al. [49]. In its simplest form, the process of producing nitrogen atoms is the cracking of N_2 gas molecules, and the way of nitrogen atoms to the core of chromium coating is according to the following steps [49]:

$$e^- + N_2 \rightarrow N + N + e^- \qquad\qquad (I-7)$$

$$e^- + N \rightarrow N^+ + 2e^- \qquad\qquad (I-8)$$

$$Energy_{N^+} \rightarrow Energy_{heat} + Energy_{impulse} \qquad\qquad (I-9)$$

$$Energy_{impulse} \rightarrow Cr(sputter) \qquad\qquad (I-10)$$

$$Cr + N \rightarrow CrN_{adsorbed} \; ; and \; 2Cr + N \rightarrow Cr_2N_{adsorbed} \qquad\qquad \text{(I-11)}$$

$$CrN + CrN \rightarrow Cr_2N + N \; (diffusing \; species) \qquad\qquad \text{(I-12)}$$
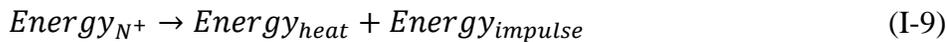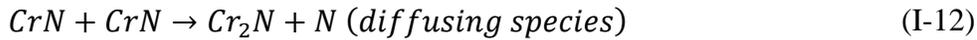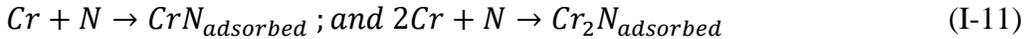
Two main methods lead to nitrogen transport from plasma to chromium surface [49]. In the first method, nitrogen ions are projected directly into the chromium surface under the effect of the electrostatic field between the cathode and the anode. In this case, the positively charged nitrogen ions are attracted to the negatively biased sample that represents the cathode. The second method is by the adsorbed chromium nitrides obtained through the interaction between the sputtered chromium and neutral nitrogen species in the plasma near the chromium coating surface. Upon arrival to chromium surface, nitrogen atoms start diffusion under the effect of temperature. Dasgupta et al. suggest that the diffusion of nitrogen into chromium is indirect [49]. In effect, the process of nitrogen diffusion starts by the formation of metastable chromium nitrides, which are subsequently transform to stable Cr_2N and diffusing nitrogen. Moreover, after the formation of a Cr_2N layer, the kinetics of nitrogen diffusion becomes slow, which delays the growth of the nitrides film.

The products of plasma nitriding of chromium coatings depend on nitriding parameters. In addition to the untransformed chromium, the products can be one of the chromium nitride types (CrN and Cr_2N) or both of them. Many researchers have investigated the chromium nitride layer obtained by plasma nitriding of hard electroplated chromium using different combination of parameters. Table I.4 presents the range of each parameter used in the plasma nitriding of hard electroplated chromium as reported in the literature.

Table I.4: Summary of plasma nitriding parameter ranges from the literature

Temperature (°C)	Time (Hours)	Gas	Gas pressure (mbar)	Substrate biasing voltage (V)
500 -1000	0.5 - 90	- Different N_2 to H_2 ratios - NH_3 - $CH_4 + NH_3$	$3 - 6.67$	450 - 800

Generally, plasma nitriding of hard electroplated chromium results in a compound layer of Cr_2N and CrN with untransformed Cr. However, some researchers have reported that the resulted layer is composed of Cr_2N and untransformed Cr [45], [49], while, another research reported a layer composed mainly of Cr_2N with traces of CrN and unreacted chromium [50]. In fact, at a nitriding temperature of about 600°C, the dominant chromium nitride phase is Cr_2N [44], [45], [51], and by increasing the nitriding temperature to about 700°C, Cr_2N phase transforms to CrN phase, which becomes the dominant phase after an extended nitriding time [51].

Affected by chromium nitrides formation, the surface morphology of the chromium coating changes after plasma nitriding. Sarraf et al. have reported that the surface color of the hard chromium electroplated layer changes to a dark gray, which is characteristic of chromium nitride phases [52]. They have reported also that chromium nitride particles have an irregular shape, and they were distributed randomly at the plasma nitrided surface. In addition, the plasma nitrided chromium surface contained an extensive network of micro-cracks. These micro-cracks disappear usually at high nitriding temperature and a long nitriding time [51]. The chromium layer surface after plasma nitriding has a rough morphology , where the roughness increases with nitriding time [53]. Figure I.18 shows surface morphology of hard chromium electroplated layer after plasma nitriding.
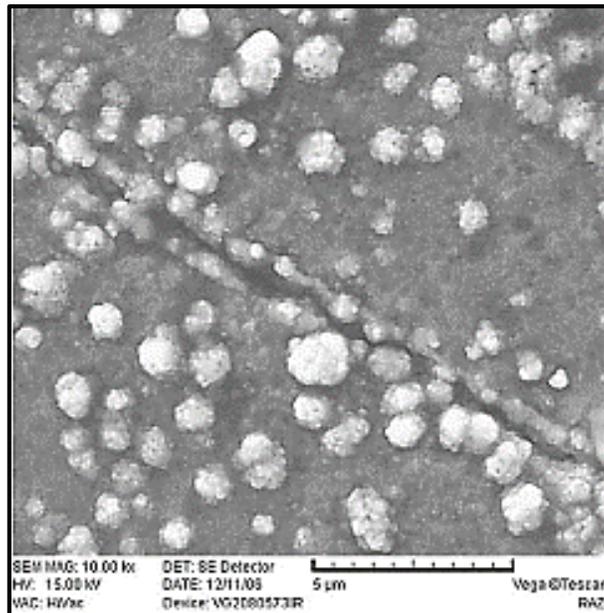
Figure I.18: Surface morphology of a hard electroplated chromium plasma nitrided at 550°C for 5 hours in a nitriding atmosphere composed of 25% hydrogen and 75% nitrogen [54]

In order to better understand the properties of plasma nitrided chromium coatings, the cross-section properties of the duplex treated substrate must be considered. Generally the cross-section has a layered morphology. Wang et al. have reported that plasma nitriding of chromium electroplated steel at about 720°C for 20 hours produces three distinct regions, an outer chromium nitrides, intermediate electroplated chromium, and inner chromium carbides, respectively [55]. The thickness of the outer chromium nitrides layer depends on nitriding temperature and time. For instance, Shen et al. have reported that the thickness of the chromium nitrides layer increases from 1.2 µm to 2.3 µm after plasma nitriding of electroplated chromium at 700°C for 2h and 4 h, respectively [50]. Moreover, the cross-section of plasma nitrided chromium electroplated samples contains micro-cracks with an orientation perpendicular to substrate surface [50]. These micro-cracks can be closed after plasma nitriding at high temperature for long nitriding time [50], [52], [55]. The main mechanism responsible of micro-cracks closure is the volume expansion induced by chromium nitrides [52]. In effect, the volume expansion accompanying the transformation of Cr to Cr_2N and CrN are 250% and 148%, respectively [39]. In addition to volume expansion, the redeposition of matter sputtered from sample and the formation of chromium nitride compounds in micro-cracks walls contribute to micro-cracks closure [56].

The distinct layers appeared in the cross-sectional view of the plasma nitrided chromium electroplated layer lead to different hardness properties due to the composition of each layer. The microhardness is generally high in the chromium nitrides layer, then, it decreases in the electroplated chromium intermediate layer, after that, it increases in the chromium carbides layer. For example, Dasgupta et al. have reported that a microhardness of about 900 HV is obtained near the surface of a chromium electroplated 316 stainless steel after plasma nitriding at 500 °C for 50 hours, under a load of 100g [49]. The hardness then decreases gradually to about 400 HV in the chromium electroplated layer, after that, it decreases again in the 316 stainless steel to about 200 HV.

The wear and friction resistance of the duplex layer obtained by chromium electroplating and plasma nitriding is related to its mechanical properties, especially, the hardness and the elastic modulus. The duplex layer is usually friction-resistant because of the existence of chromium nitrides in the outer layer [49], [57]. On the other hand, chromium nitrides can have a beneficial or deleterious effect on wear resistance of the plasma nitrided and chromium electroplated layer.

Dasgupta et al. have reported that the samples subjected to chromium electroplating and plasma nitriding at 500°C for 50 hours are resistant to abrasive wear due to the outer Cr_2N layer [49]. In contrast, Soltanieh et al. have reported that the chromium nitrides layer obtained after hard chromium electroplating and plasma nitriding either at 500 °C for 5 and 10 hours, or at 550 °C for 5 and 10 hours, is less resistant to wear due to the brittleness and low adhesive properties of the outer layer formed of chromium and iron nitrides [58].

I.6. Conclusion

In this chapter, we have presented an overview of steel types, metal coating techniques, thermochemical surface treatment techniques and a state of the art concerning the nitriding of chromium coatings, in particular the gas and plasma nitriding of electroplated chromium. Based on the state of the art, we have reported that many researchers have studied the layer obtained by plasma nitriding of hard electroplated chromium. In their research, they have used N_2 and H_2 mixture, NH_3 and NH_3+CH_4 as nitriding atmospheres for the plasma nitriding process. In addition, they have studied the surface properties resulting from the combination of chromium electroplating and plasma nitriding in the mentioned nitriding atmospheres. However, we have noted that the surface properties of the duplex layer obtained by chromium electroplating and plasma nitriding in a pure nitrogen atmosphere as well as the effect of the nitriding gas pressure have been less studied. In the next chapter, we present the experimental procedures used to perform this duplex treatment as well as the techniques used to characterise the resulting duplex layer.

EXPERIMENTAL TECHNIQUES

II. EXPERIMENTAL TECHNIQUES

II.1. Introduction

In this chapter, we present the substrate material, the experimental techniques and the characterisation methods used in our work. Firstly, the chemical composition of the substrate material is presented as well as its main characteristics. Then, we present the experimental methodology used in our work by describing each working step and the experimental equipment used, from sample preparation to plasma nitriding of the chromium electroplated samples. Finally, we present the characterisation and testing methods used to obtain the properties of the resulting surface layer.

II.2. Substrate Material

In this work, an industrial steel grade 35NCD6 (AISI 4340 steel) is used as substrate material. Its chemical composition is given in Table II.1.

Table II.1: Chemical composition of the 35NCD6 steel substrate

%C	SI	Mn	P	S	Cr	Mo	Ni
0.35	0.4	0.7	0.025	0.04	1.5	0.3	0.3

The 35NCD6 is a low alloy steel that contains a medium concentration of carbon as well as chromium, nickel, molybdenum, manganese and silicon as alloying elements. It is used in general construction applications such as in transmission shafts, crankshafts, gears…etc, because of its fatigue resistance property. In our work, this steel was chosen because of its availability and the possibility of improving its mechanical and tribological surface properties for applications that require wear resistance.

II.3. Experimental Methodology

Figure II.1 shows the flow chart of the experimental work sequence.
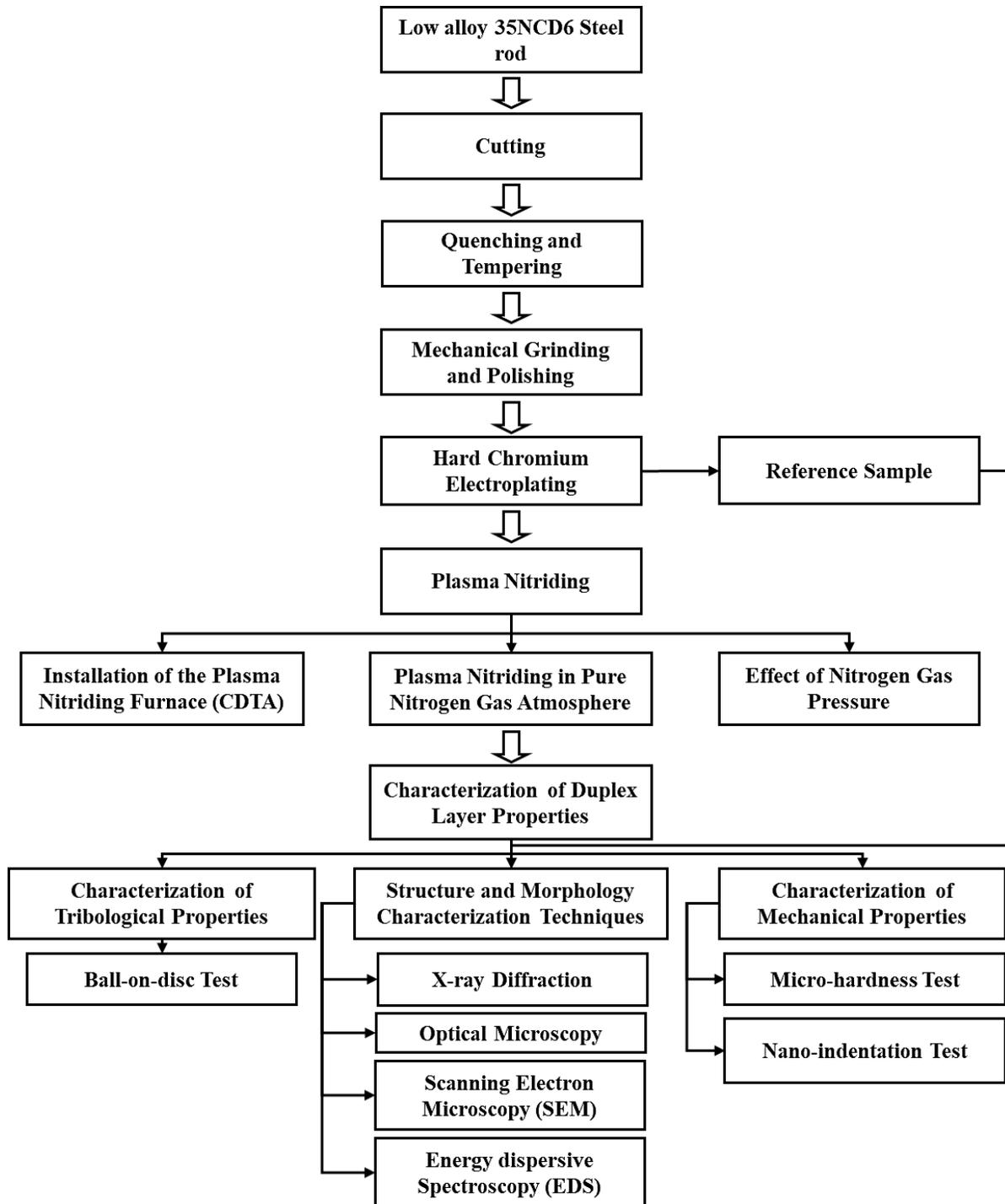
Figure II.1: Flowchart of the experimental work methodology

II.4. Preparation of Samples

The samples used in our work were obtained by cutting a 35NCD6 steel rod into disc-shaped pieces with a diameter of about 10 mm and a thickness of about 7 mm. Then, the 35NCD6 steel samples were quenched and tempered to increase their bulk hardness and to prepare them for chromium electroplating. The parameters used in the quenching and tempering processes are shown in Table II.2.

Table II.2: Quenching and tempering parameters

Treatment	Temperature (°C)	Time (min)	Medium
Austenitising	850	15	Furnace
Quenching	/	/	Oil
Tempering	180	60	Furnace

After quenching and tempering, the samples were mechanically ground up to 1200 grit SiC paper and then polished with Al_2O_3 powder.

II.5. Hard Chromium Electroplating

The quenched and tempered 35NCD6 steel samples were subjected to hard chromium electroplating in an industrial electroplating bath, which represents the first step of duplex surface treatment. The characteristics of the electroplating bath and the operating parameters are summarised in Table II.3.

Table II.3: Characteristics and operating parameters of the industrial electroplating bath

Cro_3	**1.5-1.8 g/l**
H_2So_4	**1.2-1.8 g/l**
Bath Temperature	**57±2°C**
Current Density	**40-50 A/dm^2**
Electroplating rate	**0.01mm /10-15min**

The thickness of the hard chromium electroplated layer was between 25 and 50 µm.

Although the hard chromium electroplated layer has many advantages in terms of hardness, wear resistance and corrosion resistance, it has many disadvantages such as surface micro-cracks and high internal residual stresses, which can deteriorate its good properties, especially at high loads and temperatures. Thus, the hard chromium electroplated layer can be post-treated to improve its surface properties.

II.6. Plasma Nitriding

The second step of the duplex surface treatment consists of plasma nitriding of the hard chromium electroplated layer. The plasma nitriding was performed in a laboratory-made DC plasma nitriding furnace during my internship at the Centre for Development of Advanced Technologies (CDTA) in Algiers, Algeria.

The plasma nitriding furnace consists of a cylindrical vacuum chamber, pumping system, heating system, DC suppliers, pressure and temperature controllers and a sample holder. Figure II.2 shows the laboratory-made DC plasma nitriding furnace used in our experimental work. A description of each part of the furnace is presented in the following paragraphs.
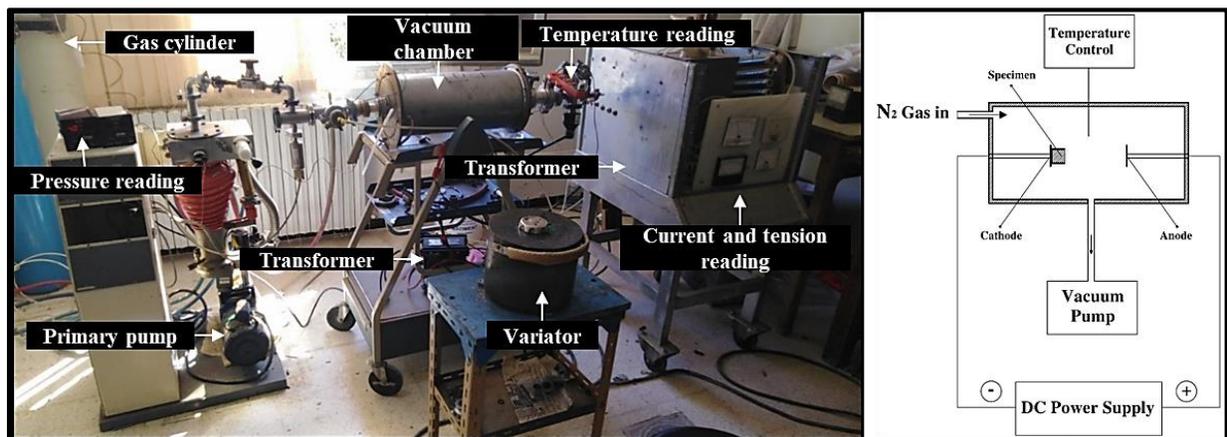
Figure II.2: The laboratory-made DC plasma nitriding furnace at the Centre for development of advanced technologies (CDTA), Algiers, Algeria

II.6.1. The plasma nitriding chamber

The plasma nitriding chamber consists of a cylindrical refractory tube and a quartz tube mounted in a coaxial configuration to maintain anode and cathode positions. The refractory tube is

inserted into a cylindrical stainless steel cover to facilitate the installation of the other furnace components.

II.6.2. Vacuum production

Generally, plasma nitriding is performed under a relatively high gas pressure compared to other PVD techniques. However, the plasma nitriding chamber must have an acceptable vacuum to reduce the amount of oxygen during the process. In order to produce the vacuum required for plasma nitriding, a primary vacuum pump (Alcatel) with a capacity of 120 m^3/h was connected to the plasma nitriding chamber by a sealed piping system. For pressure reading, a primary manometer was installed and connected to a pressure reading box.

II.6.3. DC power suppliers

We used two DC suppliers for plasma and heat generation. Each DC supplier was equipped with a variator to control the power output and a transformer to change the AC current to DC current.

II.6.4. Heating system

Plasma nitriding requires an external heat source in addition to the heat induced by ion bombardment. In our experimental work, the heat was generated by connecting a resistance wire surrounding the plasma nitriding chamber with a DC power supplier. The plasma nitriding temperature was controlled by using the variator to provide the appropriate voltage to the resistance wire and a K-type thermocouple introduced into the plasma nitriding chamber.

II.6.5. Plasma generation

Plasma was produced by connecting the sample holder (cathode) and a stainless steel cylinder (anode) to a DC supplier in the presence of nitriding gas. The bias voltage supplied to the cathode was controlled by a variator, and the reading of the plasma nitriding voltage and current was performed by a panel connected to the transformer.

II.6.6. Pressure control

To control the pressure in the plasma nitriding chamber, a gas flow valve was connected to the nitrogen gas cylinder on one side and to the plasma nitriding chamber on the other side to adjust the injected gas during the nitriding process.

II.7. Plasma Nitriding Procedure of the Hard Chromium Electroplated Layer

At the beginning, the hard chromium electroplated samples were cleaned up using ethanol, then they were placed in the sample holder, which is considered as a cathode at the same time. After that, the chamber was evacuated until a primary vacuum was obtained, and it was heated up to about 600°C using an electrical heating system. Once the working temperature was reached, nitrogen gas was injected in the chamber and the pressure in the plasma nitriding chamber was set to the working gas pressure. The plasma nitriding process was started when the cathode was negatively biased at 600 V. After 90 min, the nitriding process was completed and the samples were cooled to ambient temperature in the vacuum chamber. Figure II.3 shows the plasma luminescence during the plasma nitriding process.
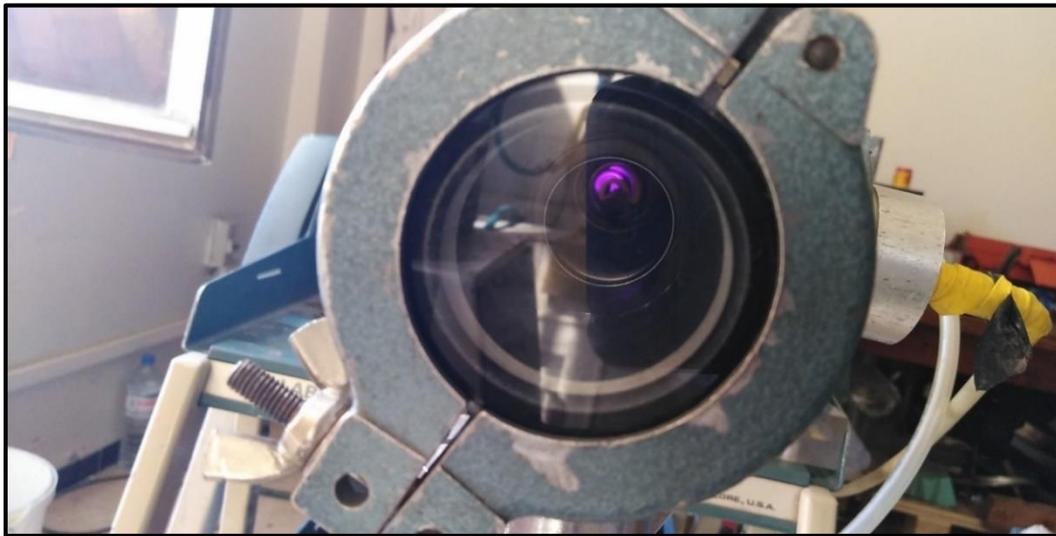
Figure II.3: Plasma luminescence during plasma nitriding

II.8. Characterisation Techniques

II.8.1. Structure and morphology characterisation techniques

II.8.1.1. X-ray diffraction

The X-ray diffraction technique is one of the basic techniques for the characterisation of coating surfaces. It is mainly used to determine the crystalline phases present in the coating layer. The working principle of the X-ray diffraction technique is based on the interference phenomenon that occurs when a polycrystalline material is subjected to a monochromatic X-ray beam. The interaction between the incident X-ray beam and the crystalline planes of the material can result in a constructive or destructive reflection. To obtain a constructive reflection, essential for the characterisation of phases, Bragg's law must be respected:

$$n\lambda = 2d_{hkl} \sin\theta \qquad\qquad\qquad \text{(II-1)}$$

Where n is the diffraction order, λ is the wavelength of the incident X-ray beam source, d is the diffraction interplanar distance and θ is the diffraction angle. A schematic illustration of Bragg's condition is presented in Figure II.4.
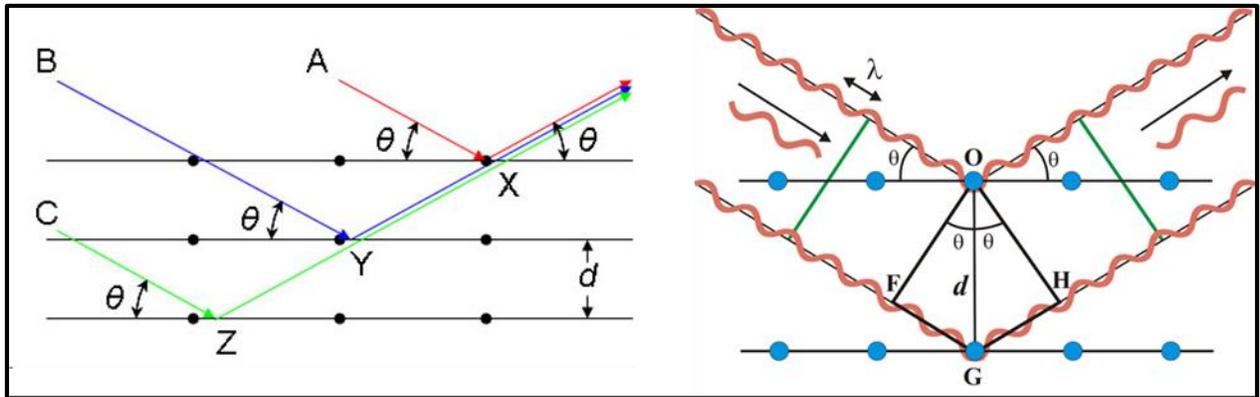
Figure II.4: Schematic illustration of Bragg's condition [59], [60]

In our experimental work, the X-ray diffraction analysis was performed by a PANalytical X'Pert PRO diffractometer (Figure II.5) using monochromatic $CuK\alpha$ radiation ($\lambda = 1.54056$ Å) with an accelerating voltage of 45 kV and a current of 40 mA in Bragg-Brentano mode (θ - 2θ).

Figure II.5: PANalytical X'Pert PRO diffractometer ("Laboratoire des Sciences et de Génie des Matériaux", University Of Science And Technology Houari Boumediene, Algiers, Algeria)

II.8.1.1.1. Estimation of the average crystallite size

A lot of crystallographic information can be derived from the X-ray diffraction pattern of a coating layer, such as lattice parameters, phase composition, crystallographic orientations, average crystallite size....etc. One of the important characteristics of a coating layer is the average crystallite size of its constituent phases which can be estimated based on Scherrer equation as follows:

$$D = \frac{K\lambda}{\beta cos\theta} \qquad\qquad \text{(II-2)}$$

Where:

- D is the average crystallite size;
- K is a constant that depends on the shape of the crystallites, but it has a typical value of about 0.9;
- λ is the X-ray wavelength in nm;
- β is the line broadening at half maximum intensity (FWHM), without the instrument-induced line broadening, in radians. A schematic illustration of the FWHM is shown in Figure II.6;
- Ѳ is the Bragg angle in radians.
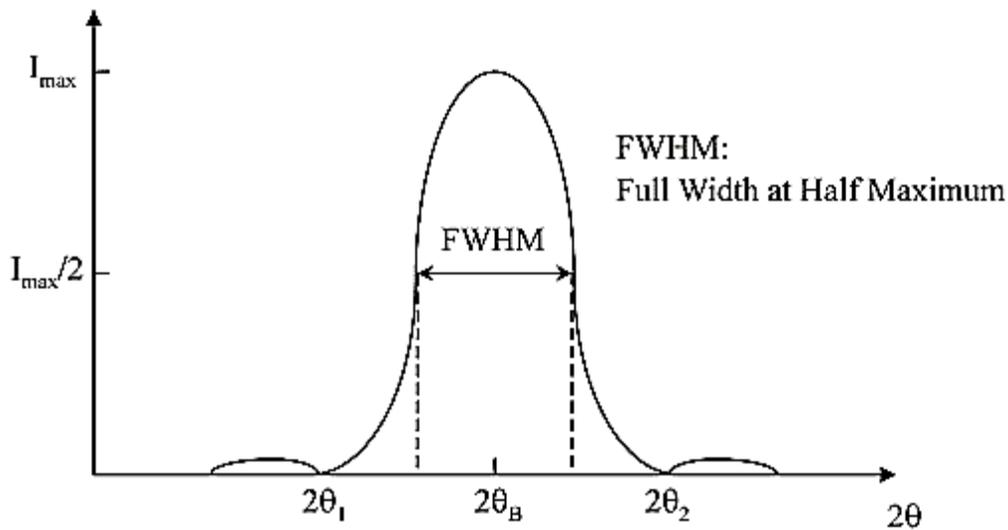
Figure II.6: Definition of the full width at half maximum [61]

II.8.1.2. Optical Microscope (OM) observation

An optical microscope (Type: Optika) equipped with an Optika 4083.11 LT camera (Figure II.6) was used for cross-sectional examination of the samples and examination of the wear tracks after the ball-on-disk test. Prior to the cross-sectional examination, the samples were mechanically ground up to 2000 grit SiC paper and then polished with Al_2O_3 powder. After that, the samples were etched with Nital ($HNO_3 + C_2H_6O$) or Aqua regia (HNO_3+HCl) diluted with ethanol (C_2H_6O) solutions.

Figure II.7: Optical microscope ("Laboratoire de Génie énergétique et matériaux (LGEM)", University of Mohamed Khider, Biskra, Algeria)

II.8.1.3. Scanning Electron Microscope (SEM) observation

The scanning electron microscope is a predominant technique in the characterisation of coating surfaces. It is based on the phenomenon of electron-material interaction. Indeed, the response of a material subjected to an electron beam can take different forms depending on the volume depth, as shown in Figure II.8. In the present study, we are interested in the response recorded by secondary electrons as it reveals the morphology of the surface layer and in the response recorded by X-ray photons that indicates the chemical composition of the surface layer.
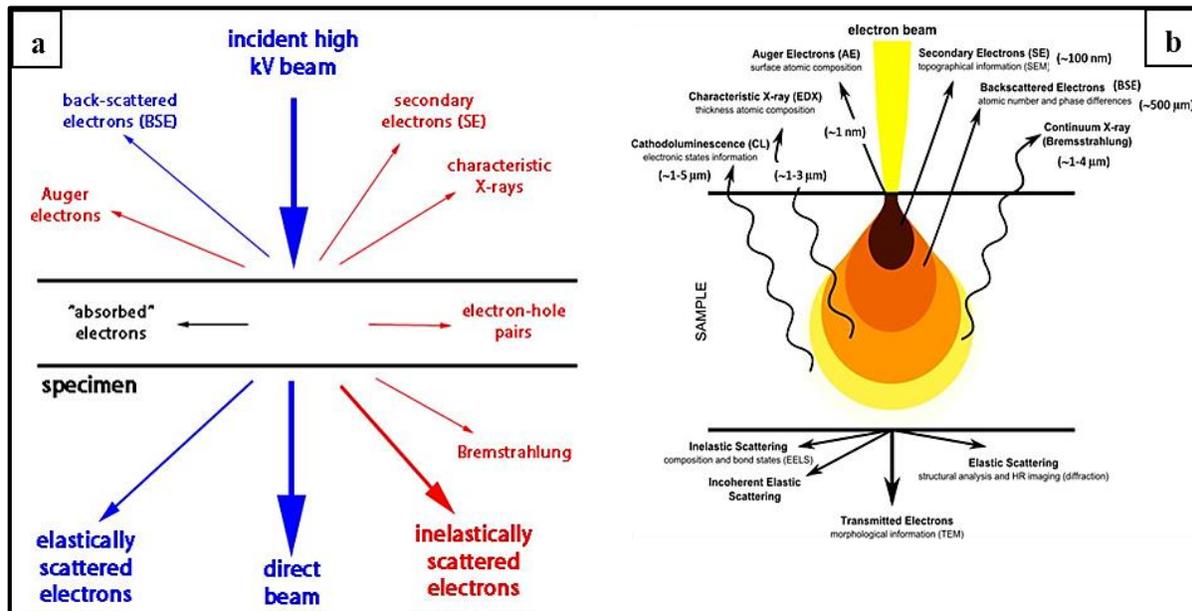
Figure II.8: a) Material response from the electrons – material interaction b) Electrons – material interaction zones [62], [63]

The scanning electron microscope consists mainly of an electron beam generating column and an analysis chamber. First, an electron beam is generated by an electron source. Then the beam is condensed by a series of electromagnetic lenses. Then, it is directed towards the surface of the target sample by means of lenses and scanning coils. As mentioned above, the interaction between the electron beam and the sample surface gives rise to different reflection patterns, each with a special detector depending on its nature. For example, secondary electrons are obtained after the ionisation of atoms near the outer surface and, due to their low energy, they only give information about the surface morphology. SEMs can have a magnification of between 10 and 100 000 [64]. A schematic illustration of the SEM operating principle is shown in Figure II.9.
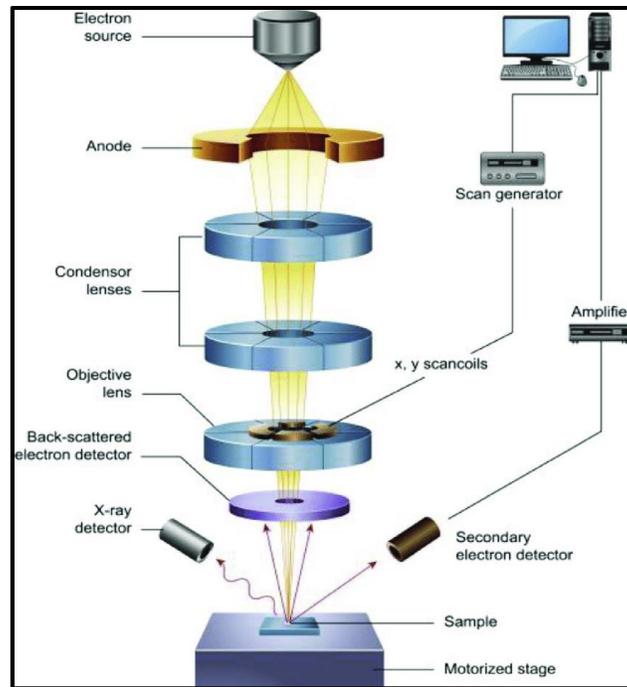
Figure II.9: Schematic illustration of SEM operating principle [65]

In the current work, two SEMs were used:

- JEOL JSM- 6360LV at the Centre for Development of Advanced Technologies (CDTA), Algiers, Algeria.

- ZEISS equipped with an Energy Dispersive Spectroscopy (EDS) section at the Research Centre in Industrial Technologies (CRTI), Algiers, Algeria.

II.8.1.3.1. Crack density measurements

The density of micro-cracks on the surface of the hard chromium electroplated layer before and after plasma nitriding was determined by analysis of representative optical and SEM images using a technique developed by Nascimento and Voorwald [66]. In this technique, horizontal lines were superimposed on the images, and the points of intersection between the micro-cracks and the horizontal lines were counted using ImageJ software. The density of the micro-cracks was then calculated as follows [66]:

$$Micro - cracks\ density = \frac{N_i}{L_t}$$ (II-3)

Where:

- N_i is the total number of line intersections with the micro-crack network;

- L_t is the total length of the horizontal lines.

The same procedure was followed with all samples maintaining a constant magnification. Figure II.10 shows an optical micrograph of the surface of the hard chromium electroplated layer with the horizontal lines and intersection points.
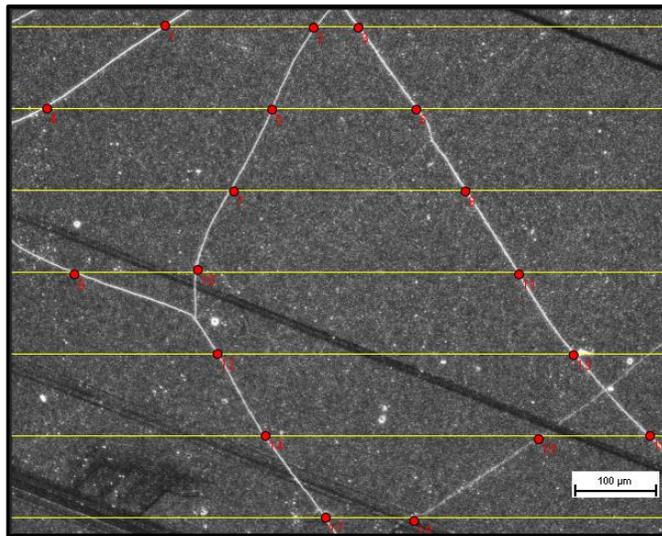
Figure II.10: Optical micrograph showing the intersection points between the micro-cracks and the horizontal lines at the surface of the hard chromium electroplated layer

II.8.1.4. Energy Dispersive Spectroscopy (EDS)

The X-ray photons emitted as a result of the interaction between an electron beam and a material can provide information about the chemical composition of the surface layer. The information recorded can be qualitative by indicating the elements present at the surface, or quantitative by giving the percentage of each element.

II.8.2. Characterisation techniques of mechanical properties

II.8.2.1. Vickers microhardness

The hardness of a material is defined as its resistance to penetration or deformation. One of the tests commonly used to measure hardness is the Vickers microhardness test. In this test, a pyramid-shaped indenter with a square base (an angle of approximately 136° between the opposing

sides) is inserted into the surface of the material under a normal load. The size of the resulting indent is then measured using an integrated optical microscope, and the hardness is calculated using the following equation:

$$Hv = 0.189 \times \frac{F}{d^2}$$ (II-4)

Where, F is the applied force or load, and d $(d = \frac{d_1 + d_2}{2})$ is the mean of the resulting indent diagonals as shown in Figure II.11.
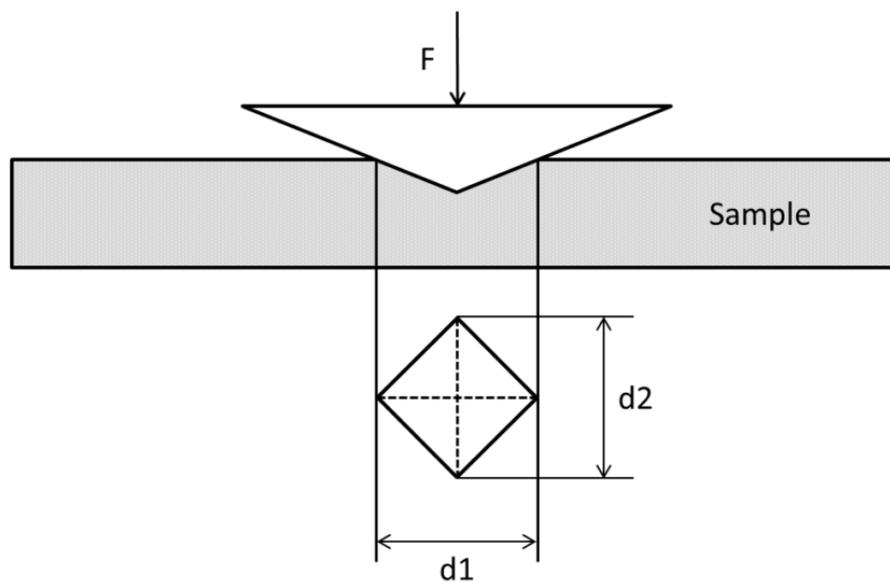
Figure II.11: Principle of the Vickers microhardness test

In the current study, the cross-sectional microhardness of samples was tested using a hardness apparatus (Figure II.12).

Figure II.12: Vickers microhardness testing apparatus ("Laboratoire de Génie énergétique et matériaux (LGEM)", University of Mohamed Khider, Biskra, Algeria)

II.8.2.2. Nanoindentation test

Nanoindentation is a technique used to characterise the mechanical properties of coatings, such as hardness and elastic modulus. In this technique, the length scale of the penetration is in the nanometre range (10^{-9}m). The principle of the nanoindentation technique is the in-situ recording of the applied load with the penetration depth to form a characteristic load-displacement curve. The information derived from this curve are used to determine the mechanical properties of the material under test based on the Olivier - Pharr model [67].

The Olivier - Pharr method was originally developed to determine the hardness and elastic modulus of a material based on the load-displacement curve of one loading-unloading cycle using a Berkovich indenter with a triangular pyramid. Typical load-displacement curve obtained with a Berkovich indenter is shown in Figure II.13. (a). The Olivier - Pharr model is based on the analysis of the unloading curve, as it results only from the elastic response of the material under test, instead of the loading curve, which results from both elastic and plastic responses. Schematic illustration of the unloading process is presented in Figure II.13. (b).
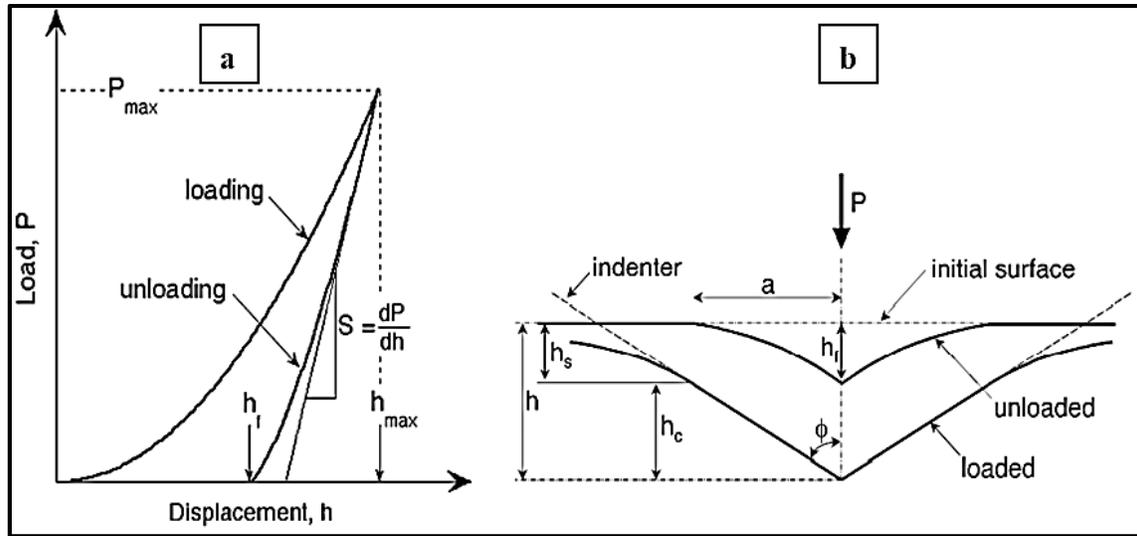
Figure II.13: Schematic illustration of: a) Load – Displacement curve with important parameters and b) Unloading process showing parameters characterising the contact geometry [67]

II.8.2.2.1. Hardness (H)

The hardness in the Olivier – Pharr model is calculated using the following equation [67]:

$$H = \frac{P_{max}}{A_c} \qquad\qquad (II\text{-}5)$$

Where, P_{max} is the maximum applied load and A_c is the contact area. A_c is defined as the area of the residual indentation (projected area), it can also be defined as the indenter area. The contact area is expressed as a function of the contact depth (h_c), and in the case of an ideal Berkovich indenter, it can be expressed as follows [67]:

$$A_c = 24.5 \times h_c^2 \qquad\qquad (II\text{-}6)$$

The contact depth (h_c) is expressed as a function of the maximum depth as follows [67]:

$$h_c = h_{max} - \varepsilon \frac{P_{max}}{S} \qquad\qquad (\text{II-7})$$

Where, h_{max} is the maximum depth under maximum load, ε is a parameter depending on the geometry of the indenter (0.75 for the Berkovich indenter), P_{max} is the maximum applied load and S is the unloading elastic stiffness, which can be defined as the slope of the upper part of the unloading curve [67].

II.8.2.2.2. Elastic modulus (E)

The elastic modulus in the Olivier - Pharr model is derived from the following equation [67]:

$$\frac{1}{E_{eff}} = \frac{1 - \nu_{sample}^2}{E_{sample}} + \frac{1 - \nu_{indenter}^2}{E_{indenter}} \qquad\qquad (\text{II-8})$$

Where, ν is the Poisson's ratio, and E_{eff} is the effective elastic modulus, which can be derived from the equation relating it to the contact area and contact stiffness. This equation is expressed as follows [67]:

$$S = \beta \frac{2}{\sqrt{\pi}} E_{eff} \sqrt{A_c} \qquad\qquad (\text{II.9})$$

Where, β is a constant that depends on the geometry of the indenter, and it is equal to 1.034 for triangular-based indenters.

II.8.2.2.3. Test parameters

In the present study, the nanoindentation tests were performed by CSM instruments Nanoindenter (Figure II.14) equipped with a Berkovich type tip under a maximum load of 60 mN.

Figure II.14: CSM instruments indenter (Centre for Development of Advanced Technologies (CDTA), Algiers, Algeria)

II.8.3. Characterisation techniques of tribological properties

Tribology is the science that studies friction between two relatively moving parts and lubrication. The study of the tribological behaviour of materials in laboratory is generally carried out using a tribometer. Its operating principle consists of moving a ball (or a pin) on the material under test in a rotating or alternating manner. Figure II.15 shows the principle of a tribological test. The ball (or pin) is usually made of a harder material than the material under test, such as 100Cr6, Al_2O_3 and WC. The tribometer is equipped with a system to record the evolution of the friction coefficient and the friction force as a function of the friction distance (friction time, friction cycles).
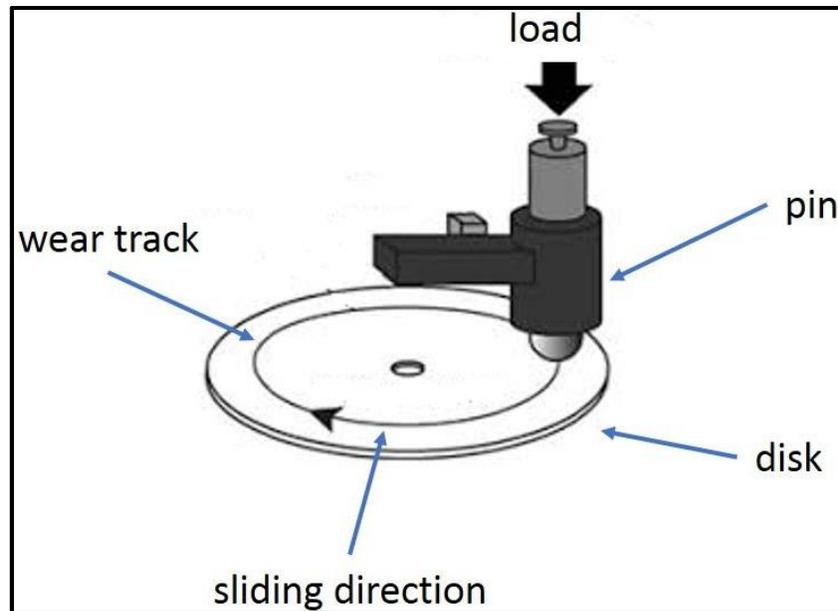
Figure II.15: Principle of the tribological test

Based on the ball-on-disk test, it is possible to estimate the wear resistance of the material under test by calculating the specific wear rate using the Archard equation as follows [68]:

$$K = \frac{V}{F_n \times l} \qquad (\text{II-10})$$

Where K (mm^3 /N.m) is the specific wear rate, V (mm^3) is the wear volume loss, Fn (N) is the normal load and l (m) is the sliding distance. The volume loss is calculated using the conversion equation from mass loss to volume loss as follows [69]:

$$\text{volume loss}(mm^3) = \frac{\text{mass loss}(g)}{\text{density}(g/cm^3)} \times 1000 \qquad (\text{II-11})$$

Mass loss is obtained by measuring the difference between the weight of the sample before and after the test.

In the present study, the ball-on-disk test was performed with a CSM instruments tribometer (Figure II.16) using a 6 mm WC ball under a 10 N load. The sliding speed and distance were 5 cm/s and 100 m, respectively. The wear tracks were then analysed by optical and scanning electron microscopes.
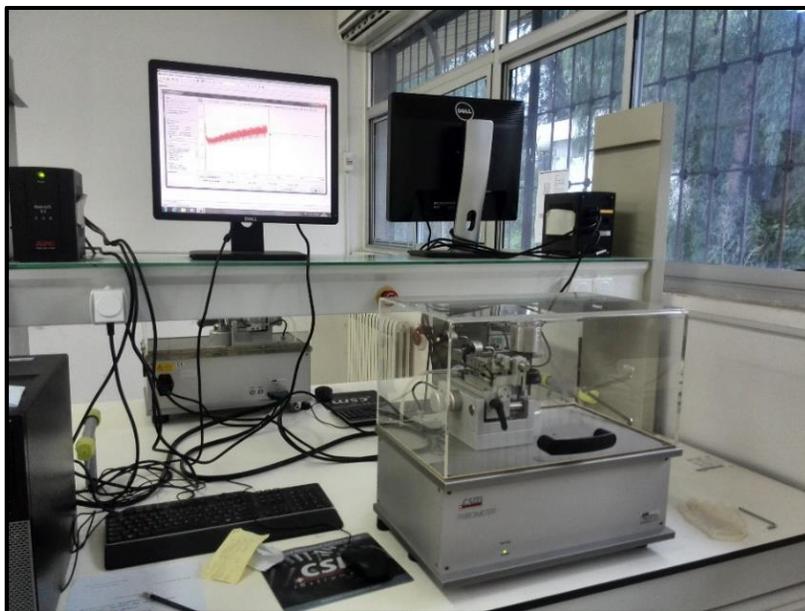
Figure II.16: CSM instruments tribometer ("Laboratoire d'analyse de surface" at the "Ecole Nationale Supérieure des Mines et de la Métallurgie", Annaba, Algeria)

RESULTS AND DISCUSSION

III. RESULTS AND DISCUSSION

III.1. Introduction

This chapter comprises the experimental results concerning the structural, morphological, mechanical and tribological properties of a duplex layer deposited on a low alloy 35NCD6 steel using a duplex surface treatment composed of chromium electroplating and plasma nitriding. The experimental results are examined and interpreted based on published scientific papers, then some correlations between the working parameters and the obtained properties are deduced. Where possible, our experimental results are compared to that existed in relevant scientific papers.

Chapter three starts by presenting the structural and mechanical properties of the substrate material (quenched and tempered 35NCD6 steel). After that, the results of surface characterisation in terms of structure, morphology, mechanical and tribological properties after chromium electroplating and then after plasma nitriding are examined and discussed in sections three and four, respectively. Finally, in section five, the effects of nitrogen pressure used in the plasma nitriding process on surface properties are discussed.

III.2. Characterisation of the Substrate

As mentioned in chapter two, the substrate is made of low alloy 35NCD6 steel (The chemical composition was presented in section II.2). The X-ray diffraction pattern of the as-received 35NCD6 steel is presented in Figure III.1.
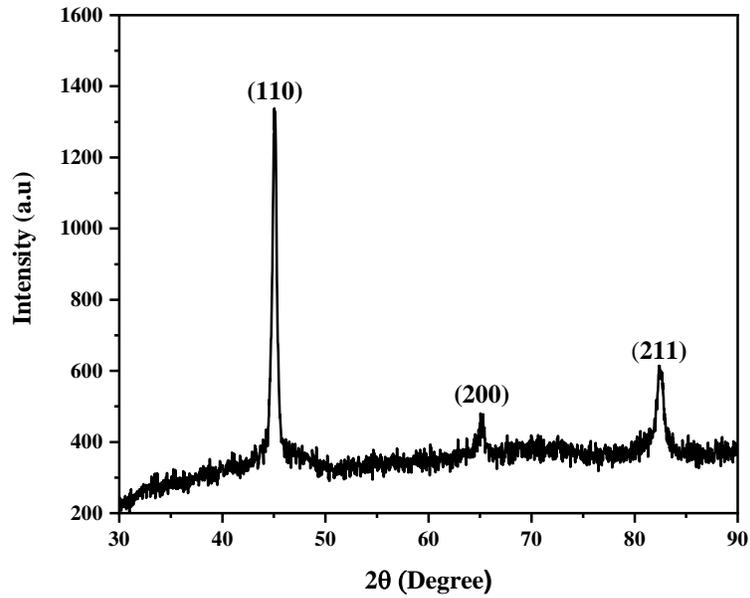
Figure III.1: X-ray diffraction pattern of the 35NCD6 steel substrate sample

As shown in Figure III.1, the X-ray diffraction pattern is composed of three peaks at 2Θ equals to 45.05°, 65.20° and 82.37°. The recorded peaks correspond to centred cubic iron (α-Fe). Figure III.2 presents the micrograph of the as-received 35NCD6 steel etched with Nital solution.
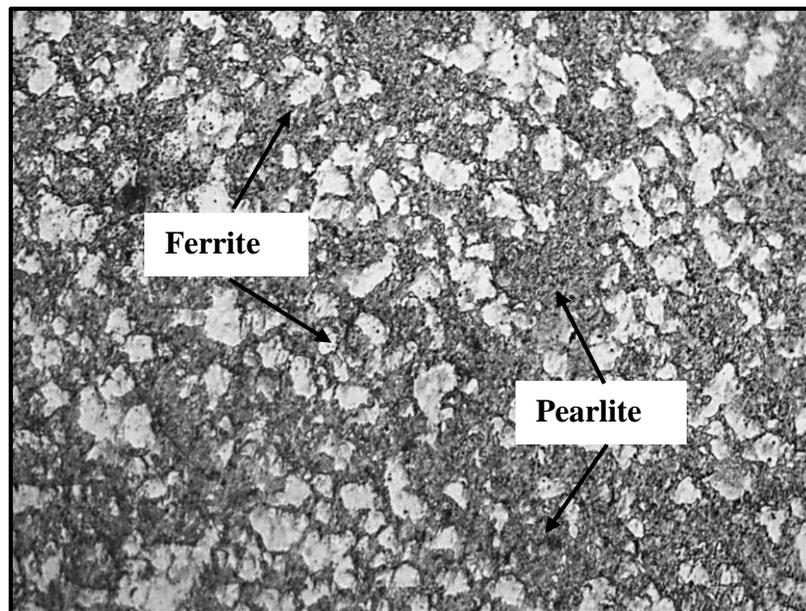
Figure III.2: Optical micrograph of the as-received 35NCD6 steel (Magnification: X1000)

The 35NCD6 steel is hypoeutectic, thus its microstructure is composed of proeutectoid ferrite and pearlite. In the microstructure of Figure III.2, the pearlite is in dark grey colour, while the ferrite is in white colour.

Before they were subjected to duplex treatment, the 35NCD6 steel samples were quenched and tempered. Figure III.3 shows the microstructure of the quenched and tempered 35NCD6 steel.
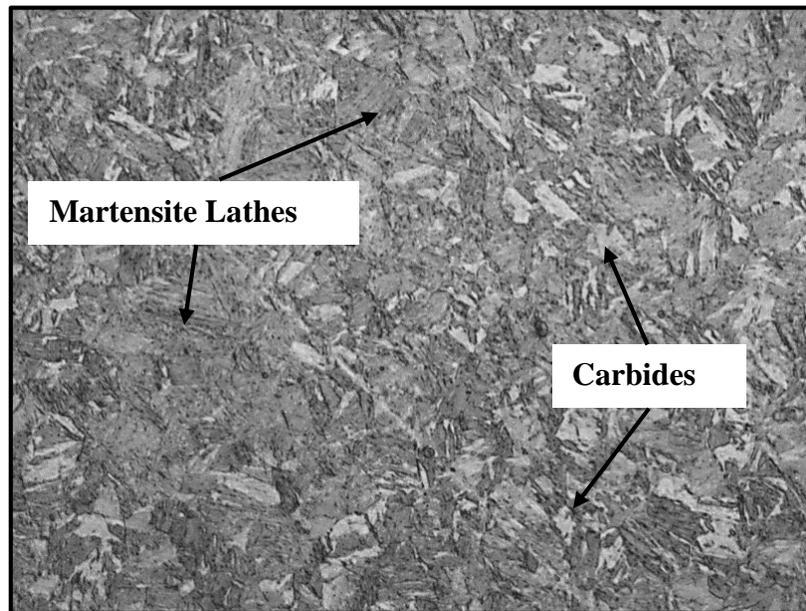
Figure III.3: Microstructure of the quenched and tempered 35NCD6 steel (Magnification X1000)

The microstructure consists of different types of carbides with various sizes and shapes dispersed in a martensite matrix [70]. The martensite matrix and carbides increase the hardness of the substrate, thus, it increases from between 14 and 18 HRC (200-230 HV) in the as-received state to between 56 and 60 HRC (600-700 HV) after quenching and tempering.

III.3. Structural, Morphological, Mechanical and Tribological Properties of the Hard Chromium Electroplated Layer

After quenching and tempering, the 35NCD6 steel samples were chromium electroplated in an electroplating bath composed mainly of trioxide chromium (CrO_3) and sulphuric acid (H_2SO_4). The deposition of chromium on a quenched and tempered steel is recommended because of the combination properties obtained at the interface [71]. In this section, we discuss the

structural, morphological, mechanical and tribological properties of the hard chromium electroplated layer deposited on 35NCD6 steel substrate.

III.3.1. Structural and morphological properties

III.3.1.1. Structural properties

Figure III.4 presents the X-ray diffraction pattern of the hard chromium electroplated layer.
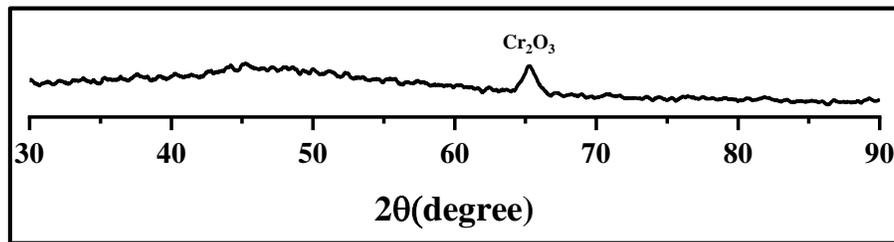
Figure III.4: X-ray diffraction pattern of the hard chromium electroplated layer

The diffraction pattern shows a small peak at 2Θ equals to $65.19°$. The shown peak corresponds to di-chromium oxide (Cr_2O_3), which can be resulted from surface oxidation. In addition, it is noted the absence of crystalline chromium peaks, which indicates that the hard chromium electroplated layer is amorphous. This result can be attributed to the properties of the industrial electroplating bath used in our experiment.

III.3.1.2. Morphological properties

III.3.1.2.1. Plan-view analysis

Figure III.5 shows optical and SEM micrographs of the surface of the hard chromium electroplated layer.
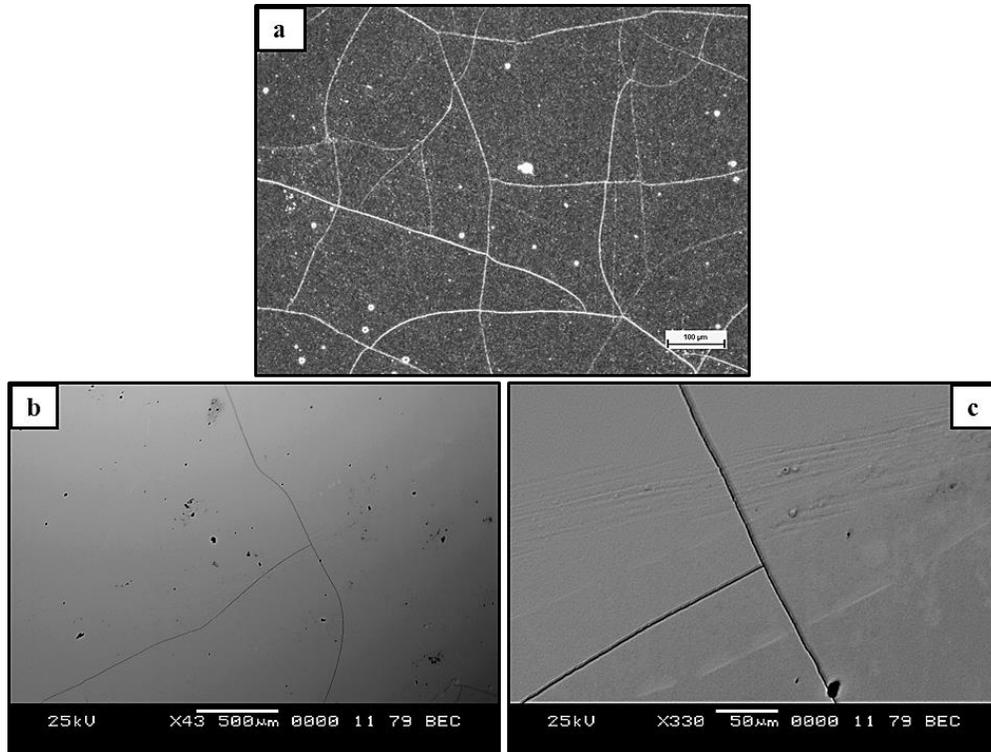
Figure III.5: a) Optical (Magnification X 100), b) and c) SEM Micrographs of the surface of the hard chromium electroplated layer

Figure III.5 shows that the surface of the hard chromium electroplated layer is uniform and smooth with presence of micro-cracks. The micro-cracks in the electroplated chromium can be originated from the shrinkage accompanying the decomposition of unstable chromium hydrides (β-Cr, with hexagonal face centred crystal structure) into stable chromium (Cr-α, with body centred crystal structure) during the electroplating process [72], [73]. Also, it can be originated from the opposing properties of low elasticity of chromium and the high residual stress induced during the electroplating process [71]. Because the X-ray diffraction pattern of the hard chromium electroplated layer indicates that the layer is amorphous, the second origin of micro-cracks in the chromium electroplated layer seems to be the adequate cause regarding our experimental conditions.

III.3.1.2.2. Cross-sectional analysis

Figure III.6 shows a cross-sectional micrograph of the hard chromium electroplated layer deposited on 35NCD6 steel sample obtained by an optical microscope.
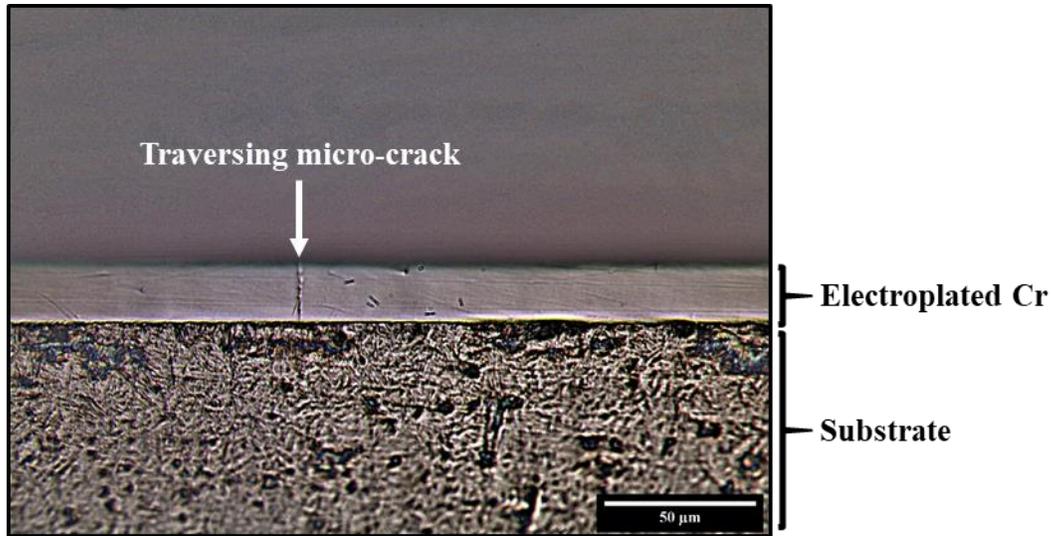
Figure III.6: Cross-sectional micrograph of the hard chromium electroplated layer

(Etched with Nital solution, Magnification: X 1000)

The cross-sectional micrograph of the hard chromium electroplated layer etched with Nital solution reveals a smooth and compact chromium layer with some micro-cracks perpendicular to the surface. The perpendicular micro-cracks that traverse the hard chromium electroplated layer were also reported by Sarraf et al. [52] .It is also noted that the microstructure of the substrate (35NCD6 steel) remains martensitic because of the low temperature of the electroplating bath (57±2 °C), which do not affect the microstructure of the quenched and tempered 35NCD6 steel. Additionally, the cross-sectional micrograph of the hard chromium electroplated layer shows the absence of a transition layer at the interface between the chromium layer and the 35NCD6 steel sample. In fact, the formation of a transition layer can take place by diffusion, which is not possible under the low heat generated in the electroplating bath.

III.3.1.3. Mechanical properties

III.3.1.3.1. Hardness and elastic modulus

The hard chromium electroplated layer was tested by a Nano-indenter equipped with a tip of Berkovich type under a maximum load of 60 mN. The experimental load-displacement curve is presented in Figure III.7.
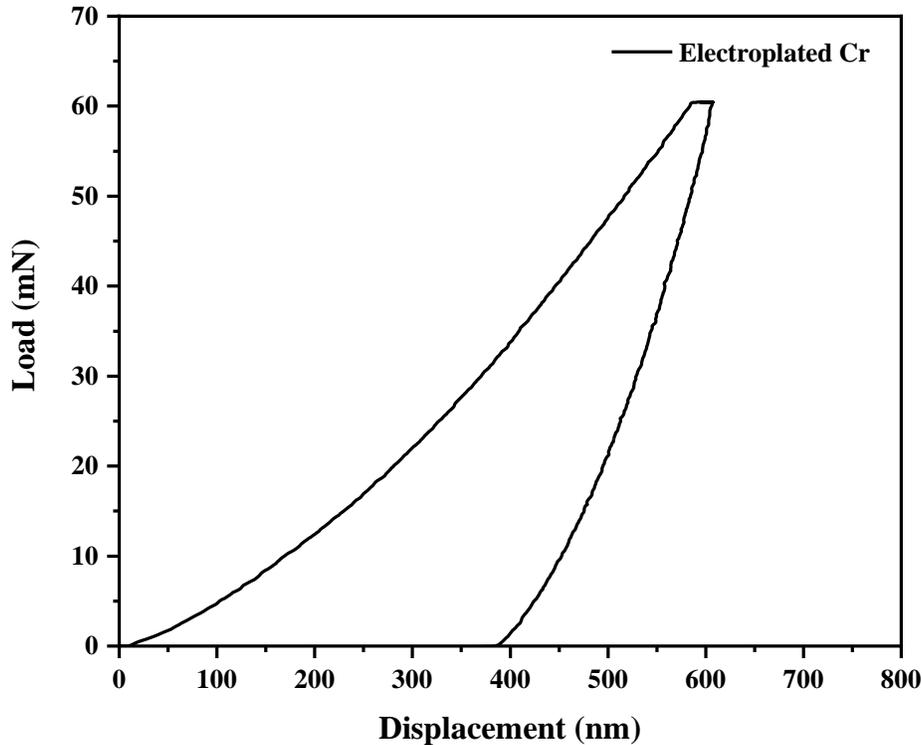
Figure III.7: Load-displacement curve of the hard chromium electroplated layer

The hardness and elastic modulus of the hard chromium electroplated layer are 14.26 GPa (~1320 HV) and 199.81 GPa, respectively. Nearly similar hardness (~13 GPa) has been reported by Vernhes et al. [74]. The high hardness of the hard chromium electroplated layer can be attributed to three factors: small grain size, internal stress and oxide inclusions [75]. However, due to the amorphous nature of the hard chromium electroplated layer in our experimental conditions, only the two latter factors can explain its high hardness.

III.3.1.3.2. Cross-sectional microhardness

The cross-sectional microhardness of the hard chromium electroplated layer was tested under an applied load of 10 gf. The microhardness of the hard chromium electroplated layer and the 35NCD6 steel substrate are 1036.6 HV and 663.74 HV, respectively. Figure III.8 shows the indentation imprints of the microhardness test.
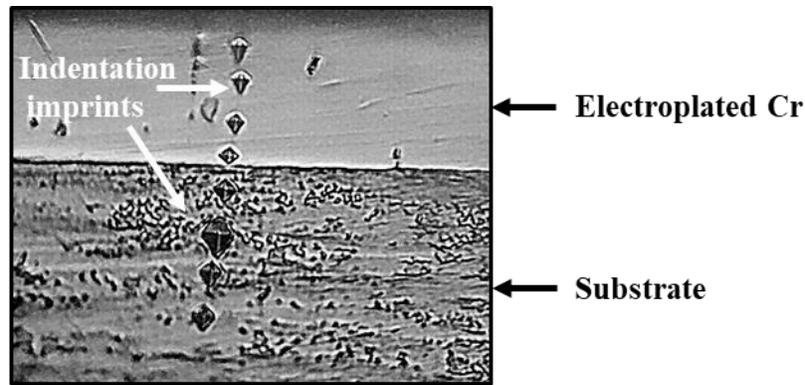
Figure III.8: Indentation imprints of the microhardness test performed on the hard chromium electroplated layer and on the 35NCD6 steel substrate (Magnification: X 500)

As shown in Figure III.8, the size of the indentation imprints in the hard chromium electroplated layer is smaller than that in the 35NCD6 steel substrate, which is in agreement with the microhardness results.

The difference in plan and cross-sectional hardness values of the hard chromium electroplated layer can be attributed to the oxide inclusions at the surface as well as to the difference in testing techniques.

III.3.1.4. Tribological properties

III.3.1.4.1. Frictional behaviour

Figure III.9 presents the evolution of friction coefficient of the hard chromium electroplated layer as a function of sliding distance. The hard chromium electroplated layer was tested using a WC ball under a normal load of 10 N and a sliding speed of 5 cm/s in dry condition at room temperature.
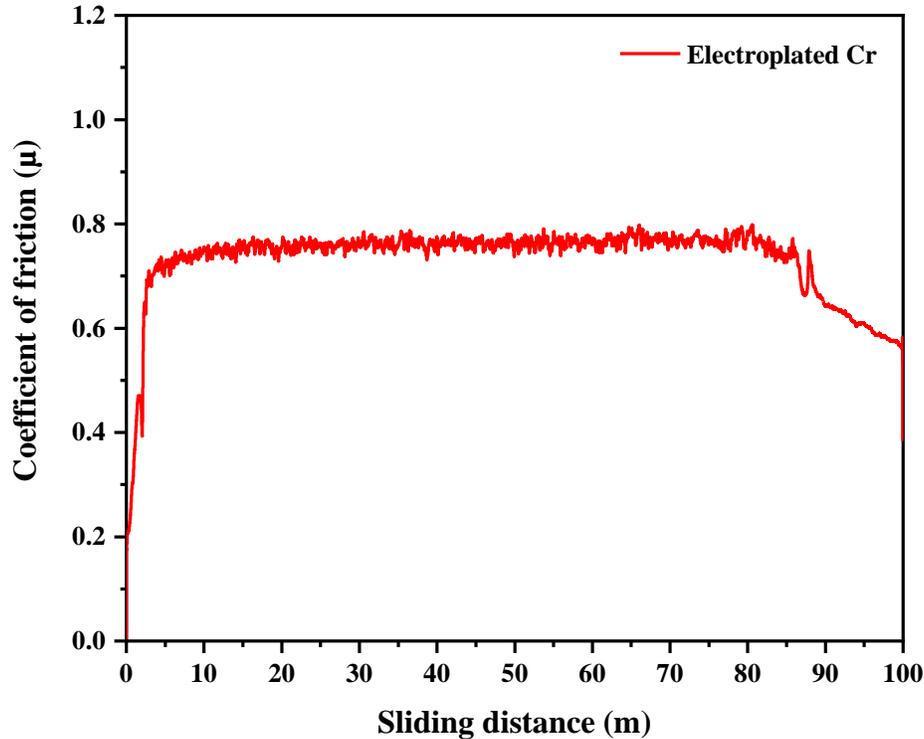
Figure III.9: Frictional behaviour of the hard chromium electroplated layer

Figure III.9 shows that the friction coefficient of the hard chromium electroplated layer increases rapidly at the beginning of the test, after that, it fluctuates around 0.73 for the majority of testing time, then it decreases to about 0.6 for the rest of the experiment. Noll has reported an average friction coefficient of 0.65 for an alumina ball against hard chromium electroplated disk [76]. The coefficient of friction is directly related to friction force. At the beginning, the first contact between the two sliding parts induces an increase in the coefficient of friction, and after about 3 m of sliding a second increase is observed, which can be attributed to the increase in friction force caused by the labouring of the hard chromium electroplated layer by the WC ball. After about 5 m, the coefficient of friction fluctuates around 0.73 until about 80 m of sliding distance. The cause of the relatively stable coefficient of friction in this stage can be the formation of an intermediate layer from the debris of the hard chromium electroplated layer between the WC ball and the tested sample. After that, the observed drop in the coefficient of friction after 80 m of sliding distance can be explained by the formation of a chromium oxide layer, which is generally harder than electroplated chromium, under the effect of the heat generated during the sliding process. The relatively high coefficient of friction recorded in this WC/hard chromium

electroplated layer pair have been also reported in other research papers for Al_2O_3/ Hard chromium electroplated layer and Si_3N_4/hard chromium electroplated layer pairs [2], [77].

III.3.1.4.2. Wear behaviour

Table III.1 presents the main tribological properties of the hard chromium electroplated layer. As noted in the table, the hard chromium electroplated layer has a relatively high wear rate, which is in good agreement with the high coefficient of friction recorded in the sliding test.

Table III.1: Summary of the main tribological properties of the hard chromium electroplated layer

	Weight loss (g)	Density (g/cm^3)	Wear volume (mm^3)	Wear rate (mm^3/m.N)
Hard chromium electroplated layer	0.0018	7.11	0.253165	0.000253

Moreover, the high wear rate explains the wide wear track shown in the SEM images of the hard chromium electroplated layer surface in Figure III.10. The cause of the relatively high wear rate in the electroplated chromium can be the brittleness of the hard chromium electroplated layer because of its high hardness. The wear track at the surface of the hard chromium electroplated layer contains microgrooves, wear debris, delaminated surfaces and some micro-cracks (Figure III.10). The microgrooves and wear debris indicate that the surface was plastically deformed. On the other hand, the delaminated surface indicates that the surface was subjected to tearing. Based on these observations, it is suggested that the abrasive and adhesive wear mechanisms are present, but the predominant wear mechanism is abrasion. Vernhes et al. have reported that in the case of hard counterparts like WC and alumina, the high wear rate is observed because of the brittle cracking of the hard chromium electroplated layer [74]. The wear mechanism depends on many factors, such as the components of the tribosystem, the environment, and the surface properties. For instance, Bolelli et al. [77] have reported that the wear mechanism that governed the sliding of an Al_2O_3 ball on electroplated chromium is abrasion, while, Zeng et al. [2] have reported that it is delamination in the case of a Si_3N_4 ball sliding on electroplated chromium.
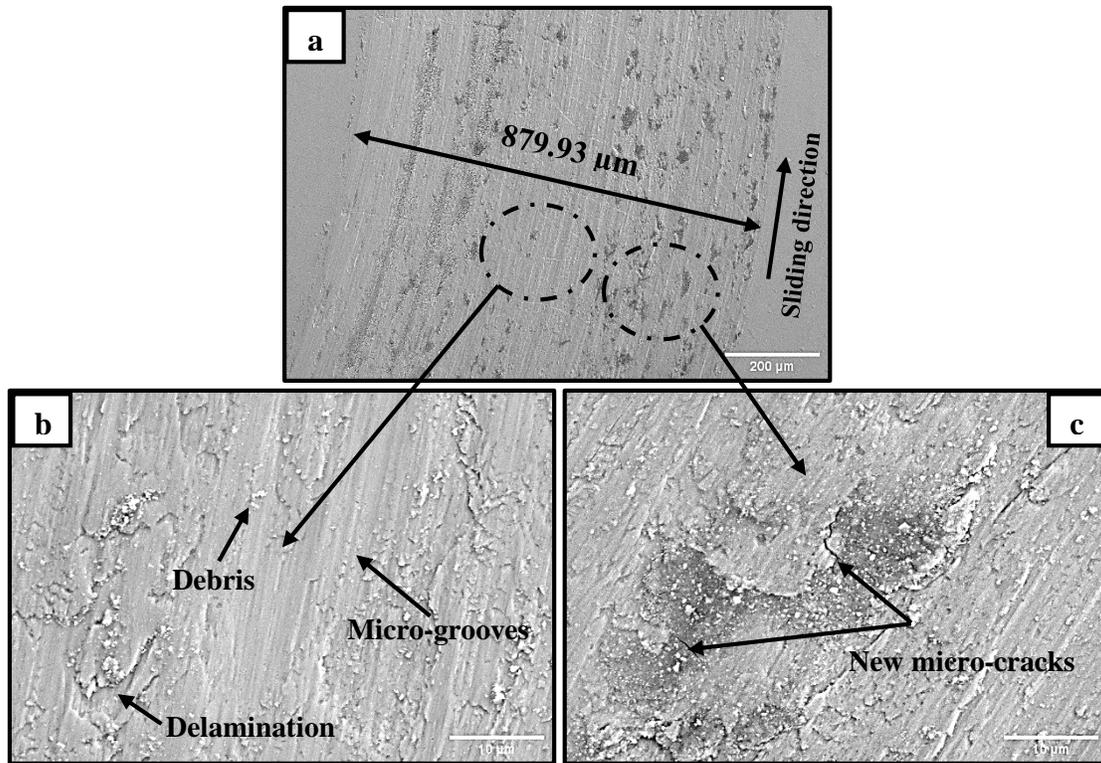
Figure III.10: SEM images of the wear track at the surface of the hard chromium electroplated layer [78]

III.4. Structural, Morphological, Mechanical and Tribological Properties of the Plasma Nitrided Hard Chromium Electroplated Layer

In this section, we present and discuss the morphological, structural, mechanical and tribological properties of the hard chromium electroplated layer surface after plasma nitriding at 600°C for 90 min in a pure nitrogen atmosphere, using a nitrogen pressure of 3 Torr.

III.4.1. Structural and morphological properties

III.4.1.1. Structural properties

Figure III.11 presents the X-ray diffraction pattern of the hard chromium electroplated layer after plasma nitriding at 3 Torr.
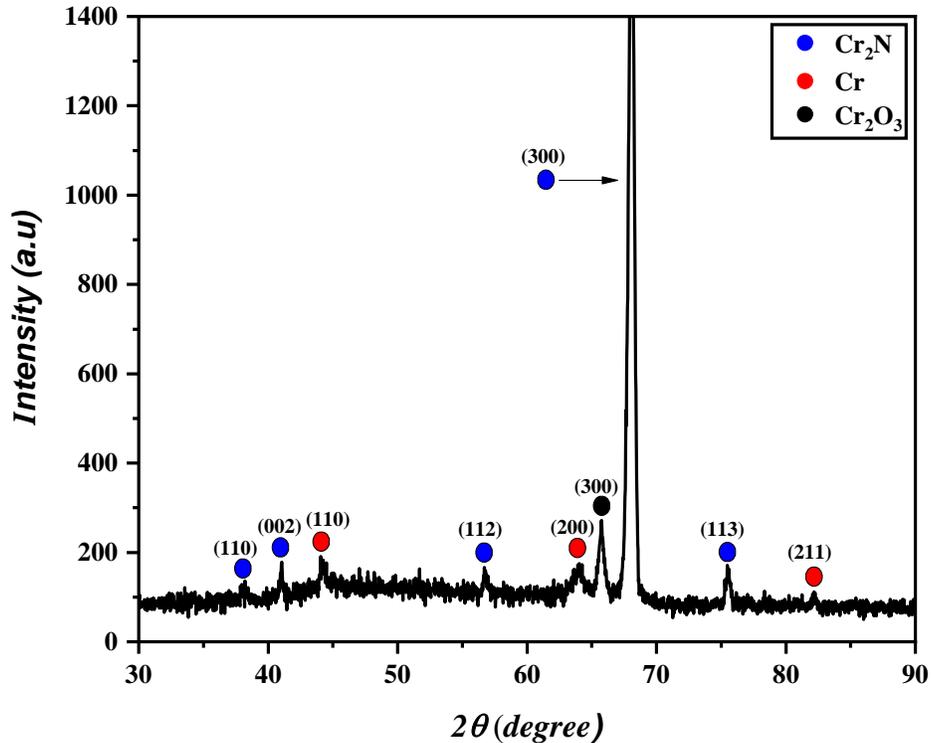
Figure III.11: X-ray diffraction pattern of the hard chromium electroplated layer after plasma nitriding at 3 Torr

Figure III.11 shows that the diffraction pattern is composed mainly of hexagonal chromium nitride (Cr_2N) and centred cubic Cr peaks, in addition to one chromium oxide (Cr_2O_3) peak at 66°. Similar observation have been reported by many researchers after gas nitriding [41], [47] and after plasma nitriding [45], [49], [50] of a chromium layer. The presence of Cr peaks after plasma nitriding (2Θ: 44.2°, 64.0°, 82.3°) is attributed to the crystallisation of chromium atoms in bcc crystal structure during the preheating and nitriding processes. The crystallisation of chromium takes place between 300°C and 500°C as reported by Snavely et al. [79]. The diffraction peaks of Cr_2N at 38.40°, 40.99°, 56.68°, 68.05°and 75.44° confirm the nitridation of the surface of the hard chromium electroplated layer, as the nitridation of chromium starts generally at about 600°C, where its products until 700°C are crystallised chromium and Cr_2N [41].

Formation of chromium nitrides during plasma nitriding of chromium can take place by the contribution of two mechanisms: the first is the re-deposition of chromium nitrides issued from the interaction between sputtered chromium atoms and neutral nitrogen species in the plasma, and the second is the diffusion of nitrogen atoms into the crystalline lattice of chromium [49].

The high intensity of the Cr_2N peak at 68.05° indicates that the Cr_2N crystals have a preferred growth orientation parallel to the (300) plane. The same texturing observation was noted in the research work of other authors after plasma nitriding [55], [80] and after gas nitriding [46] of electroplated chromium.

III.4.1.2. Morphological properties

III.4.1.2.1. Plan-view analysis

SEM micrographs of the surface of the hard chromium electroplated layer after plasma nitriding at 3 Torr are shown in Figure III.12.
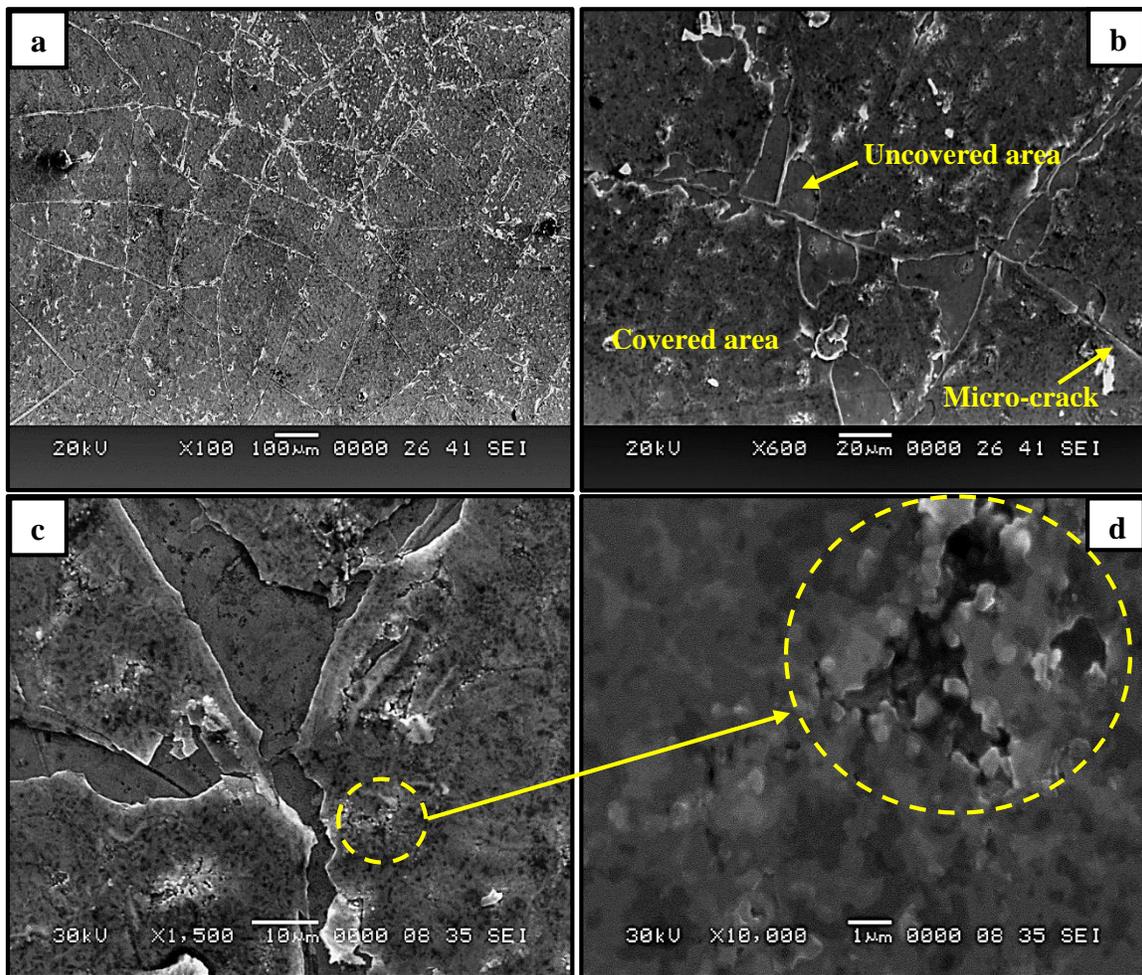
Figure III.12: Surface morphology after plasma nitriding of hard chromium electroplated layer at 3 Torr

Figure III.12 shows that the surface morphology is significantly different from that before plasma nitriding (Figure III.5). The surface of the plasma nitrided hard chromium electroplated layer contains a network of micro-cracks with covered and uncovered areas, and it is noted that the uncovered areas are localised especially along micro-cracks. The uncovered area looks smooth with low roughness in comparison to the covered area that looks rough and porous. The morphology of the surface in the covered areas can be attributed to the formation of Cr_2N compounds as a result of the diffusion of attracted nitrogen ions into the crystalline lattice of the hard electroplated chromium. Based on the SEM micrographs and the X-ray diffraction pattern of the surface after plasma nitriding at 3 Torr, we suggest that the covered areas correspond to a diffusion layer rich with Cr_2N compounds, while the uncovered areas correspond to the hard chromium electroplated layer. The uncovered areas can be resulted from the detachment of the hard Cr_2N-rich regions due to ionic bombardment and surface tensile stress. In other words, the high kinetic energy of nitrogen ions, at this relatively low nitrogen pressure, increases the ionic bombardment of the surface, which results in the detachment of some parts of the diffusion layer in the Cr_2N-rich regions due to its low thickness. Takahashi et al. have reported that the sputtering effect of ions becomes significant at nitriding pressure less than 3 Torr and a total voltage higher than 600 V [81]. The nitriding conditions reported by Takahashi et al. are similar to that used in the present experiment, which can enhance our suggestion about the detachment of the Cr_2N-rich diffusion layer.

III.4.1.2.2. Cross-sectional analysis

Figure III.13 presents a cross-sectional micrograph of the hard chromium electroplated layer after plasma nitriding at 3 Torr.
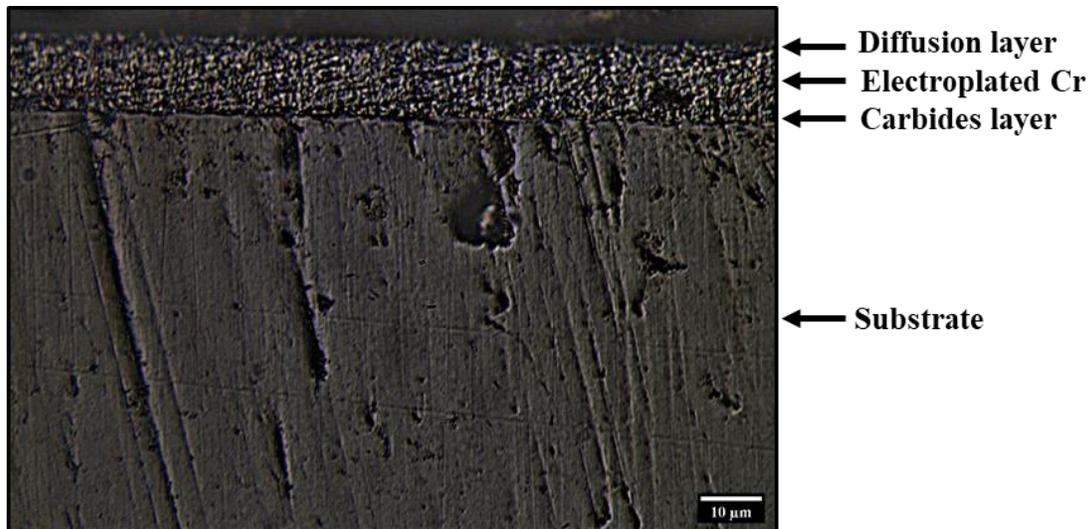
Figure III.13: Cross-sectional micrograph of the hard chromium electroplated layer after plasma nitriding at 3 Torr (Etching solution: Aqua regia, Magnification: X 1000)

The cross-sectional micrograph in Figure III.13 shows that the hard chromium electroplated layer is transformed to three layers: upper diffusion layer, intermediate unchanged chromium electroplated layer and inner chromium carbides layer. This cross-sectional morphology is commonly observed when a chromium layer deposited on steel substrate is subjected to a post-nitriding at high temperature [82]. The diffusion layer in the cross-sectional micrograph confirms the plan-view observation (Figure III.12).The formation of the diffusion layer takes place when the attracted nitrogen ions are diffused into the surface of the hard chromium electroplated layer. On the other hand, the chromium carbides layer is formed as a result of the diffusion of carbon atoms from the steel substrate towards the hard chromium electroplated layer under the effect of the heat generated in the pre-heating step and during the plasma nitriding process.

III.4.2. Mechanical properties

III.4.2.1. Hardness and Elastic modulus

The surface of the plasma nitrided hard chromium electroplated layer was tested using a Nano-indenter equipped with a Berkovich type tip under a maximum applied load of 60 mN. The experimental load – displacement curve is presented in Figure III.14.
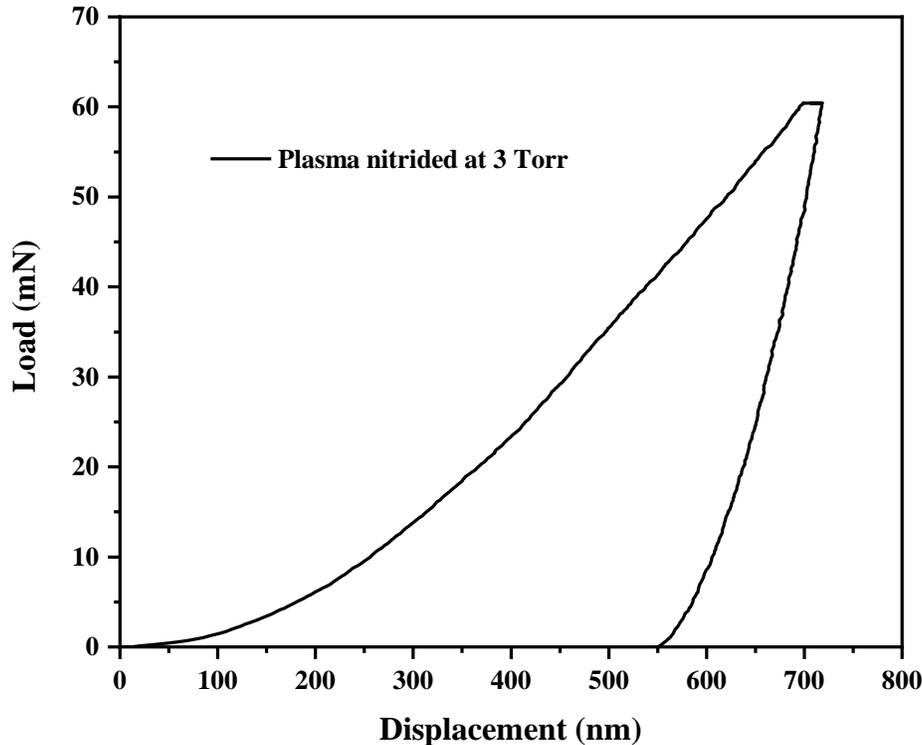
Figure III.14: Load-displacement curve of the hard chromium electroplated layer after plasma nitriding at 3 Torr

Figure III.14 shows that the load - displacement curve is smooth (without discontinuities), which indicates that no significant cracking took place during the test. The hardness and the elastic modulus recorded in this test are about 10.64 GPa and 247.84 GPa, respectively, with a maximum displacement depth (h_{max}) of about 731.59 nm. It is noted that the hardness after plasma nitriding at 3 Torr, is lower than that at the surface of the hard chromium electroplated layer, and the maximum displacement is about 73 % of the diffusion layer thickness (~ 1µm). It is known that the substrate contribution to hardness is included in the recorded values when the maximum displacement of the indenter exceeds 10 % of the coating thickness [83]. As a consequence, the recorded hardness and elastic modulus after plasma nitriding at 3 Torr do not correspond to the diffusion layer only, instead they correspond to the diffusion layer with contribution from the hard chromium electroplated layer. The decrease of surface hardness after plasma nitriding at 3 Torr can be attributed to the degradation of the mechanical properties of the hard chromium electroplated layer under the effect of heat generated before and during plasma nitriding. The degradation of mechanical properties of electroplated chromium after annealing and after plasma nitriding has been reported by many researchers [54], [84], [85].

III.4.2.2. Cross-sectional microhardness

The cross-sectional microhardness of the hard chromium electroplated layer after plasma nitriding at 3Torr was tested using a microhardness apparatus under a load of 10 gf. As mentioned earlier, the cross-sectional micrograph of the sample nitriding at 3Torr (Figure III.13) showed the formation of two new layers: nitrogen diffusion layer and chromium carbides layer. While the microhardness of the diffusion layer was difficult to measure because of its small thickness compared to the size of the Vickers indenter, the microhardness of the unchanged chromium electroplated layer and the chromium carbides layer as well as the microhardness of the substrate were easily tested. The recorded microhardness values for the unchanged chromium electroplated layer, the chromium carbides layer and the 35NCD6 steel substrate are 495.18 HV, 603.13 HV and 291.3 HV, respectively. It should be noted that the microhardness of the hard chromium electroplated layer decreased after plasma nitriding at 3 Torr, which confirms the earlier explanation about the decrease of surface hardness after plasma nitriding at 3 Torr (Section III.4.2.1). Moreover, the microhardness of the 35NCD6 steel substrate decreased from about 664 HV to about 291 HV because of the heat generated before and during plasma nitriding. Lee and Su have reported that the hardness and strength of the AISI 4340 steel (AFNOR designation: 35NCD6 steel) decrease with increasing tempering temperature [70]. Figure III.15 shows the difference in indent size between the unchanged chromium electroplated layer, the chromium carbide layer and the 35NCD6 steel substrate.
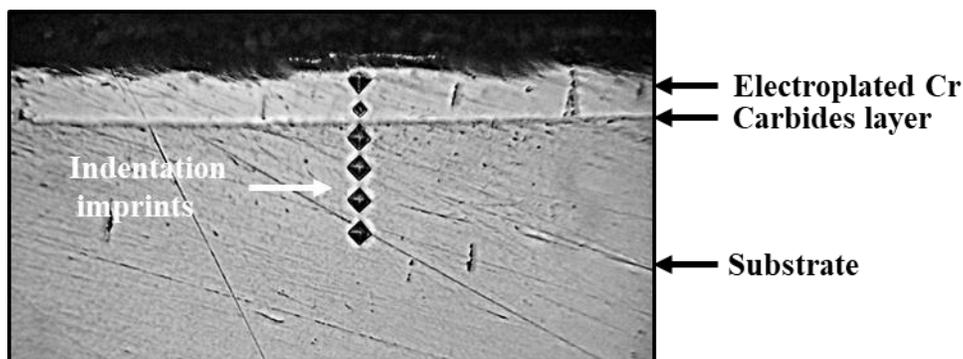
Figure III.15: Indentation imprints of the microhardness test performed on the hard chromium electroplated layer after plasma nitriding at 3 Torr (Magnification: X 500)

III.4.3. Tribological properties

III.4.3.1. Frictional behaviour

The plasma nitrided hard chromium electroplated layer was tested under the same conditions as those used for testing the hard chromium electroplated layer. The evolution of the friction coefficient as a function of sliding distance is presented in Figure III.16.
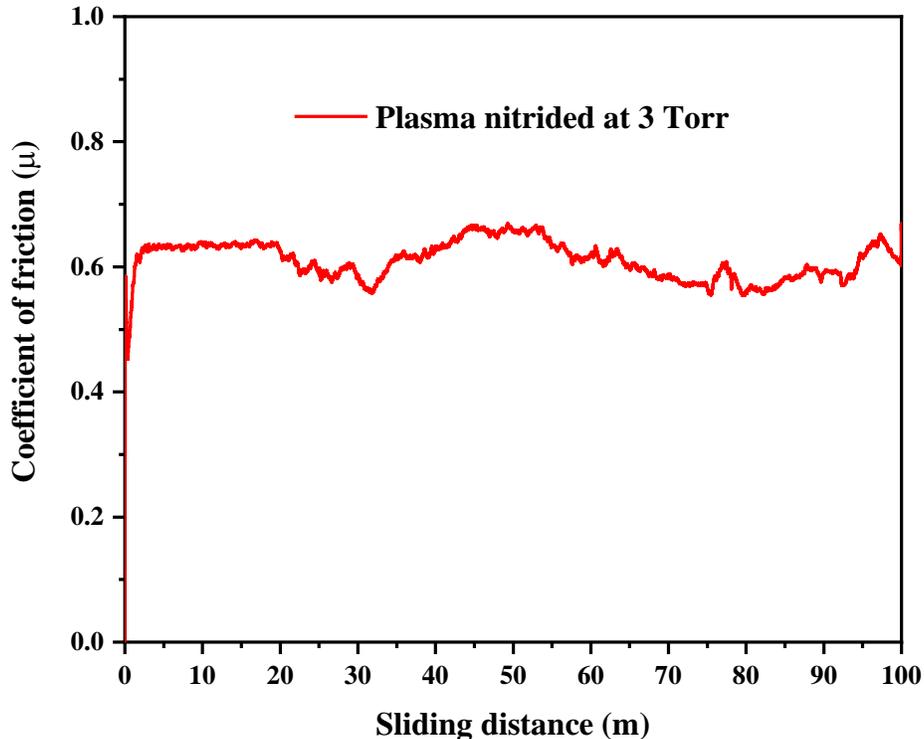
Figure III.16: Evolution of friction coefficient as a function of sliding distance of the hard chromium electroplated layer after plasma nitriding at 3 Torr

Figure III.16 shows that, the coefficient of friction increases rapidly at the beginning of the test because of the high frictional force accompanying the first contact between the two sliding parts. After that, it evolves in an unstable manner until the end of the test. The unstable evolution of the friction coefficient can be attributed to the inhomogeneous surface morphology after plasma nitriding at 3 Torr (see Section III.4.1.2). The inhomogeneous surface morphology formed of hard Cr_2N-rich covered areas and ductile electroplated Cr-rich uncovered areas can induce different friction forces in the sliding track during the test, which can explain the unstable behaviour of the friction coefficient evolution. The average friction coefficient of the hard chromium electroplated

layer after plasma nitriding at 3 Torr is about 0.61. It should be noted that the friction coefficient of the plasma nitrided hard chromium electroplated layer is lower than the friction coefficient of the hard chromium electroplated layer before plasma nitriding (0.73), which can be due to the presence of the hard Cr_2N compounds in addition to the ductile electroplated chromium. The ductile chromium exhibits high resistance to plastic deformation, and the Cr_2N compounds can withstand load because of their high hardness, thus the presence of both ductile chromium and Cr_2N can enhance the tribological properties of the layer[86].

III.4.3.2. Wear behaviour

The residual wear track obtained on the plasma nitrided hard chromium electroplated layer was analysed using an optical microscope, and the obtained micrographs are presented in Figure III.17.
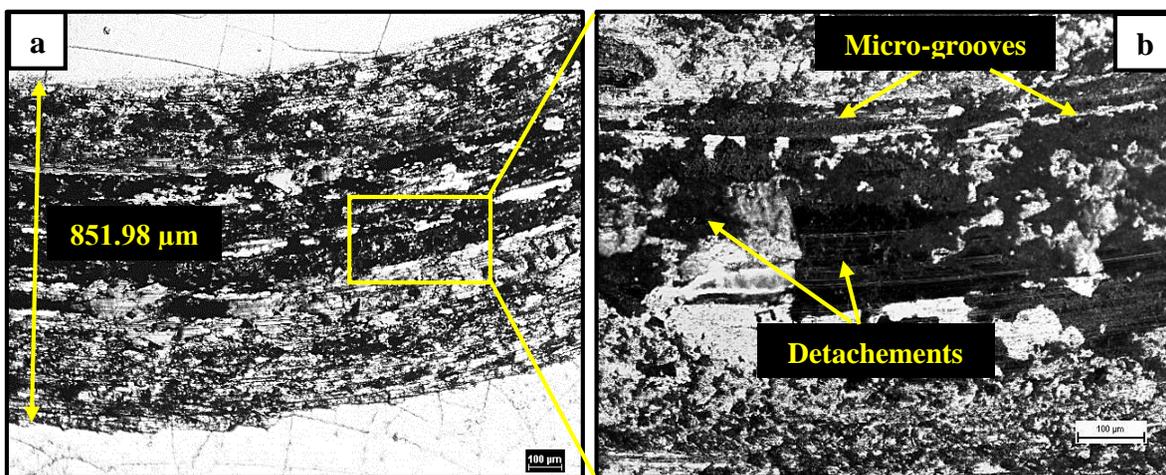
Figure III.17: Optical micrographs of wear track at the surface of the hard chromium electroplated layer after plasma nitriding at 3 Torr: a) X 50 and b) X 100 magnification

The wear track in the plasma nitrided hard chromium electroplated layer shows a number of microgrooves as well as some surface detachments, especially in the centre area, which indicates that the surface of the plasma nitrided hard chromium electroplated layer was subjected to abrasive and adhesive wears. However, the amount of the detached surface indicates that the adhesive wear mechanism is dominant. The morphology of the wear track surface can be resulted from the difference in the mechanical properties of surface components that is composed of hard Cr_2N and ductile electroplated chromium. This difference in the mechanical properties of surface components induces different responses towards the sliding WC ball.

The wear track width in the plasma nitrided hard chromium electroplated layer is slightly smaller than that in the hard chromium electroplated layer (~ 879.93 µm), while the weight loss is almost similar in both samples. The weight loss in the plasma nitrided hard chromium electroplated layer was about 0.002 g, and it was about 0.0018 g for the hard chromium electroplated layer. As a consequence, the wear properties of the surface of the hard chromium electroplated layer have not changed significantly after plasma nitriding at 3 Torr.

III.5. Effect of Nitrogen Pressure on the Structural, Morphological, Mechanical and Tribological Properties of the Plasma Nitrided Hard Chromium Electroplated Layer

To explore the effect of nitrogen pressure, the hard chromium electroplated layer was plasma nitrided at 600°C for 90 min at different nitrogen pressures: 3, 3.5, 4, 4.5 and 5 Torr. The effect of nitrogen pressure on the structural, morphological, mechanical and tribological properties of the obtained layer is presented in this section.

III.5.1. Effect of nitrogen pressure on structural properties

Figure III.18 presents the X-ray diffraction patterns of the hard chromium electroplated layer after plasma nitriding at 3, 3.5, 4, 4.5 and 5 Torr.
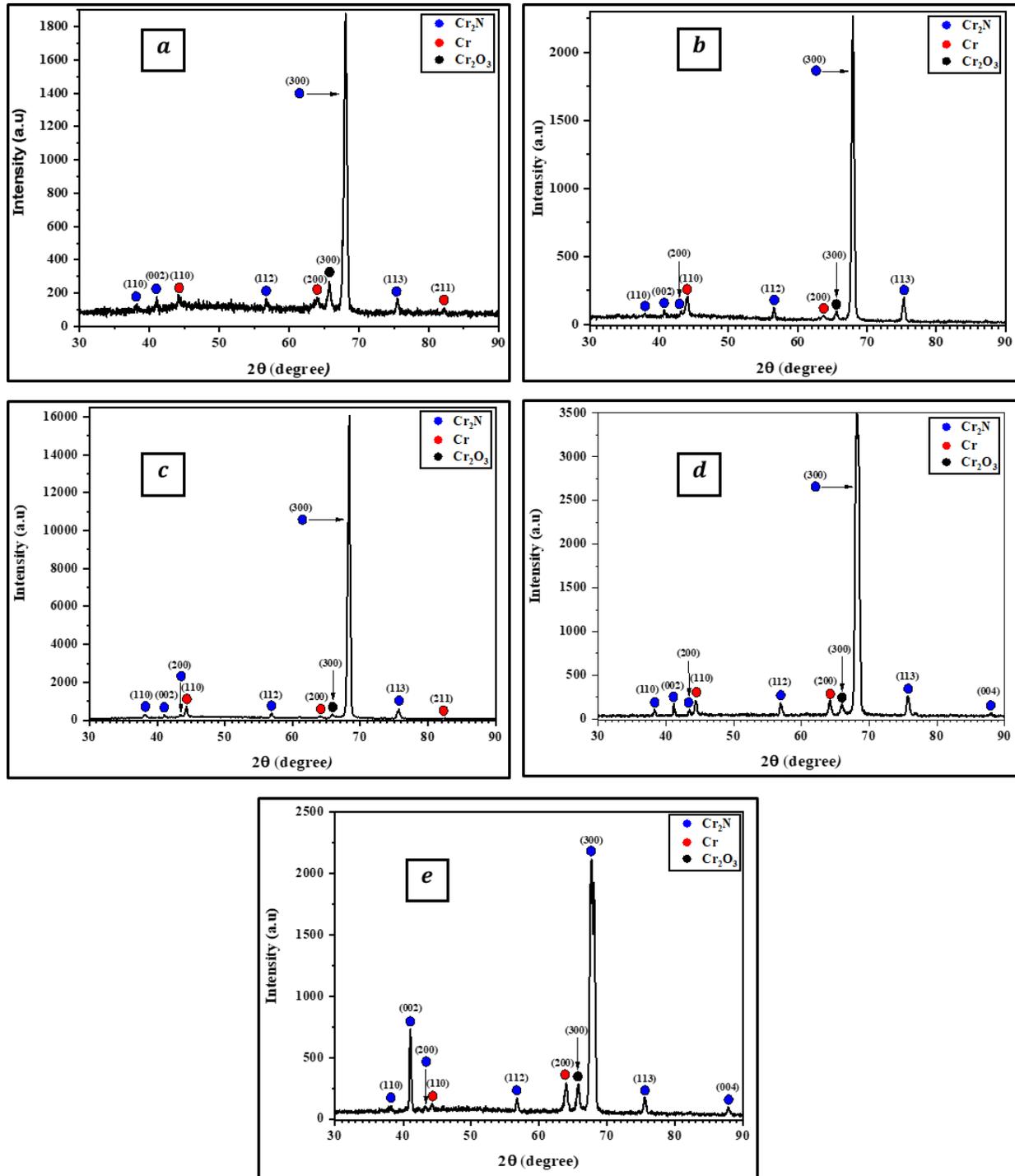
Figure III.18: X-ray difraction patterns of the hard chromium electroplated layer after plasma nitriding at: a) 3, b) 3,5, c) 4, d) 4.5 and e) 5 Torr

The X-ray diffraction patterns show that the surface of the hard chromium electroplated layer after plasma nitriding at the five nitrogen pressures is composed of Cr_2N (PDF-2 database card N°: 00 – 001 – 1232) , crystalline Cr (PDF-2 database card N°: 00 – 001 – 1251) and Cr_2O_3

(PDF-2 database card N°: 01 – 084 – 0313) peaks. However, the diffraction peaks of the Cr_2N phase are dominant in all diffraction patterns. Moreover, the five X-ray diffraction patterns show that the Cr_2N has a preferred growth orientation parallel to the (300) plane. By comparing the five diffraction patterns, we note the absence of the (200) plane peak in the diffraction pattern of the sample nitrided at 3 Torr. The absence of the (200) plane peak can be attributed to the absence of Cr_2N crystals growing parallel to the (200) plane because of the lack of sufficient nitrogen atoms. On the other hand, we note the presence of a new Cr_2N diffraction peak at about 87.96 ° corresponding to the (004) plane after plasma nitriding at 4.5 and 5 Torr. The emergence of a new Cr_2N peak can be attributed to the formation of new Cr_2N crystals because of the high amount of nitrogen atoms. The diffraction pattern of the sample nitrided at 5 Torr shows also a noticeable increase in the Cr_2N peak intensity of the (200) plane compared to the other Cr_2N peaks. The increase of the peak intensity of the (200) plane can be attributed to an increase in the Cr_2N crystals that grow parallel to the (200) plane.

Three intense peaks in the diffraction pattern of the Cr_2N phase corresponding to the (300), (112) and (113) planes were chosen to follow the evolution of their intensities with the change of nitrogen pressure. The evolution of the intensities of the chosen peaks as a function of nitrogen pressure is presented in Figure III.19.
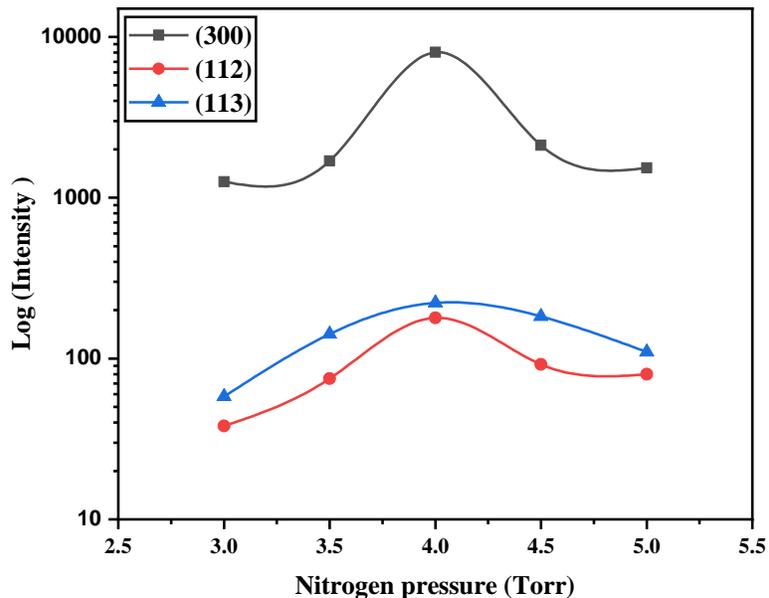
Figure III.19: Evolution of the intensities of Cr_2N main peaks as a function of nitriding nitrogen pressure

Figure III.19 shows that the Cr_2N peak corresponding to the (300) plane is the most intense followed by that corresponding to the (113) plane, and finally the peak corresponding to the (112) plane for all nitriding pressures. Also, it should be noted that for each diffraction plane, the intensities of the chosen Cr_2N peaks increase with increasing nitrogen pressure up to 4 Torr, then they decrease after plasma nitriding at 4.5 and 5 Torr. This evolution trend of the intensities of nitride peaks has also been reported by Borgioli et al. after plasma nitriding of AISI 316L austenitic stainless steel at about 430 °C for 5 h at a working pressure ranging between 1.13 and 15 Torr (1.5 – 20 hPa) [87]. The increase in Cr_2N peak intensities with increasing nitrogen pressure up to 4 Torr can be attributed to the increase in the amount of crystallised Cr_2N compounds. In effect, increasing nitrogen pressure up to 4 Torr in the plasma nitriding chamber results in an increase in the amount of nitrogen atoms that reach the surface of the hard chromium electroplated layer, which promotes the formation of Cr_2N compounds under the thermodynamic conditions carried out in the chamber. On the other hand, the decrease in the intensities of the Cr_2N peaks after plasma nitriding at 4.5 Torr can be attributed to grains rotation. Stinville et al. have reported that during the formation of the nitride layer, the grains on the surface tend to rotate [88]. The effect of nitrogen pressure of plasma nitriding on surface texture will be more developed in future works.

The chemical composition of a representative spot on the surface of the hard chromium electroplated layer after plasma nitriding at 4 Torr was measured by EDS, and the results are shown in Figure III.20.
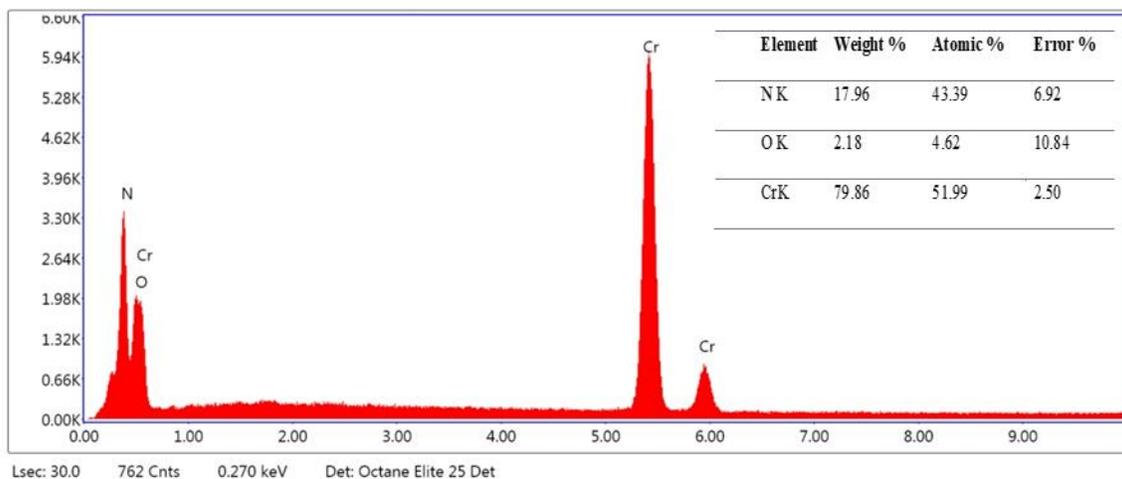
Figure III.20: EDS results of the hard chromium electroplated layer after plasma nitriding at 4 Torr

The EDS results indicate that the surface layer contains chromium and nitrogen elements with an oxygen atomic percentage of less than 5%, which indicates that the layer is not highly contaminated. The EDS spectrum reveals a nitrogen ray at about 0.333 keV and chromium L_α, K_α and K_β rays at about 0.5 keV, 5.476 keV and 6 keV, respectively. The ratio of chromium to nitrogen is close to CrN rather than Cr_2N. However, the X-ray diffraction pattern of the hard chromium electroplated layer after plasma nitriding at 4 Torr did not show any CrN peaks. This difference indicates that the amount of CrN compounds was small, thus they were not detected by the X-ray Diffractometer. The difference between the X-ray diffraction pattern and the EDS results of a plasma nitrided hard chromium electroplated layer has also been reported by Shen et al.[50]. However, they attributed this difference to a very thin CrN layer at the surface, as they noted two very weak peaks of CrN in the X-ray diffraction pattern of the characterised sample.

The average crystallite size of the Cr_2N compounds was estimated using the most intense peak, corresponding to the (300) plane, based on Scherrer's equation. The obtained value was in the order of nanometres in all nitriding pressure conditions, and it ranged between about 16 and 29 nm. The recorded average crystallite size is acceptable with regard to our plasma nitriding conditions (temperature of 600 °C and time of 90 min), and compared to Kocabaş et al. who have reported an average crystallite size of about 50 nm in a chromium nitrides layer obtained by hard chromium electroplating and plasma nitriding at 700 °C for a relatively long nitriding time [53].

III.5.2. Effect of nitrogen pressure on surface morphological properties

III.5.2.1. Plan-view analysis

Figure III.21 presents SEM micrographs of the surface of the hard chromium electroplated layer after plasma nitriding at 3, 3.5, 4, 4.5 and 5 Torr.
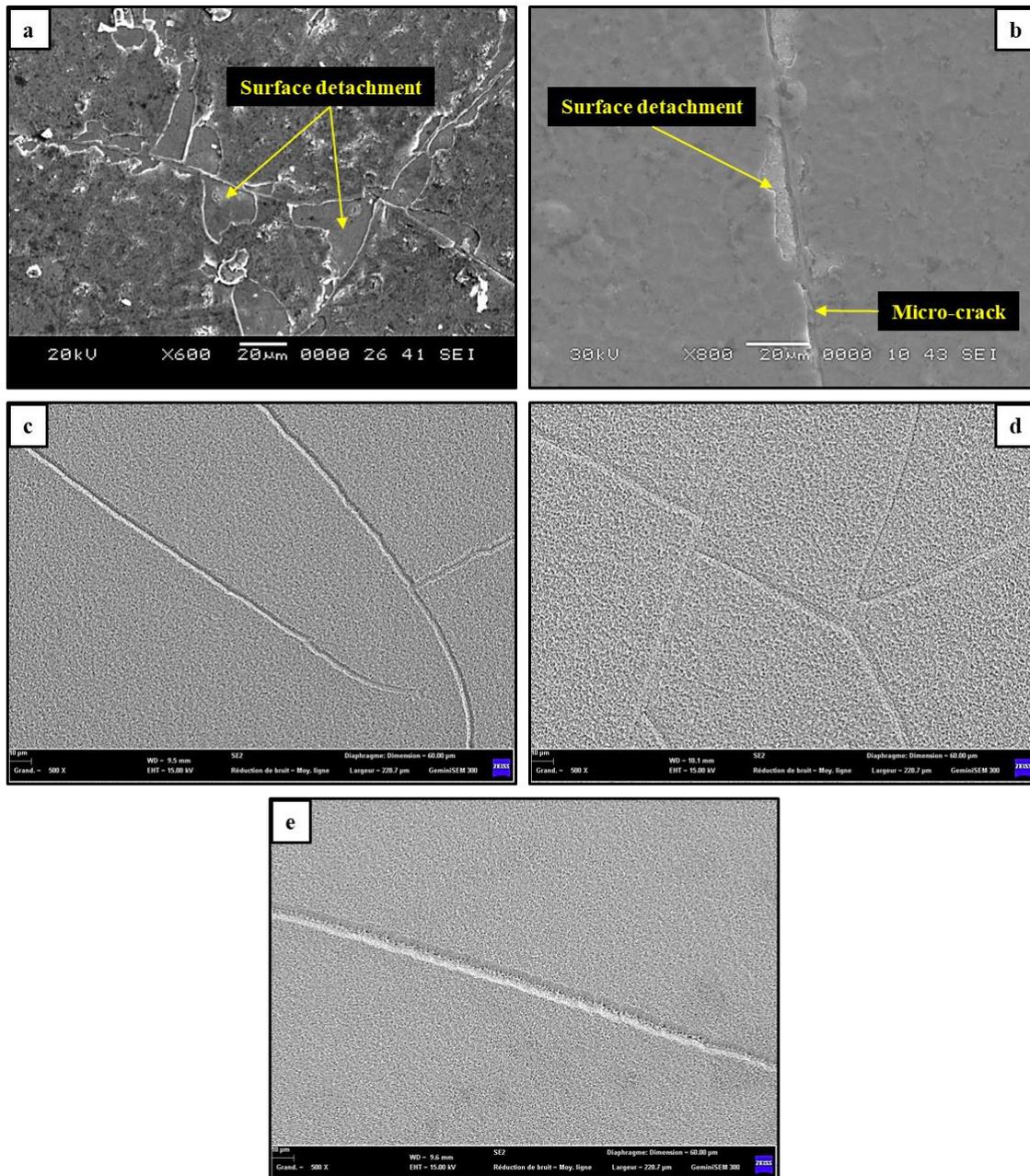
Figure III.21: SEM micrographs showing the surface morphology of the hard chromium electroplated layer after plasma nitriding at a) 3 Torr, b) 3.5 Torr, c) 4 Torr, d) 4.5 Torr and e) 5 Torr

Figure III.21 shows that the surface of the hard chromium electroplated layer after plasma nitriding at 3 and 3.5 Torr contains detached areas. However, the detached areas in the sample nitrided at 3.5 Torr exist only along some micro-cracks. On the other hand, the surface of the hard chromium electroplated layer after plasma nitriding at 4, 4.5 and 5 Torr does not contain detached areas, and it is covered homogeneously. The decrease in the number of the detached areas after

plasma nitriding at 3.5 Torr and their absence after plasma nitriding at 4, 4.5 and 5 Torr can be due to the increase in the amount of crystallised Cr_2N compounds in the diffusion layer at the surface of the hard chromium electroplated layer with increasing nitrogen pressure. The high amount of crystallised Cr_2N compounds increases the compactness of the diffusion layer because of the compressive stresses induced by volume expansion. Buijnsters et al. have reported that the volume expansion that accompanies the transformation of chromium to Cr_2N is about 250 % [39]. Figure III.21 also shows the presence of micro-cracks after plasma nitriding at the five nitrogen pressure conditions. The morphology and the density of micro-cracks will be discussed in the next section.

Figure III.22 shows that the surface between micro-cracks after plasma nitriding at the five nitrogen pressure conditions is rough and porous. The surface porosity and roughness after nitridation of chromium have also been reported in the literature [39], [89]. The shown surface morphology can be attributed to the formation and growth mechanisms of the Cr_2N compounds at the surface of the hard chromium electroplated layer as well as to the ionic bombardment during the plasma nitriding process.
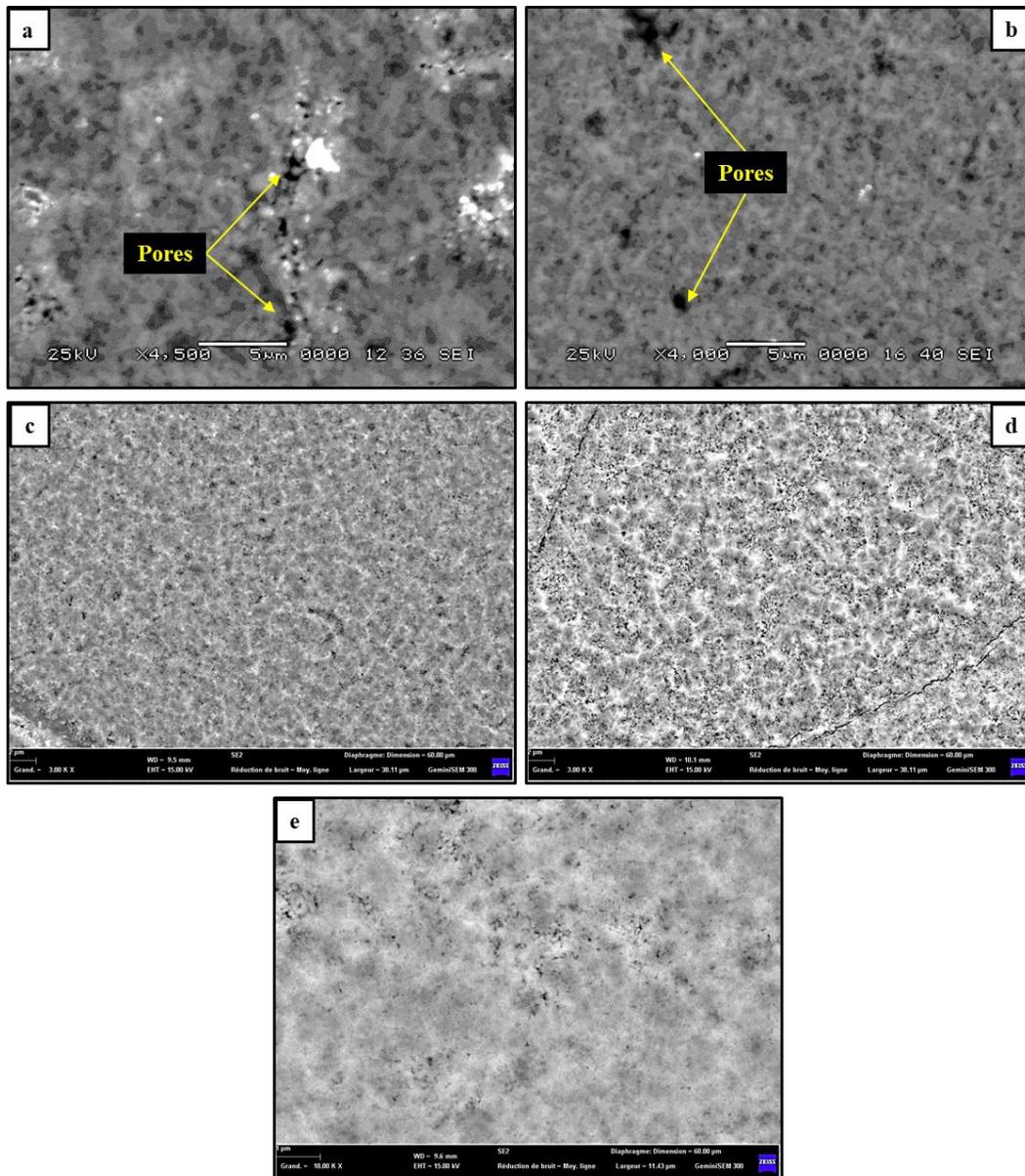
Figure III.22: SEM micrographs showing the morphology of surface between micro-cracks after plasma nitriding of the hard chromium electroplated layer at a) 3 Torr, b) 3.5 Torr, c) 4 Torr, d) 4.5 Torr and e) 5 Torr

III.5.2.2. Analysis of micro-cracks

III.5.2.2.1. Micro-cracks density

Figure III.23 presents some representative SEM micrographs of the micro-cracks distribution at the surface of the hard chromium electroplated layer after plasma nitriding at 3, 3.5, 4, 4.5 and 5 Torr.
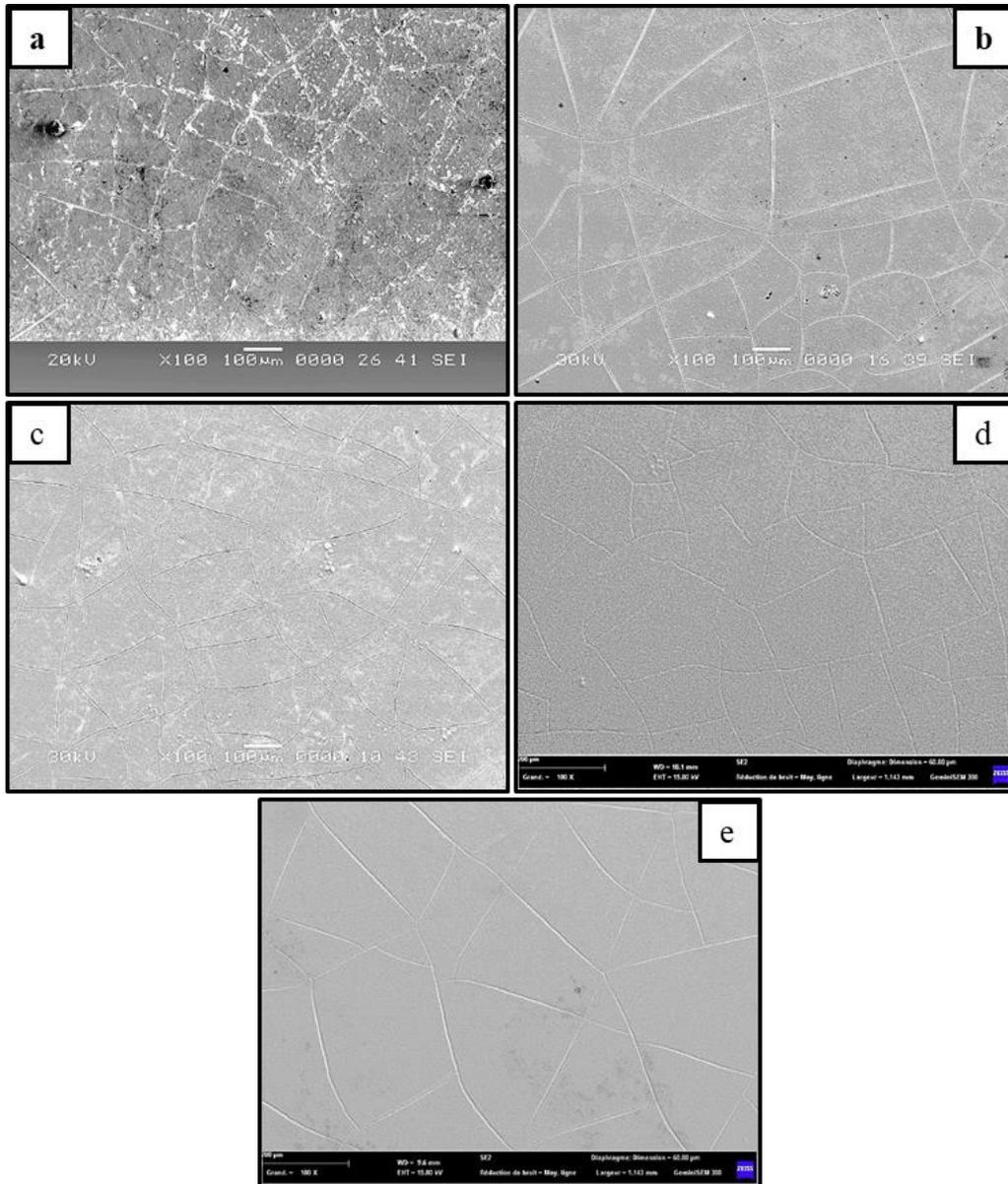
Figure III.23: SEM micrographs of the distribution of micro-cracks after plasma nitriding at:
a) 3 Torr, b) 3.5 Torr, c) 4 Torr, d) 4.5 Torr, e) 5 Torr

The SEM micrographs in Figure III.23 show that the density of micro-cracks change with the change of nitriding nitrogen pressure. By using a technique developed by Nascimento and Voorwald (see Section II.8.1.3.1), the density of micro-cracks as a function of the nitriding nitrogen pressure is presented in Figure III.24.
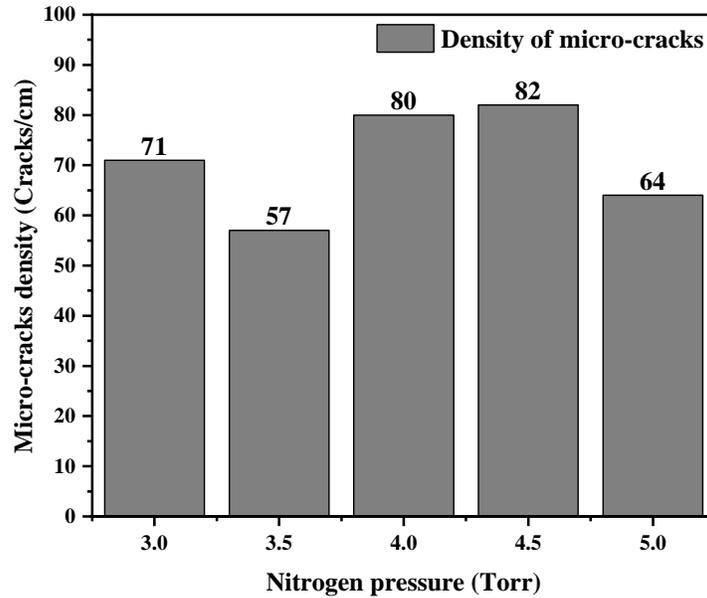
Figure III.24: Micro-cracks density as a function of nitriding nitrogen pressure

Figure III.24 shows that in general, the micro-cracks density increases with increasing nitriding nitrogen pressure up to 4.5 Torr, then it decreases after plasma nitriding at 5 Torr. The increase in micro-cracks density with increasing nitrogen pressure up to 4.5 Torr can be attributed to tensile stresses induced by the release of internal stresses from the hard chromium electroplated layer due to the heat generated on the sample surface by ion bombardment during plasma nitriding. Sarraf et al. have reported that at high-temperature conditions in conventional plasma nitriding, the internal stresses in the hard chromium electroplated layer are relieved due to the formation of intermediate unstable chromium hydrides, and then the decomposition of the hydrides results in a volume shrinkage of 18% [52]. This volume shrinkage causes the tensile stresses that induce cracking [52]. In contrast, the decrease in the density of micro-cracks after plasma nitriding at 5 Torr can be attributed to the decrease in the heat generated by ionic bombardment due to the decrease in the nitrogen ions attracted to the surface of the electroplated chromium. The decrease of the density of nitrogen ions and charged particles at high nitriding pressure have been reported in the literature [81]. It should be noted that the micro-cracks density after plasma nitriding at the five nitriding nitrogen pressure is higher than that after hard chromium electroplating (~ 49 cracks/cm).

III.5.2.2.2. Micro-cracks morphology

Figure III.25 presents SEM micrographs showing the morphology of the micro-cracks after plasma nitriding of hard chromium electroplated layer at 3.5, 4, 4.5 and 5 Torr. The morphology of micro-cracks in the sample nitrided at 3 Torr will not be discussed because of the high amount of detached areas.
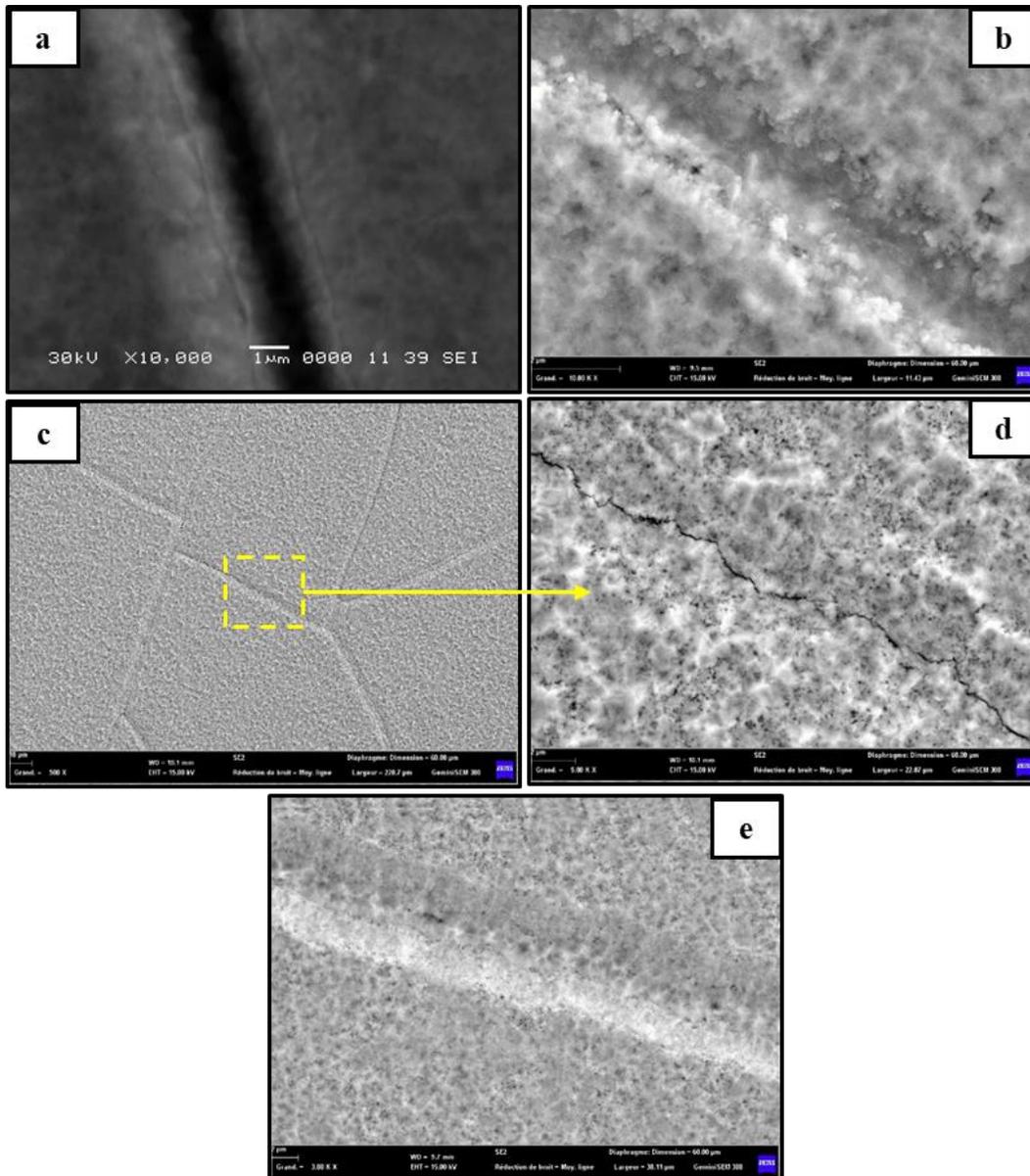
Figure III.25: SEM micrographs showing the micro-cracks morphology at the surface of the hard chromium electroplated layer after plasma nitriding at: a) 3.5 Torr, b) 4 Torr, c) and d) 4.5 Torr and e) 5 Torr

By examining Figure III.25, it is noted that the micro-crack in the sample nitrided at 3.5 Torr is unfilled and that it has a white zone along its edges. The white zone can be attributed to the high amount of nitrogen atoms attracted to the edges of the micro-crack because of the change in the morphology of the surface near the micro-crack. In contrast, the micro-crack in the sample nitrided at 4 Torr is partially filled. The area within the micro-crack was characterised by EDS, and the results are shown in Figure III.26.

	Weight %	Atomic %	Error %
N K	19.87	46.67	6.85
O K	1.85	3.80	12.74
Cr K	78.28	49.53	2.52
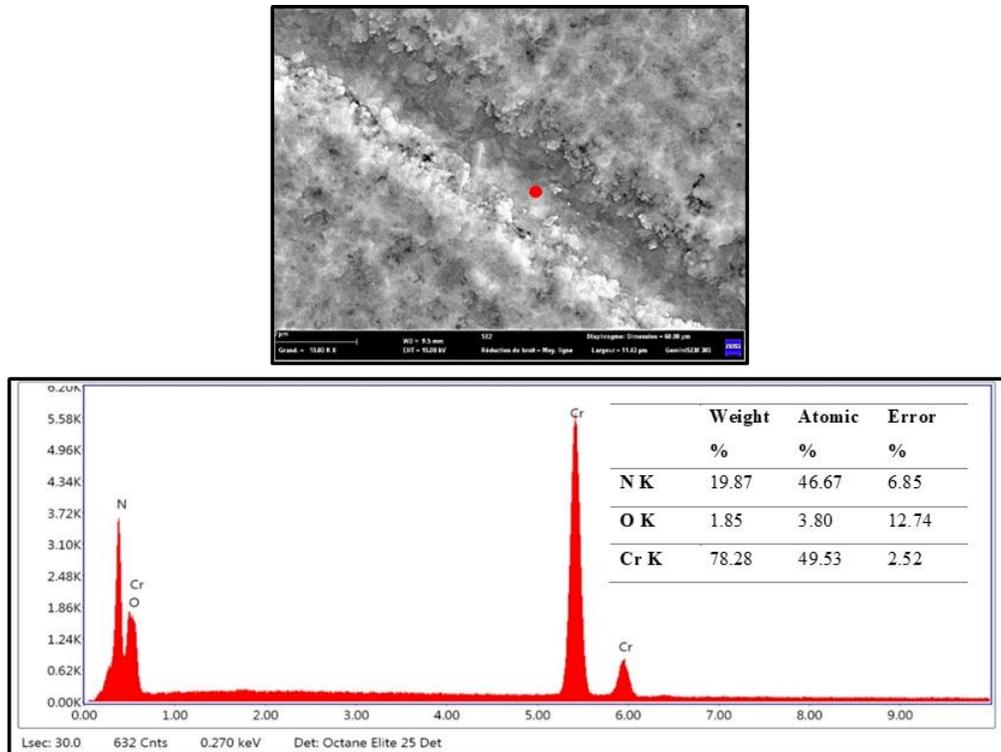
Figure III.26: EDS results of the area inside the micro-crack observed in the surface after plasma nitriding at 4 Torr

The EDS results indicate that the micro-crack is filled with chromium nitrides because it has the same elemental composition and relatively the same atomic ratio of chromium to nitrogen as that recorded on the surface of the hard chromium electroplated layer after plasma nitriding at 4 Torr (see Section III.5.1). After plasma nitriding at 4.5 and 5 Torr, the micro-crack is almost filled with chromium nitrides. The filling of the micro-cracks is attributed to the volume expansion induced by the formation of chromium nitrides [52].

III.5.3. Effect of nitrogen pressure on cross-sectional morphology

Figure III.27 presents the cross-sectional micrographs of the hard chromium electroplated layer after plasma nitriding at 3, 3.5, 4, 4.5 and 5 Torr.
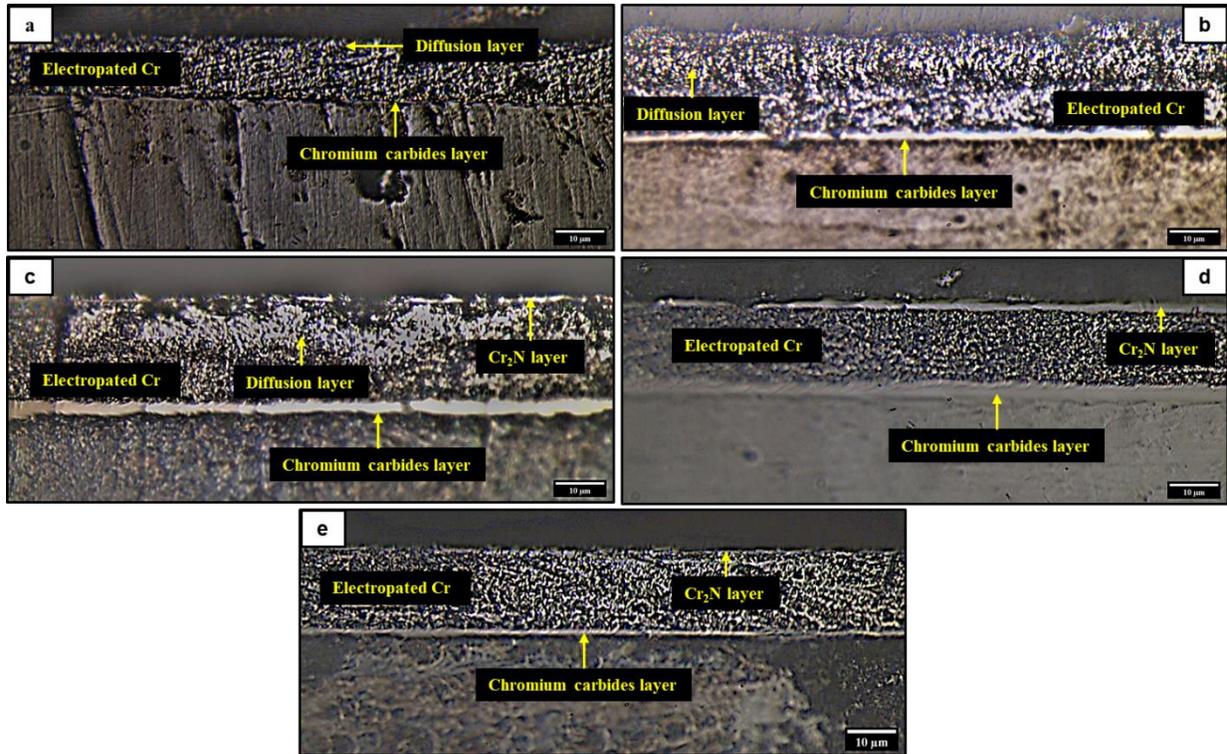
Figure III.27: Cross-sectional micrographs of the samples after plasma nitriding at: a) 3 Torr, b) 3.5 Torr, c) 4 Torr, d) 4.5 Torr and e) 5 Torr (Etching: Aqua regia solution, Magnification X1000)

The cross-sectional micrographs shown in Figure III.27 show that new layers are formed within the hard chromium electroplated layer after plasma nitriding at the five nitriding nitrogen pressures. According to several research articles in the literature [48], [55], [82], the newly formed layers are the chromium carbides layer, the diffusion layer and the Cr_2N layer.

The chromium carbides layer is formed at the interface between the hard chromium electroplated layer and the 35NCD6 steel substrate by the diffusion of carbon atoms from the substrate to the chromium electroplated layer. In effect, the diffusion of carbon atoms takes place due to the high affinity of carbon to chromium compared to its affinity to iron [55].

Figure III.28 presents the evolution of the thickness of the chromium carbides layer as a function of nitriding nitrogen pressure. However, the thickness of the chromium carbides layer in the sample nitrided at 3 Torr is not presented as it cannot be clearly defined.
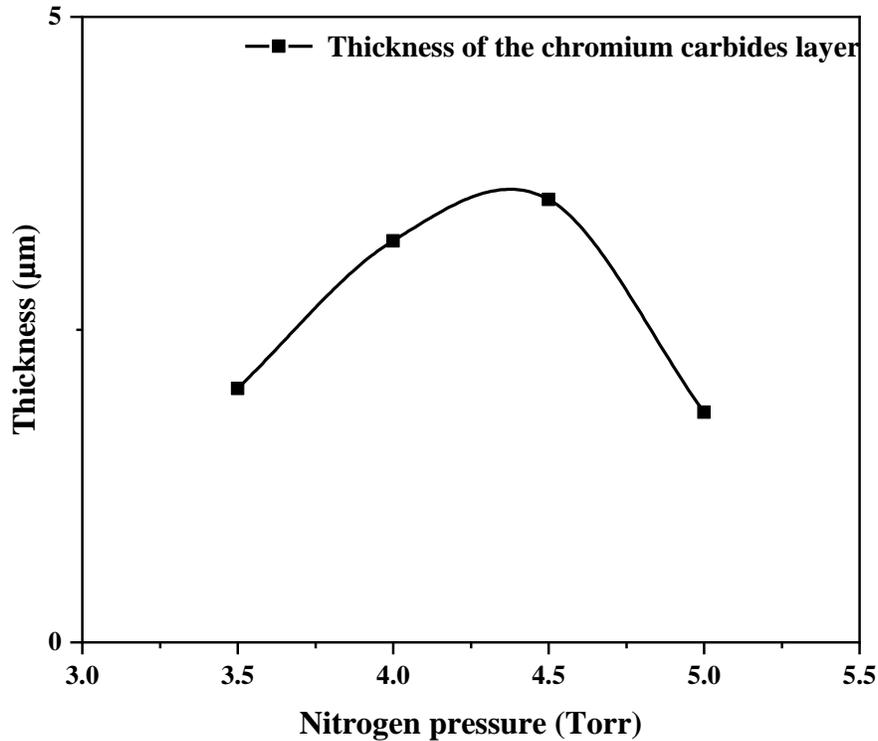
Figure III.28: Evolution of the thickness of the chromium carbides layer as a function of nitrogen pressure

The thickness of the chromium carbides layer increases from about 2.03 µm after plasma nitriding at 3.5 Torr to about 3.54 µm after plasma nitriding at 4.5 Torr, and then decreases to about 1.84 µm after plasma nitriding at 5 Torr. The change in thickness of the chromium carbides layer can be attributed to the change in the temperature of samples during the plasma nitriding process due to ionic bombardment.

By examining the cross-sectional micrographs shown in Figure III.28, it is noted that the diffusion layer is observed only in the samples plasma nitrided at 3, 3.5 and 4 Torr. The thickness of the diffusion layer is about 1µm in the sample nitrided at 3 Torr, 11.26 µm in the sample nitrided at 3.5 Torr and 7.87 µm in the sample nitrided at 4 Torr. The increase in the thickness of the diffusion layer after increasing the nitrogen pressure from 3 to 3.5 Torr is due to the increase in the amount of nitrogen ions attracted to the surface of the hard chromium electroplated layer and the

heat generated by ionic bombardment. Then, the decrease in the thickness of the diffusion layer in the sample nitrided at 4 Torr is attributed to the formation of a Cr_2N layer from the diffusion layer. The formed Cr_2N layer acts as a diffusion barrier that limits the diffusion of nitrogen atoms into the surface of the hard chromium electroplated layer. Dasgupta et al. have reported that the diffusion kinetics may become slow as a result of the retard in the diffusion of nitrogen atoms into the stable Cr_2N layer that forms at the beginning of the nitriding process at relatively high nitriding pressure [49]. In contrast, the absence of the diffusion layer in the samples nitrided at 4.5 and 5 Torr can be attributed to the rapid conversion of the diffusion layer into a Cr_2N layer due to the increased amount of nitrogen.

The Cr_2N layers observed in the samples nitrided at 4, 4.5 and 5 Torr have thicknesses of about 1.44 µm, 1.96 µm and 1.03 µm, respectively. The slight increase in the thickness of the Cr_2N layer after increasing nitrogen pressure from 4 to 4.5 Torr can be attributed to the increase of temperature at the surface of the sample due to ionic bombardment in addition to the increase of the amount of nitrogen atoms at the surface of the hard chromium electroplated layer because of the increased amount of attracted nitrogen ionic species. After that, the decrease of the Cr_2N layer thickness in the sample plasma nitrided at 5 Torr can be caused by the decrease in sample's temperature owing to the decrease in ionic bombardment as well as the decrease of attracted nitrogen ionic species that reach the surface of the hard chromium electroplated layer at high nitriding pressures.

III.5.4.   Effect of nitrogen pressure on mechanical properties

III.5.4.1. Cross-sectional microhardness

The microhardness of the chromium carbides layer, the unchanged chromium electroplated layer, and the substrate in the samples nitrided under the five nitrogen pressure conditions was tested using an indenter equipped with Vickers tip under a load of 10 gf. However, the chromium nitrides layer was not tested because it was difficult to perform the test near the edge of the sample (edge effect). Figure III.29 shows the evolution of microhardness of the chromium carbides layer, the unchanged chromium electroplated layer, and the substrate as a function of nitriding nitrogen pressure.
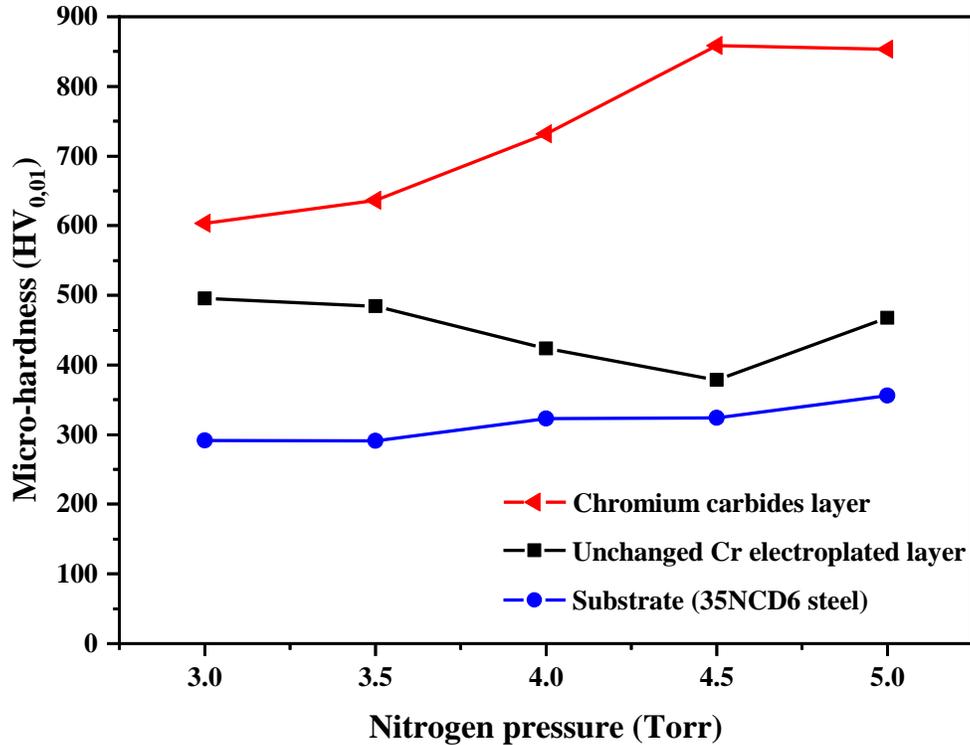
Figure III.29: Evolution of microhardness of the chromium carbides layer, unchanged chromium electroplated layer and substrate as a function of nitrogen pressure

Figure III.29 shows that the chromium carbides layer is harder than the unchanged chromium electroplated layer and the substrate material after plasma nitriding at the five nitrogen pressure conditions. Moreover, the unchanged chromium electroplated layer is harder than the 35NCD6 steel substrate.

The microhardness of the 35NCD6 steel substrate after plasma nitriding under all pressure conditions is similar, and it is lower than that before plasma nitriding (see Section III.2). This decrease in substrate microhardness is due to the change in microstructure of the 35NCD6 steel caused by the nitriding temperature and holding time. A similar decrease in hardness has been reported by Lee and Su who have noted a decrease in hardness of quenched AISI 4340 steel from about 660 HV to about 356 HV after tempering at 650 °C for 2 hours, with a change in microstructure from martensitic to ferritic [70].

The microhardness of the chromium carbides layer increases from about 603 HV after plasma nitriding at 3 Torr to about 858 HV after plasma nitriding at 4.5 Torr, then, it slightly decreases to about 853 HV after plasma nitriding at 5 Torr. The microhardness of the chromium

carbides layer is directly related to its thickness. As reported earlier, the thickness of the chromium carbides layer increases with increasing nitrogen pressure up to 4.5 Torr, then it decreases after plasma nitriding at 5 Torr, which is in good agreement with the evolution of microhardness of the chromium carbides layer.

For the unchanged chromium electroplated layer, the microhardness decreases with increasing nitriding nitrogen pressure up to 4.5 Torr, then it increases slightly when the nitrogen pressure increases up to 5 Torr. The hardness of the unchanged chromium electroplated layer is affected by the heat generated during the preparation step prior to plasma nitriding and that generated during plasma nitriding. Many published scientific papers have reported that the heat generated during gas and plasma nitriding induces a decrease in the hardness of the electroplated chromium [43], [46], [54]. The generated heat releases the residual stress and the entrapped hydrogen that are responsible for the hardness of the electroplated chromium [43].

III.5.4.2. Surface mechanical properties

In order to study the mechanical properties of the surface after plasma nitriding at 3, 3.5, 4, 4.5 and 5 Torr, the samples were tested using a Nano-indenter equipped with a Berkovich type tip, under a maximum load of 60 mN. The experimental load-displacement curves of the tested samples are presented in Figure III.30 and the obtained mechanical properties are summarised in Table III.3.
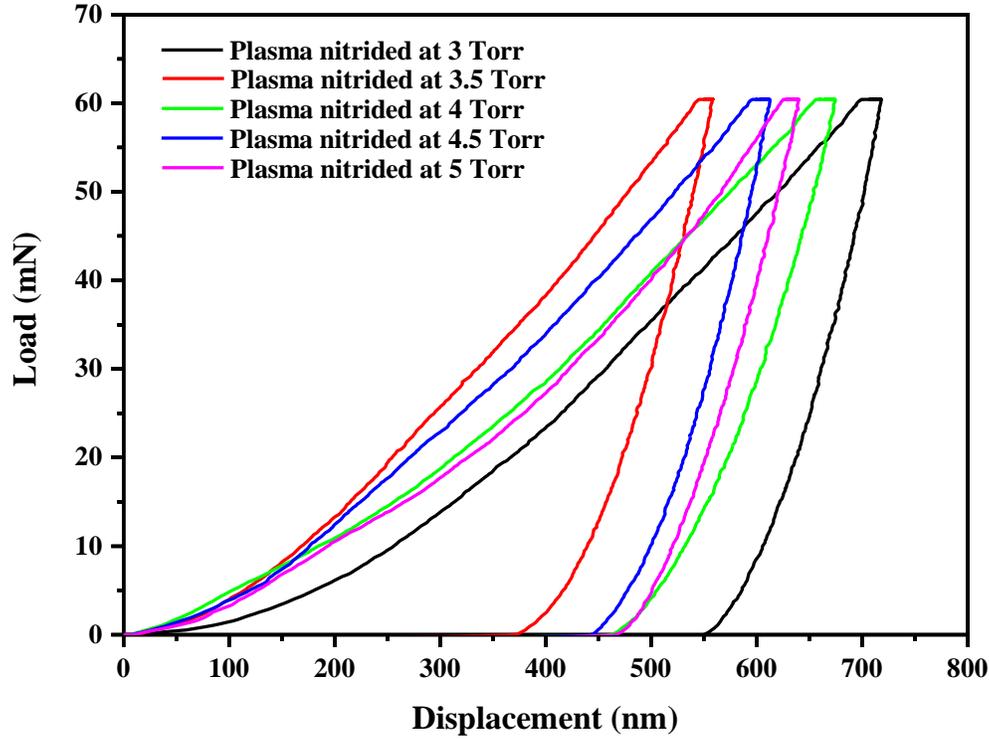
Figure III.30: Load-displacement curves of the hard chromium electroplated layer after plasma nitriding at 3, 3.5, 4, 4.5 and 5 Torr

Table III.2: Mechanical properties of the surface of the hard chromium electroplated layer after plasma nitriding at 3, 3.5, 4, 4.5 and 5 Torr

Sample	H (Gpa)	E (Gpa)	H/E	H^3/E^2 (GPa)	Maximum depth, h_{max} (nm)
Plasma nitrided at 3Torr	10.65	247.84	0.043	0.020	731.59
Plasma nitrided at 3.5Torr	15.19	302.84	0.050	0.038	557.62
Plasma nitrided at 4Torr	12.45	206.24	0.060	0.045	661.51
Plasma nitrided at 4.5 Torr	13.08	264.62	0.049	0.032	623.09
Plasma nitrided at 5 Torr	12.38	233.47	0.053	0.035	657.2

By examining Figure III.30, It is noted that the load-displacement curves of the samples plasma nitrided at 3.5, 4, 4.5, and 5 Torr superimpose for the first 50 nm of the penetration depth, indicating that elastic deformation is dominant at this stage [90] due to the shallow outer surface modified by ion bombardment. Furthermore, the shape of the load-displacement curves indicates that all samples have an elasto-plastic response [91].

III.5.4.2.1. Effect of nitrogen pressure on hardness and elastic modulus

Figure III.31 presents the evolution of hardness and elastic modulus as a function of nitriding nitrogen pressure.
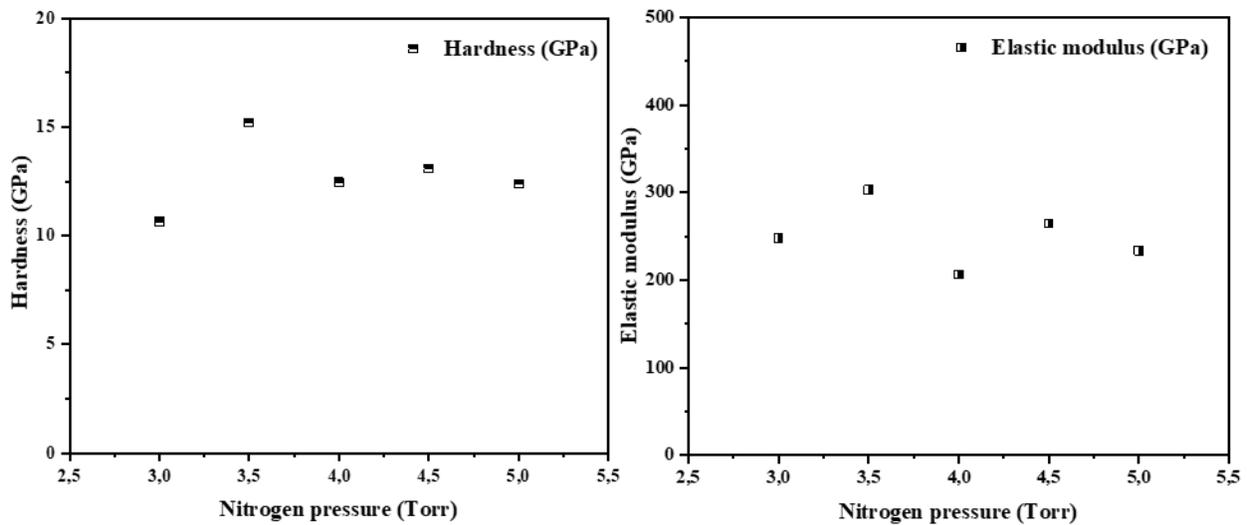
Figure III.31: Evolution of hardness and elastic modulus as a function of nitriding nitrogen pressure

Figure III.31 shows that the hardness increases from about 10.65 GPa for the sample nitrided at 3 Torr to about 15.19 GPa after plasma nitriding at 3.5 Torr, and it shows relatively comparable hardness values for the samples nitrided at 4, 4.5, and 5 Torr. In fact, the slightly higher hardness values of the samples nitrided at 4 and 4.5 Torr compared to the sample nitrided at 5 Torr are attributed to the slightly thick Cr_2N layer on their surfaces. Guan et al. have reported that increasing the thickness of the Cr_2N monolayer in a Cr_2N/Cr multilayer results in an increase in hardness [86]. In contrast, the high hardness in the sample nitrided at 3.5 Torr is attributed to the high thickness of the diffusion layer. Knowing that the thickness of the diffusion layer is about 11μm and the maximum penetration depth recorded in the sample nitrided at 3.5 Torr is about 558 nm, it can be concluded that the recorded hardness corresponds to the diffusion layer only because the maximum penetration depth is less than the 10th of the diffusion layer thickness. The decrease

in hardness of the nitrided samples at 4, 4.5, and 5 Torr, although they all have a well-defined Cr_2N layer on their surfaces, can be attributed to the contribution of the soft chromium electroplated layer in the recorded hardness because the maximum penetration depth in all the three samples (see Table III.3) exceeds the 10th of the thickness of the Cr_2N layer (see Section 5.4). The surface hardness of the Cr_2N/ Cr-electroplated layer for all nitrided samples is higher than that obtained by Tabrizi et al. who have reported a surface hardness of about 1109 $HV_{0.25}$ (~ 10.88 GPa) for a sample chromium electroplated and plasma nitrided at 600°C for 8 hours [92].

The elastic modulus values of the nitrided samples at 3, 4, 4.5, and 5 Torr are almost similar (see Table III.3) due to the explicit contribution of the chromium electroplated layer in the elastic response during the Nanoindentation test, which is not the case for the sample nitrided at 3.5 Torr.

III.5.4.2.2. Effect of nitrogen pressure on the elasto-plastic behaviour

The elasto-plastic behaviour of the nitrided hard chromium electroplated layer can be discussed based on the (H/E) and (H^3/E^2) ratios [93]. The values of these ratios for all nitriding pressure conditions are summarised in Table III.3. As mentioned earlier, the (H/E) ratio represents the elastic deformation to failure, and the (H^3/E^2) ratio represents the plastic deformation to failure. The highest values of these ratios ((H/E) = 0.06 and (H^3/E^2) = 0.045 GPa) were reported for the sample nitrided at 4 Torr. This result is attributed to the low elastic modulus recorded in the sample nitrided at 4 Torr compared to that recorded in the samples nitrided at the other nitrogen pressure conditions. Moreover, the high value of the (H^3/E^2) ratio indicates that the sample nitrided at 4 Torr has the best resistance to plastic deformation because it has the best combination of hardness and ductility. The good elasto-plastic behaviour of the sample nitrided at 4 Torr can be attributed to the synergistic effect of the mechanical properties of the hard Cr_2N layer, the diffusion layer, the ductile unchanged chromium electroplated layer and the chromium carbides layer. On the other hand, the samples nitrided under the other nitrogen pressure conditions have comparable elasto-plastic behaviour, except for the sample nitrided at 3 Torr.

III.5.5. Effect of nitrogen pressure on tribological properties

To study the tribological behaviour of the hard chromium electroplated layer after plasma nitriding at 3, 3.5, 4, 4.5, and 5 Torr, the samples were tested using the ball-on-disk experiment.

The test was performed in dry conditions using a WC ball under a normal load of 10 N and a sliding speed of 5 cm/s to pass a distance of 100 meters.

III.5.5.1. Effect of nitrogen pressure on frictional behaviour

Figure III.32 presents the evolution of friction coefficient of the hard chromium electroplated layer after plasma nitriding at 3, 3.5, 4, 4.5 and 5 Torr.
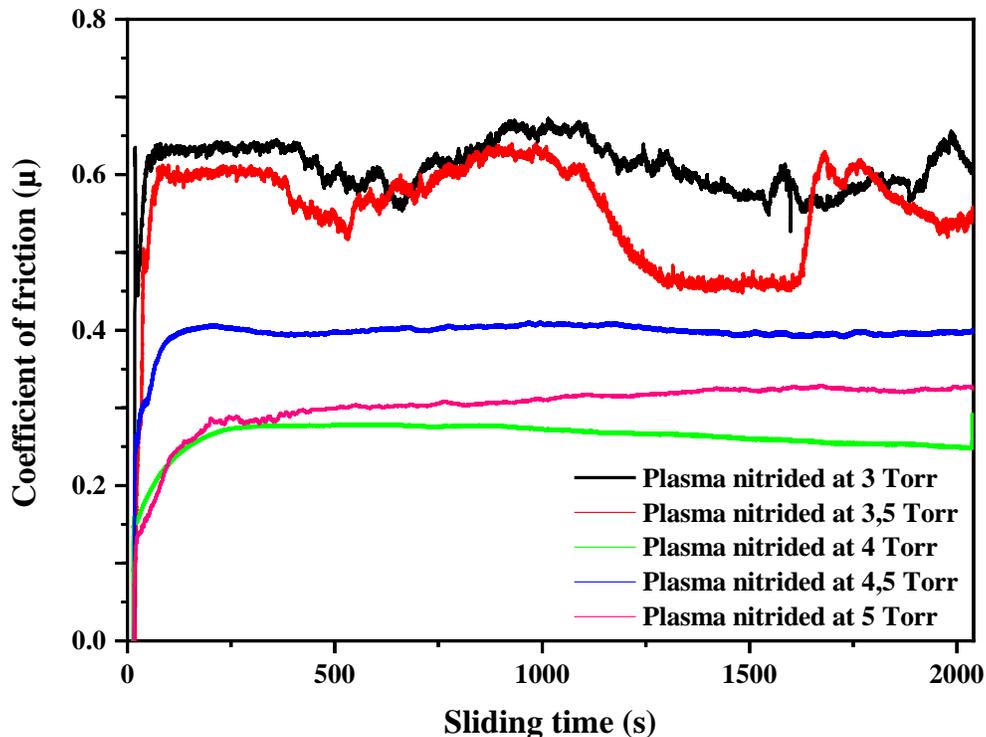
Figure III.32: Evolution of friction coefficient as a function of sliding time during ball-on-disk test on samples plasma nitrided at 3, 3.5, 4, 4.5 and 5 Torr

Figure III.32 shows that the friction coefficient increases rapidly at the beginning of the test for all samples (short phase of rapid growth) due to the first contact between the sliding ball and the surface. Furthermore, it is noted that the friction behaviour is comparable in the samples nitrided at 3 and 3.5 Torr as well as in the samples nitrided at 4, 4.5 and 5 Torr. The evolution of the friction coefficient in the samples nitrided at 3 and 3.5 Torr is unstable because the surface of both samples is not homogeneous. In fact, the surface is composed of hard Cr_2N particles from the diffusion layer and of ductile electroplated chromium. The inhomogeneity of the surface leads to varying frictional forces and different reactions towards the sliding WC ball. On the other hand, the surface of the samples nitrided at 4, 4.5 and 5 Torr is composed of a Cr_2N layer, as shown in

the cross-sectional micrographs, so its response to the sliding WC ball is homogeneous with a stable evolution of the friction coefficient.

Figure III.33 shows the evolution of mean friction coefficient as a function nitrogen pressure.
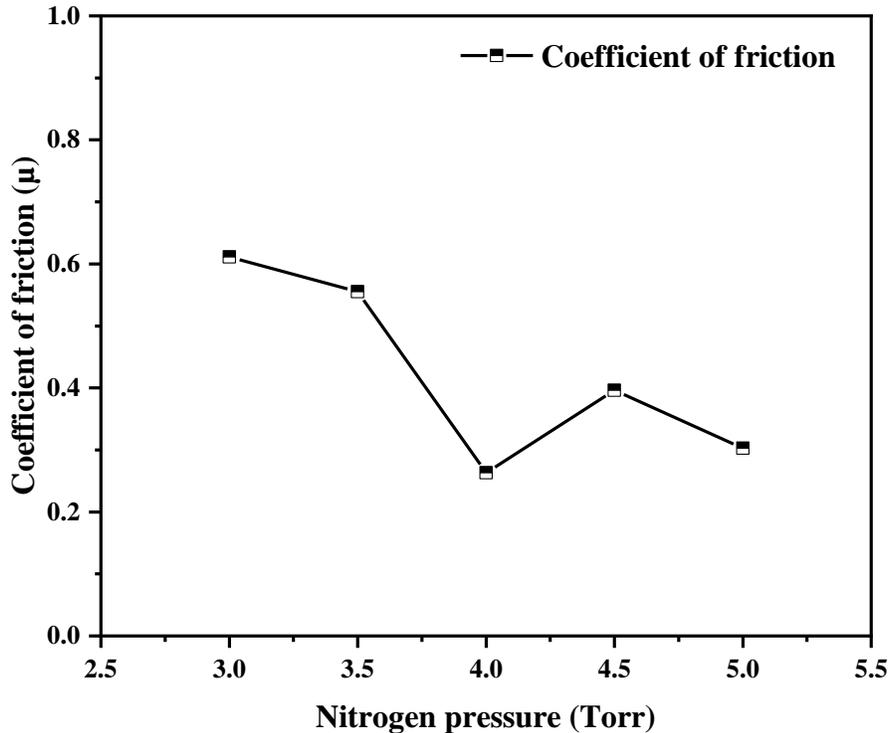
Figure III.33: Evolution of friction coefficient as a function of nitrogen pressure

The coefficient of friction decreases from about 0.61 for the sample nitrided at 3 Torr to 0.26 for the sample nitrided at 4 Torr, then, it increases to about 0.40 for the sample nitrided at 4.5 Torr and finally, it decreases again to about 0.30 for the sample nitrided at 5 Torr. It can be seen that the coefficients of friction of the samples nitrided at 4, 4.5 and 5 Torr are explicitly lower than those of the samples nitrided at 3 and 3.5 Torr. This difference in friction coefficient can be attributed to the frictional properties of the hard Cr_2N layer. Numerous published scientific articles have reported that the two types of chromium nitride (CrN and Cr_2N) have a low friction coefficient [86], [94], [95]. The sample nitrided at 4.5 Torr shows an increase in the friction coefficient compared to the samples nitrided at 4 and 5 Torr. This increase can be attributed to its high surface roughness caused by the energetic ion bombardment by nitrogen ionic species. It is known that surface roughness affects significantly the wear properties [96].

III.5.5.2. Effect of nitrogen pressure on wear behaviour

III.5.5.2.1. Weight loss analysis

The weight loss during the ball-to-disk test was measured by weighing each sample before and after the test using a balance with an accuracy of 0.0001g, and the results are shown in Figure III.34.
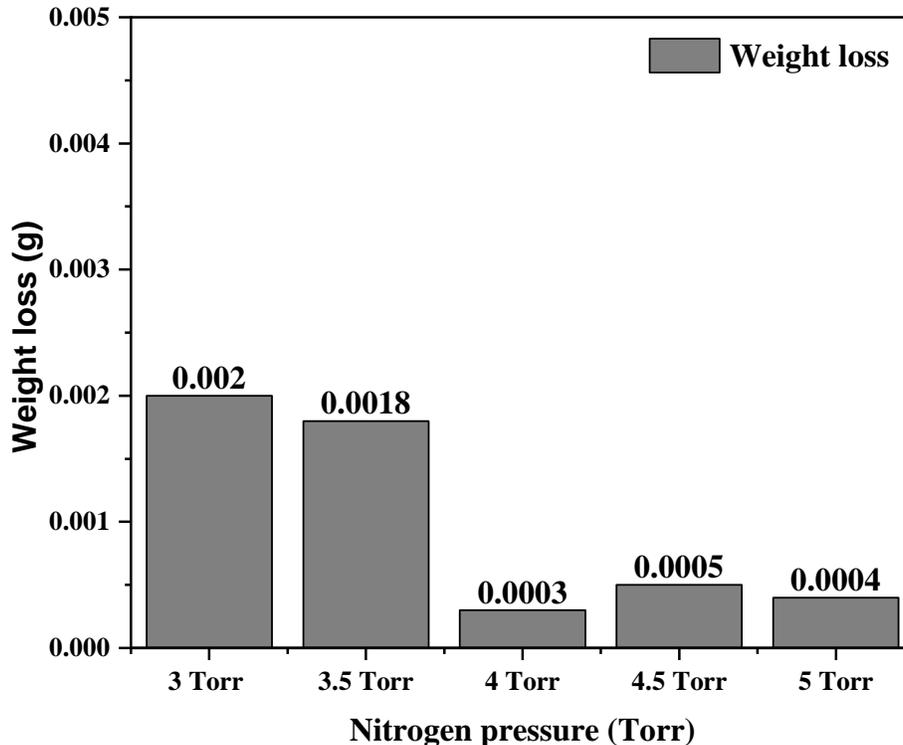
Figure III.34: Weight loss as a function of nitriding nitrogen pressure

Figure III.34 shows that the weight loss decreases slightly with increasing nitrogen pressure from 3 to 3.5 Torr, then, it decreases significantly when the nitrogen pressure is increased to 4 Torr. And after increasing the nitrogen pressure to 4.5 and 5 Torr, the weight loss increases slightly. The slight decrease in weight loss in the sample nitrided at 3.5 Torr is attributed to the increased amount of Cr_2N compounds formed from its thick diffusion layer. Increasing the amount of Cr_2N improves the mechanical properties of the surface as indicated by the H/E and H^3/E^2 ratios, which increased from 0.043 and 0.020 for the sample nitrided at 3 Torr to 0.050 and 0.038 for the sample nitrided at 3.5 Torr, respectively. On the other hand, the considerable decrease in weight loss (about 70%) in the samples nitrided at 4, 4.5 and 5 Torr can be attributed to the hard Cr_2N layer at the surface

layer. Wei et al. have reported that Cr_2N is the most effective wear resistance coating compared to Cr and CrN coatings [94].

III.5.5.2.2. Wear track analysis

Figure III.35 shows optical micrographs of the wear tracks in the samples nitrided at 3, 3.5, 4, 4.5 and 5 Torr.
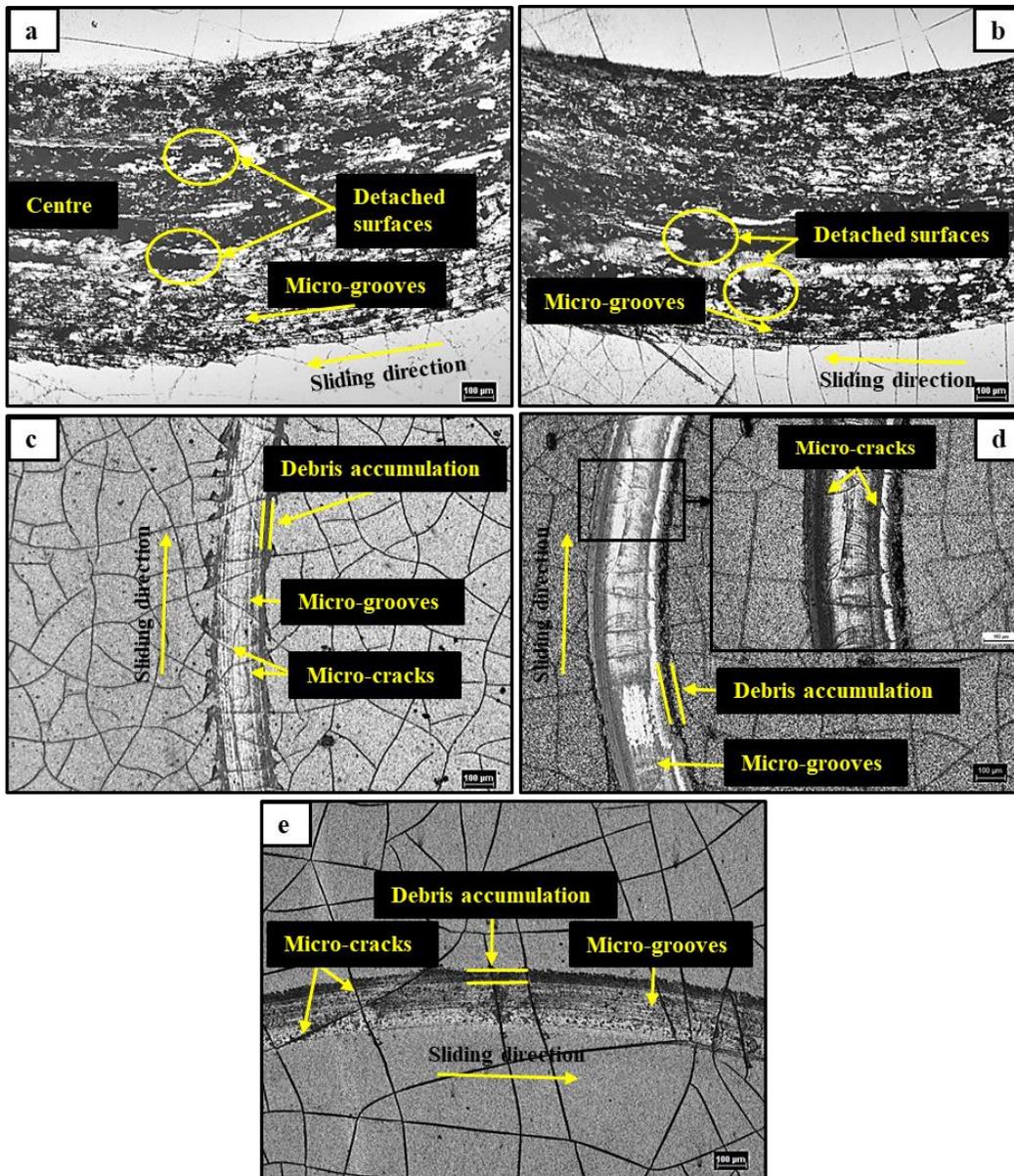
Figure III.35: optical micrographs of the wear tracks obtained after a ball-on-disk test on samples plasma nitrided at: a) 3 Torr, b) 3.5 Torr, c) 4 Torr, d) 4.5 Torr and e) 5 Torr

By examining the micrographs in Figure III.35, it can be noted that the width of the wear track changes with the change in nitrogen pressure. Figure III.36 presents the evolution of wear track width as a function of nitrogen pressure.
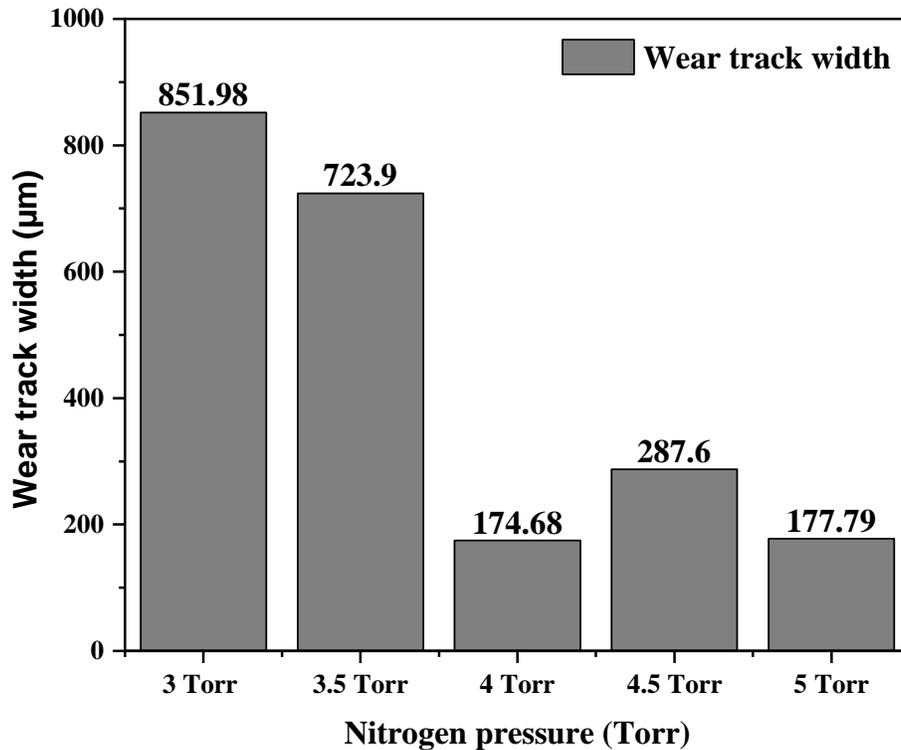
Figure III.36: Wear track width as a function of nitrogen pressure

Figure III.35 shows that the samples nitrided at 3 and 3.5 Torr have different wear track morphology than those nitrided at 4, 4.5, and 5 Torr, which may explain the significant change in the width of the wear track after plasma nitriding at 4 Torr, as shown in Figure III.36. This observation is in good agreement with the results of weight loss and coefficient of friction. The morphology of the wear track in the sample nitrided at 3 Torr is comparable to that of the sample nitrided at 3.5 Torr. Indeed, the wear track in both samples has a highly deformed area in the centre and a relatively less deformed area at the periphery. This difference can be attributed to the small area of contact between the sliding WC ball and the sample surface. The wear tracks in the samples nitrided at 3 and 3.5 Torr show several detached surfaces and microgrooves. These observations suggest that both adhesive and abrasive wear mechanisms are present. However, the adhesive wear is more dominant owing to the high amount of detached surfaces.

On the other hand, the wear track in the samples nitrided at 4, 4.5, and 5 Torr is smooth, and it shows several microgrooves and accumulation of wear debris at its periphery, suggesting that the wear mechanism is dominantly abrasive. It is important to note that the wear tracks of all three samples are crossed by the already existing micro-cracks. However, these micro-cracks did not affect the wear track area due to the presence of the Cr_2N particles that supported the surface against fracture. Guan et al. have reported that the hard Cr_2N phase in a Cr/Cr_2N nano-multilayer coatings can withstand the high applied load owing to its high hardness and adhesion strength [86].

The wear track properties and weight loss can be correlated to the mechanical properties of the surface based on the plastic deformation to failure ratio (H^3/E^2). The sample nitrided at 4 Torr has the highest H^3/E^2 ratio, which correlates well with its wear properties, as it has the lowest coefficient of friction, weight loss, and wear track width compared to the samples nitrided at the other nitrogen pressure conditions. This correlation is also maintained for the samples nitrided at 3, 4.5 and 5 Torr. However, it is not maintained for the sample nitrided at 3.5 Torr.

GENERAL CONCLUSION AND FUTURE WORKS

GENERAL CONCLUSION AND FUTURE WORKS

The objectives of this thesis were to produce a chromium nitrides layer by plasma nitriding of hard chromium electroplated layer in a pure nitrogen gas atmosphere, and to study the effect of nitrogen pressure of plasma nitriding on the structural, morphological, mechanical and tribological properties of the resulting chromium nitrides layer. The hard chromium electroplated layer was deposited on a low alloy 35NCD6 steel substrate in an industrial electroplating facility. After that, the hard chromium electroplated layer was plasma nitrided in a laboratory-made DC plasma nitriding furnace at the Centre for Development of Advanced Technologies (CDTA). The main results and conclusions that can be drawn from this research work are as the following:

- The hard chromium electroplated layer was successfully deposited on the low alloy 35NCD6 steel substrate.

The obtained hard chromium electroplated layer has the following characteristics:

- Amorphous structure and smooth surface with some micro-cracks;
- High surface hardness and a relatively low elastic modulus;
- High coefficient of friction and wear loss under a relatively severe conditions.

Thus, the characteristics of the obtained hard chromium electroplated layer indicate that it cannot be used as a protective coating against wear under severe working conditions.

The hard chromium electroplated layer was plasma nitrided in a pure nitrogen atmosphere at about 600 °C for 90 min, at a pressure of 3 Torr. The main results can be summarised in the following points:

- The main components of the surface layer were Cr_2N and chromium.
- The surface layer was characterised by detachments and micro-cracks.
- The hard chromium electroplated layer was transformed into three layers: nitrogen diffusion layer, unchanged chromium electroplated layer and chromium carbides layer.
- The hardness of the hard chromium electroplated layer decreased from about 1036 $HV_{0.01}$ to about 495 $HV_{0.01}$.

- The hardness of the diffusion layer with the contribution of the hardness of the unchanged chromium electroplated layer was about 10.65 GPa.

- The surface of the diffusion layer showed unstable frictional behaviour and low wear resistance.

Based on the above-mentioned results, we can conclude that plasma nitriding of hard chromium electroplated layer at a relatively low pressure of 3 Torr slightly increases the mechanical and tribological properties of the hard electroplated chromium surface layer.

To investigate the effect of nitrogen pressure on the structural, morphological, mechanical and tribological properties, the hard chromium electroplated layer was also plasma nitrided at 3.5, 4, 4.5 and 5 Torr. The main results can be summarised in the following points:

- The main surface components after plasma nitriding of the hard chromium electroplated layer under the five nitrogen pressure conditions were Cr_2N and Cr.

- The Cr_2N crystals had a preferred growth orientation parallel to the (300) plane.

- The increase of nitrogen pressure resulted in an increase in the amount of Cr_2N crystals.

- The average crystallite size of the formed Cr_2N crystals was in the order of nanometres.

- Surface detachments decreased after plasma nitriding at 3.5 Torr, and disappeared after plasma nitriding at 4, 4.5 and 5 Torr.

- After plasma nitriding of the hard chromium electroplated layer at 4, 4.5 and 5 Torr, a well-defined Cr_2N layer was formed on the surface.

- The surface layer after plasma nitriding was rough and porous.

- The micro-cracks were partially filled with chromium nitrides after plasma nitriding at 4 Torr, and almost filled after plasma nitriding at 4.5 and 5 Torr.

- The hard chromium electroplated layer was transformed into a diffusion layer, an unchanged chromium electroplated layer and a chromium carbides layer after plasma nitriding at 3, 3.5 Torr.

- The hard chromium electroplated layer was transformed into Cr_2N layer, diffusion layer, unchanged chromium electroplated layer and chromium carbides layer after plasma nitriding at 4 Torr.

- The hard chromium electroplated layer was transformed into Cr_2N layer, unchanged chromium electroplated layer and chromium carbides layer after plasma nitriding at 4.5 and 5 Torr.

- The maximum thickness of the Cr_2N layer was about 2μm, recorded for the sample plasma nitrided at 4.5 Torr.

- The soft chromium electroplated layer beneath the Cr_2N layer influenced the surface hardness results for the samples plasma nitrided at 4, 4.5 and 5 Torr.

- The maximum hardness of the (Cr_2N/electroplated-Cr) layer was about 13 GPa, recorded for the sample that was plasma nitrided at 4.5 Torr.

- The best tribological properties were obtained for the samples plasma nitrided at 4, 4.5 and 5 Torr.

These results indicate that the nitrogen pressure used for plasma nitriding significantly influences the morphological, mechanical and tribological properties of the hard chromium electroplated layer. Therefore, it is important to choose the nitriding pressure of plasma nitriding appropriately. In the case where the nitriding gas is pure nitrogen, we suggest a nitriding pressure between 4 and 4.5 Torr.

Future Works

- The present research work represents a starting point in the study of layers obtained with duplex surface treatment techniques. In the future, we aim to :

- Improve the mechanical and tribological properties of the plasma nitrided hard chromium electroplated layer in pure nitrogen atmosphere by optimising other nitriding parameters, such as temperature and time.

- Study in detail the phenomenon of micro-cracks and the possible ways to control it.

- Study in detail the effect of nitrogen pressure on the surface texture of the hard chromium electroplated layer after plasma nitriding.

- Study the effect of corrosion on the plasma nitrided hard chromium electroplated layer.

REFERENCES

REFERENCES

[1] T. Bell, H. Dong, and Y. Sun, "Realising the potential of duplex surface engineering," *Tribol. Int.*, vol. 31, no. 1–3, pp. 127–137, 1998.

[2] Z. Zeng, L. Wang, L. Chen, and J. Zhang, "The correlation between the hardness and tribological behaviour of electroplated chromium coatings sliding against ceramic and steel counterparts," *Surf. Coatings Technol.*, vol. 201, no. 6, pp. 2282–2288, 2006.

[3] W. D. Callister, *Materials science and engineering an introduction*. John Wiley, 2007.

[4] H. Berns and W. Theisen, *Ferrous materials: steel and cast iron*. Springer Science & Business Media, 2008.

[5] C. P. Sharma, *Engineering materials: properties and applications of metals and alloys*. PHI Learning Pvt. Ltd., 2003.

[6] A. S. M. H. Committee, "Properties and Selection: Irons, Steels, and High-Performance Alloys." ASM International, Jan. 01, 1990.

[7] F. Masuyama, "Low-alloyed steel grades for boilers in ultra-supercritical power plants," A. B. T.-M. for U.-S. and A. U.-S. P. P. Di Gianfrancesco, Ed. Woodhead Publishing, 2017, pp. 53–76.

[8] N. E. Prasad and R. J. H. Wanhill, *Aerospace materials and material technologies*, vol. 3. Springer, 2017.

[9] A. P. B. T.-I. to A. M. Mouritz, Ed., "Steels for aircraft structures," Woodhead Publishing, 2012, pp. 232–250.

[10] J. Dutta Majumdar and I. Manna, "Laser surface engineering of titanium and its alloys for improved wear, corrosion and high-temperature oxidation resistance," in *Woodhead Publishing Series in Electronic and Optical Materials*, J. Lawrence and D. G. B. T.-L. S. E. Waugh, Eds. Woodhead Publishing, 2015, pp. 483–521.

[11] T. Burakowski and T. Wierzchon, *Surface engineering of metals: principles, equipment, technologies*. CRC press, 1998.

[12] K. A. Chandler, *Marine and offshore corrosion: marine engineering series*. Elsevier, 2014.

[13] R. H. Madon, M. Fawzi, K. I. Sarwani, S. A. Osman, M. Azahari, and A. W. M. Razali, "Effect of Reaction Temperature on Steam Methane Reforming's yield over Coated Nickel Aluminide (Ni_3Al) Catalyst in Micro Reactor," *Energy*, vol. 1, p. 2, 2018.

[14] M. Pfeifer, *Materials enabled designs: The materials engineering perspective to product design and manufacturing*. Butterworth-Heinemann, 2009.

[15] Q. Zhang, D. Sando, and V. Nagarajan, "Chemical route derived bismuth ferrite thin films and nanomaterials," *J. Mater. Chem. C*, vol. 4, no. 19, pp. 4092–4124, 2016.

[16] G. Galvanotechnik eV, "Gütesicherung in der Galvanotechnik, Saulgau: Eugen G." Leuze

Verlag, 1987.

[17]   N. Kanani, *Electroplating: basic principles, processes and practice*. Elsevier, 2004.

[18]   L. M. Moretto and R. Seeber, "Controlled Potential Techniques in Amperometric Sensing," in *Environmental Analysis by Electrochemical Sensors and Biosensors*, Springer, 2014, pp. 239–282.

[19]   H. SILMAN, "Chromium Coatings," L. L. Shreir, R. A. Jarman, and G. T. B. T.-C. (Third E. Burstein, Eds. Oxford: Butterworth-Heinemann, 1994, pp. 13:99-13:110.

[20]   J. K. Dennis and T. E. Such, "Chapter 8 - Chromium plating," in *Woodhead Publishing Series in Metals and Surface Engineering*, J. K. Dennis and T. E. B. T.-N. and C. P. (Third E. Such, Eds. Woodhead Publishing, 1993, pp. 205–244.

[21]   M. P. Nascimento, R. C. Souza, I. M. Miguel, W. L. Pigatin, and H. J. C. Voorwald, "Effects of tungsten carbide thermal spray coating by HP/HVOF and hard chromium electroplating on AISI 4340 high strength steel," *Surf. Coatings Technol.*, vol. 138, no. 2–3, pp. 113–124, 2001.

[22]   O. G. Palanna, *Engineering chemistry*. Tata McGraw-Hill Education, 2009.

[23]   E. J. Mittemeijer and M. A. J. Somers, *Thermochemical surface engineering of steels*. Woodhead Publishing, 2015.

[24]   J. R. Davis, *Surface hardening of steels: understanding the basics*. ASM international, 2002.

[25]   https://www.industrialheating.com/articles/89973-principles-of-gas-nitriding-part-2 (accessed Oct. 01, 2020).

[26]   Z. Xu and F. F. Xiong, *Plasma surface metallurgy*. Springer, 2008.

[27]   Y. Sun and E. Haruman, "Effect of carbon addition on low-temperature plasma nitriding characteristics of austenitic stainless steel," *Vacuum*, vol. 81, no. 1, pp. 114–119, 2006.

[28]   Z. Xu and F. F. Xiong, *Plasma Surface Metallurgy*. 2017.

[29]   J. P. De Luca and J. M. Leitnaker, "Review of Thermodynamic Properties of the Cr-N System," *J. Am. Ceram. Soc.*, vol. 56, no. 3, pp. 126–129, 1973.

[30]   C. Rebholz, H. Ziegele, A. Leyland, and A. Matthews, "Structure, mechanical and tribological properties of nitrogen-containing chromium coatings prepared by reactive magnetron sputtering," *Surf. Coatings Technol.*, vol. 115, no. 2–3, pp. 222–229, 1999.

[31]   G. Bertrand, C. Savall, and C. Meunier, "Properties of reactively RF magnetron-sputtered chromium nitride coatings," *Surf. Coatings Technol.*, vol. 96, no. 2–3, pp. 323–329, 1997.

[32]   M. Pakala and R. Y. Lin, "Reactive sputter deposition of chromium nitride coatings," *Surf. Coatings Technol.*, vol. 81, no. 2–3, pp. 233–239, 1996.

[33]   P. Hones, R. Sanjines, and F. Lévy, "Sputter deposited chromium nitride based ternary compounds for hard coatings," *Thin Solid Films*, vol. 332, no. 1–2, pp. 240–246, 1998.

[34]   J.-N. Tu, J.-G. Duh, and S.-Y. Tsai, "Morphology, mechanical properties, and oxidation

behavior of reactively sputtered Cr–N films," *Surf. Coatings Technol.*, vol. 133, pp. 181–185, 2000.

[35] Z. B. Zhao, Z. U. Rek, S. M. Yalisove, and J. C. Bilello, "Phase formation and structure of magnetron sputtered chromium nitride films: in-situ and ex-situ studies," *Surf. Coatings Technol.*, vol. 185, no. 2–3, pp. 329–339, 2004.

[36] A. P. Ehiasarian, P. E. Hovsepian, L. Hultman, and U. Helmersson, "Comparison of microstructure and mechanical properties of chromium nitride-based coatings deposited by high power impulse magnetron sputtering and by the combined steered cathodic arc/unbalanced magnetron technique," *Thin Solid Films*, vol. 457, no. 2, pp. 270–277, 2004.

[37] R. R. Aharonov, B. F. Coll, and R. P. Fontana, "Properties of chromium nitride coatings deposited by cathodic arc evaporation," *Surf. Coatings Technol.*, vol. 61, no. 1–3, pp. 223–226, 1993.

[38] B. Warcholinski and A. Gilewicz, "Effect of substrate bias voltage on the properties of CrCN and CrN coatings deposited by cathodic arc evaporation," *Vacuum*, vol. 90, pp. 145–150, 2013.

[39] J. G. Buijnsters, P. Shankar, J. Sietsma, and J. J. Ter Meulen, "Gas nitriding of chromium in NH3-H2 atmosphere," *Mater. Sci. Eng. A*, vol. 341, no. 1–2, pp. 289–295, 2003.

[40] W. Mayr, W. Lengauer, P. Ettmayer, D. Rafaja, J. Baue, and M. Bohn, "Phase equilibria and multiphase reaction diffusion in the Cr-C and Cr-N systems," *J. Phase Equilibria*, vol. 20, no. 1, pp. 35–44, 1999.

[41] M. Taguchi and J. Kurihara, "Effect of surface nitriding on corrosion resistance of chromium in sulfuric acid solution," *Mater. Trans. JIM*, vol. 32, no. 12, pp. 1170–1176, 1991.

[42] E. Menthe and K. T. Rie, "Plasma nitriding and plasma nitrocarburizing of electroplated hard chromium to increase the wear and the corrosion properties," *Surf. Coatings Technol.*, vol. 112, no. 1–3, pp. 217–220, 1999.

[43] A. Basu *et al.*, "Microstructural and texture studies of gas-nitrided Cr-coated low-alloy high-carbon steel," *Surf. Coatings Technol.*, vol. 201, no. 16–17, pp. 6985–6992, 2007.

[44] J. Y. Eom, V. Shankar Rao, H. S. Kwon, K. S. Nam, and S. C. Kwon, "Experiments and modeling study on growth behavior of Cr-nitrides formed on electroplated hard Cr during ion-nitriding," *J. Mater. Res.*, vol. 18, no. 4, pp. 861–867, 2003.

[45] P. Kuppusami, A. Dasgupta, and V. S. Raghunathan, "A new surface treatment by pulsed plasma nitriding for chromium plated austenitic stainless steel," *ISIJ Int.*, vol. 42, no. 12 SPEC., pp. 1457–1460, 2002.

[46] P. K. Ajikumar *et al.*, "Morphology and growth aspects of Cr(N) phases on gas nitridation of electroplated chromium on AISI 316 LN stainless steel," *Surf. Coatings Technol.*, vol. 201, no. 1–2, pp. 102–107, 2006.

[47] D. G. Nam and H. C. Lee, "Thermal nitridation of chromium electroplated AISI316L stainless steel for polymer electrolyte membrane fuel cell bipolar plate," *J. Power Sources*, vol. 170, no. 2, pp. 268–274, 2007.

[48] A. Basu, J. Dutta Majumdar, and I. Manna, "Structure and properties of Cr xN coating," *Surf. Eng.*, vol. 28, no. 3, pp. 199–204, 2012.

[49] A. Dasgupta, P. Kuppusami, M. Vijayalakshmi, and V. S. Raghunathan, "Pulsed plasma nitriding of large components and coupons of chrome plated SS316LN stainless steel," *J. Mater. Sci.*, vol. 42, no. 20, pp. 8447–8453, 2007.

[50] H. Shen, L. Wang, and J. Sun, "Characteristics and properties of Cr[sbnd]N compound layer produced by plasma nitriding of Cr-electroplated of AISI 304 stainless steel," *Surf. Coatings Technol.*, vol. 385, no. February, p. 125450, 2020.

[51] L. Wang, K. S. Nam, and S. C. Kwon, "Effect of plasma nitriding of electroplated chromium coatings on the corrosion protection C45 mild steel," *Surf. Coatings Technol.*, vol. 202, no. 2, pp. 203–207, 2007.

[52] S. H. Sarraf, M. Soltanieh, and H. Aghajani, "Repairing the cracks network of hard chromium electroplated layers using plasma nitriding technique," *Vacuum*, vol. 127, pp. 1–9, 2016.

[53] M. Kocabaş, M. Danişman, N. Cansever, and Ş. Ülker, "Effect of plasma nitriding time on surface properties of hard chromium electroplated AIS1 1010 steel," *Mater. Test.*, vol. 57, no. 5, pp. 437–442, 2015.

[54] M. Keshavarz Hedayati, F. Mahboubi, and T. Nickchi, "Comparison of conventional and active screen plasma nitriding of hard chromium electroplated steel," *Vacuum*, vol. 83, no. 8, pp. 1123–1128, 2009.

[55] L. Wang, K. S. Nam, and S. C. Kwon, "Transmission electron microscopy study of plasma nitriding of electroplated chromium coating," *Appl. Surf. Sci.*, vol. 207, no. 1–4, pp. 372–377, 2003.

[56] L. Wang, D. S. Kim, K. S. Nam, M. Kim, and S. C. Kwon, "Microstructure of electroplated hard chromium coatings after plasma nitrocarburizing," *Surf. Coatings Technol.*, vol. 190, no. 2–3, pp. 151–154, 2005.

[57] I. Pokorska, "Properties of composite layers obtained by combined treatment," *Met. Sci. Heat Treat.*, vol. 47, no. 11–12, pp. 520–521, 2005.

[58] M. Soltanieh, H. Aghajani, F. Mahboubi, and K. A. Nekouee, "Surface characterization of multiple coated H11 hot work tool steel by plasma nitriding and hard chromium electroplating processes," *Vacuum*, vol. 86, no. 10, pp. 1470–1476, 2012.

[59]   https://chem.libretexts.org/Bookshelves/Analytical_Chemistry/Supplemental_Modules_(Analytical_Chemistry)/Instrumental_Analysis/Diffraction_Scattering_Techniques/Bragg%27s_Law (accessed Mar. 25, 2021).

[60] https://www.xtal.iqfr.csic.es/Cristalografia/parte_05_5-en.html (accessed Mar. 25, 2021).

[61] M. Lee, *X-Ray diffraction for materials research: from fundamentals to applications*. CRC Press, 2017.

[62] W. C. Contributors, "File:Electron Interaction with Matter.svg," *Wikimedia Commons, the free media repository*. https://commons.wikimedia.org (accessed Mar. 29, 2021).

[63] https://iubemc.sitehost.iu.edu/eftem.html (accessed Mar. 29, 2021).

[64] B. JP and D. JM, "Des matériaux," *Press. Int. Polytech. Ec. Polytech. Montréal*, 2000.

[65] A. S. Ali, "Application of nanomaterials in environmental improvement," in *Nanotechnology and the Environment*, IntechOpen, 2020.

[66] M. P. Do Nascimento and H. J. C. Voorwald, "The significance and determination by image analysis of microcrack density in hard chromium plating," *Plat. Surf. Finish.*, vol. 95, no. 4, pp. 36–42, 2008.

[67] W. C. Oliver and G. M. Pharr, "An impoved technique for determining hardness and elastic modulus using load and displacement sensing indentation experiments," *Journal of Materials Research*, vol. 7, no. 06. pp. 1564–1583, 1992.

[68] J. Archard, "Contact and rubbing of flat surfaces," *J. Appl. Phys.*, vol. 24, no. 8, pp. 981–988, 1953.

[69] A. Designation, "G99-95a (2000) e1," *Stand. test method wear Test. with a pin-on-disk Appar.*

[70] W. Lee and T. Su, "Mechanical properties and microstructural features of AISI 4340 high-strength alloy steel under quenched and tempered conditions," vol. 87, pp. 198–206, 1999.

[71] J. Simão and D. K. Aspinwall, "Hard chromium plating of EDT mill work rolls," *J. Mater. Process. Technol.*, vol. 92, pp. 281–287, 1999.

[72] M. H. Sohi, A. A. Kashi, and S. M. M. Hadavi, "Comparative tribological study of hard and crack-free electrodeposited chromium coatings," *J. Mater. Process. Technol.*, vol. 138, no. 1–3, pp. 219–222, 2003.

[73] K.-M. Yin and C. M. Wang, "A study on the deposit uniformity of hard chromium plating on the interior of small-diameter tubes," *Surf. Coatings Technol.*, vol. 114, no. 2–3, pp. 213–223, 1999.

[74] L. Vernhes, M. Azzi, and J. E. Klemberg-Sapieha, "Alternatives for hard chromium plating: Nanostructured coatings for severe-service valves," *Mater. Chem. Phys.*, vol. 140, no. 2–3, pp. 522–528, 2013.

[75] A. Brenner, P. Burkhead, and C. Jennings, "Physical properties of electrodeposited chromium," *J. Res. Natl. Bur. Stand. (1934).*, vol. 40, pp. 31–59, 1948.

[76] K. E. Noll, "Effects of Ion Implantation on Electroplated Chromium.," ARMY ARMAMENT RESEARCH DEVELOPMENT AND ENGINEERING CENTER WATERVLIET NY …, 1995.

[77] G. Bolelli, V. Cannillo, L. Lusvarghi, and S. Riccò, "Mechanical and tribological properties of electrolytic hard chrome and HVOF-sprayed coatings," *Surf. Coatings Technol.*, vol. 200, no. 9, pp. 2995–3009, 2006.

[78]   S. Mokhtara, M. Zidani, M. M. Alim, and S. Mechachti, "Plasma Nitriding of Hard Chromium Electroplated Low Alloy AISI 4340 Steel in Pure Nitrogen Gas Atmosphere," in *Journal of Nano Research*, 2020, vol. 65, pp. 135–144.

[79]   C. A. Snavely and C. L. Faust, "Studies on the Structure of Hard C h r o m i u m Plate," 1949.

[80]   E. Lunarska, K. Nikiforow, T. Wierzchon, and I. Ulbin-Pokorska, "Effect of plasma nitriding on hydrogen behavior in electroplated chromium coating," *Surf. Coatings Technol.*, vol. 145, no. 1–3, pp. 139–145, 2001.

[81]   Y. Takahashi, K. Inoue, Y. Li, and I. Kawaguchi, "Glow Plasma Behaviour in Nitriding Process (Physics, Process, Instruments & Measurements)," *Trans. JWRI*, vol. 22, no. 1, pp. 13–19, 1993.

[82]   H. Cifuentes Aya and J. J. Olaya Flórez, "A review of producing hard coatings by means of duplex treatments using an electroplated coating-thermochemical treatment combination," *Ing. e Investig.*, vol. 31, no. 3, pp. 6–16, 2011.

[83]   J. B. Pethica and W. C. Oliver, "Mechanical properties of nanometre volumes of material: use of the elastic response of small area indentations," *MRS Online Proc. Libr.*, vol. 130, no. 1, pp. 13–23, 1988.

[84]   N. M. Martyak, J. E. McCaskie, B. Voos, and W. Plieth, "Microcracks in chromium electrodeposits," *J. Mater. Sci.*, vol. 32, no. 22, pp. 6069–6073, 1997.

[85]   C. P. Brittain and G. C. Smith, "The Influence of Annealing on the Structure and Hardness of Electrodeposited Chromium," *Trans. IMF*, vol. 31, no. 1, pp. 146–152, 1954.

[86]   X. Guan, Y. Wang, Q. Xue, and L. Wang, "Toward high load bearing capacity and corrosion resistance Cr/Cr2N nano-multilayer coatings against seawater attack," *Surf. Coatings Technol.*, vol. 282, pp. 78–85, 2015.

[87]   F. Borgioli, A. Fossati, E. Galvanetto, T. Bacci, and G. Pradelli, "Glow discharge nitriding of AISI 316L austenitic stainless steel: Influence of treatment pressure," *Surf. Coatings Technol.*, vol. 200, no. 18–19, pp. 5505–5513, 2006.

[88]   J. C. Stinville, J. Cormier, C. Templier, and P. Villechaise, "Modeling of the lattice rotations induced by plasma nitriding of 316L polycrystalline stainless steel," *Acta Mater.*, vol. 83, pp. 10–16, 2015.

[89]   S. Taktak, I. Gunes, S. Ulker, and Y. Yalcin, "Effect of N2 + H2 gas mixtures in plasma nitriding on tribological properties of duplex surface treated steels," *Mater. Charact.*, vol. 59, no. 12, pp. 1784–1791, 2008.

[90]   X. Cai *et al.*, "Microstructural characterization of a V2C and V8C7 ceramic-reinforced Fe substrate surface compound layer by EBSD and TEM," *J. Alloys Compd.*, vol. 747, pp. 8–20, 2018.

[91]   V. Domnich and Y. Gogotsi, "PHASE TRANSFORMATIONS IN SILICON UNDER CONTACT LOADING," no. June, 2014.

[92] A. Taghizadeh Tabrizi, H. Aghajani, and F. Farhang Laleh, "Tribological characterization of hybrid chromium nitride thin layer synthesized on titanium," *Surf. Coatings Technol.*, vol. 419, no. May, p. 127317, 2021.

[93] A. Leyland and A. Matthews, "On the significance of the H/E ratio in wear control: A nanocomposite coating approach to optimised tribological behaviour," *Wear*, vol. 246, no. 1–2, pp. 1–11, 2000.

[94] G. Wei, T. W. Scharf, J. N. Zhou, F. Huang, M. L. Weaver, and J. A. Barnard, "Nanotribology studies of Cr, Cr2N and CrN thin films using constant and ramped load nanoscratch techniques," *Surf. Coatings Technol.*, vol. 146–147, pp. 357–362, 2001.

[95] V. L. Dubonosov, L. V. Krichkovskaya, D. V. Demyanenko, G. S. Khrypunov, and O. S. Vodoriz, "Prospectives for applying of nanocoatings on instrumental tools," *2020 IEEE 4th Int. Conf. Intell. Energy Power Syst. IEPS 2020 - Proc.*, pp. 291–295, 2020.

[96] A. W. Batchelor, L. N. Lam, and M. Chandrasekaran, *Materials degradation and its control by surface engineering*. World Scientific, 2011.

APPENDICES

APPENDICES

A

Scientific activities

1- **International publications**

- S. MOKHTARA, M. ZIDANI, M. M. ALIM, S.Mechachti, "Plasma Nitriding of Hard Chromium Electroplated Low Alloy AISI 4340 Steel in Pure Nitrogen Gas Atmosphere", Journal of Nano Research, Vol. 65, pp 135-144 (online: 14 – 12 – 2020).

2- **International conferences**

- S. MOKHTARA, M. ZIDANI, M. M. ALIM, "Structural morphological and mechanical properties of a chromium nitride layer obtained by duplex treatment", 3nd international conference on physical chemistry & functional materials (PCFM 2020),, Battalgazi/Malatya, Turkey, September 22-24 (2020) (Online presentation).

- S.MOKHTARA, M.ZIDANI, L.MEBARKI, "The effect of quenching and tempering on the tribological behaviour of AISI 4340 steel", International Conference on Welding, No Destructive Testing and Materials and Alloys Industry (IC-WNDT-MI'18), Skikda, Algeria, 07 -08 November (2018).

- S.MOKHTARA, M.ZIDANI, L.MEBARKI, "Frictional and wear behaviour of heat-treated and duplex-coated 35NCD6 steel", International Conference on Materials Science (ICMS2018), SETIF1University, Algeria, September 12-14 (2018).

3- **National conferences**

- S.MOKHTARA, M.ZIDANI, MM.ALIM, S.Mechachti, "Structural and Morphological Properties of a Duplex Layer Deposited on Low Alloy Steel", Algerian Symposium on Renewable Energy and Materials ASREM2020, Médéa, Algeria, December 16-17 (2020) (Online presentation).

- S.MOKHTARA, M.ZIDANI, "Duplex treatment of 35NCD6", Journée de métallurgie, University Mohamed Khider, Biskra, Algeria, November 10 (2019).

4- Teaching activities

- Teaching physics module 01 - practical work - first semester (2020/2021).
- Teaching physics module 02 - practical work - second semester (2020/2021)

5- Other

- One year internship in Centre for Development of Advanced Technologies (CDTA) in "Ionised Environment and Laser" (MIL) division, Baba Hassen, Algiers, Algeria (2019).
- Five months as an Erasmus exchange student at the University of Politecnico di Milano Italy (2020).